David Publishing Company
www.davidpublishing.com

Volume 2, Number 1, January 2014

Journal of Pharmacy and Pharmacology

ISSN 2328-2150 (Print)

From Knowledge to Wisdom

Journal of Pharmacy and Pharmacology
Volume 2, Number 1, January 2014 (Serial Number 2)

Journal of Pharmacy and Pharmacology

Volume 2, Number 1, January 2014 (Serial Number 2)

David Publishing Company
www.davidpublishing.com

Publication Information
Journal of Pharmacy and Pharmacology is published monthly in hard copy (ISSN 2328-2150) by David Publishing Company located at 240 Nagle Avenue #15C, New York, NY 10034, USA.

Aims and Scope
Journal of Pharmacy and Pharmacology, a monthly professional academic journal, covers all sorts of researches on Pharmacokinetics, Biopharmaceutics, Pharmaceutical Analysis, Pharmaceutical Biotechnology and Drug Delivery, Pharmaceutical Outcomes and Policy, Pharmacy Administration, Advanced Pharmacology, Experimental Method and Technique of Pharmacology, Clinical Pharmacology, Medical Statistics, Pathophysiology, and Medicinal Chemistry, as well as other issues related to Pharmacy and Pharmacology.

Manuscripts and correspondence are invited for publication. You can submit your papers via E-mail to pharmacy@davidpublishing.com or pharmacy@davidpublishing.org. Submission guidelines are available at http://www.davidpublishing.com.

Editorial Office
240 Nagle Avenue #15C, New York, NY 10034, USA
Tel: 1-323-984-7526, 323-410-1082; Fax: 1-323-984-7374, 323-908-0457
E-mail: pharmacy@davidpublishing.com, pharmacy@davidpublishing.org

Abstracted / Indexed in
Database of EBSCO, Massachusetts, USA
Universe Digital Library S/B, ProQuest
Summon Serials Solutions, USA
Google Scholar (scholar.google.com)
Chinese Database of CEPS, American Federal Computer Library Center (OCLC), USA
Universe Digital Library Sdn Bhd (UDLSB), Malaysia
China National Knowledge Infrastructure (CNKI), China

Subscription Information
Price (per year): Print $520, Online $320, Print and Online $600.

David Publishing Company
240 Nagle Avenue #15C, New York, NY 10034, USA
Tel: 1-323-984-7526, 323-410-1082; Fax: 1-323-984-7374, 323-908-0457
E-mail: order@davidpublishing.org
Digital Cooperative Company: www.bookan.com.cn

Journal of
Pharmacy and Pharmacology

Volume 2, Number 1, January 2014 (Serial Number 2)

Contents

Reviews

Original Articles

Journal of Pharmacy and Pharmacology 2 (2014) 1-18

An Overview of *Entada phaseoloides*: Current Research and Future Prospects

Chandana Choudhury Barua[1], Mousumi Hazorika[1] and Jyoti Misri[2]

1. Department of Pharmacology and Toxicology, Assam Agricultural University, Guwahati, Assam 781022, India

2. Department of Animal Health, ICAR, Krishi Anusandhan Bhavan (Pusa), New Delhi 110001, India

Received: September 22, 2013 / Accepted: November 25, 2013 / Published: February 28, 2014.

Abstract: In recent times, focus on plant research and herbal products has increased tremendously in the western world as well as in developed and developing countries. *Entada phaseoloides*, a well-known creeper widely used therapeutically in the orient and has become increasingly popular as an important medicinal plant. Many studies have been carried out on this medicinal plant and have generated immense data about the morphology, chemical composition, corresponding to biological activity of extracts and isolated secondary metabolites. Biological studies and traditional clinical practice demonstrated that *Entada phaseoloides* and its bioactive compounds possess various pharmacological properties. The plant has been traditionally used in Ayurvedic medicine for centuries as an anti-inflammatory, analgesic, antipyretic, antiarthritis, antidiabetic, antioxidant, cytotoxic, antimicrobial and molluscidal agent. The present review summarizes current knowledge on morphology, major bioactive(s) constituents and its chemistry, reported medicinal properties, pharmacological actions, folklore uses and the possibility of interactions of the herb with the conventional drugs. Despite this, further investigations are required to explore *Entada phaseoloides* and to evaluate the different biological activities of either its extracts or the isolated compounds with probable modes of action.

Key words: *Entada phaseoloides*, morphology, bioactive constituents, folklore uses.

1. Introduction

Throughout the ages, humans have traditionally relied on plants, animals and minerals for their basic needs, such as food, protection against enemies, hunting, and healing of infections and health disorders. A number of traditional medicinal systems have evolved that have been used for centuries and today, are still a source of interesting drugs for phytotherapy [1]. Nature always stands as a gold mark to exemplify the outstanding phenomenon of symbiosis [2, 3]. Interest in the use of herbal products has grown dramatically in the western world [4] as well as in developed countries [5]. The herbal vendors are the mobile men seen on the busy streets of many Indian cities selling crude medicinal plants and its products. They prescribe herbal treatment for several diseases, a skill they inherited from their forefathers through several generations of experience [6]. One of the important medicinal plants, widely used therapeutically in the orient and becoming increasingly popular is *Entada phaseoloides*, a creeper, of genus *Entada* which consists of 30 species of trees, shrubs and tropical lianas. About 21 species are known from Africa, six from Asia, two from the American tropics and one with a pan tropical distribution [7]. *Entada phaseoloides* is a very large woody climber belonging to Order Fabales, Family Fabaceae or Leguminosae, Subfamily Mimosoideae and Tribe of Mimoseae. Botanical name is *Entada phaseoloides* (L.) Merril [8]. Synonyms of *Entada phaseoloides* is *Entada scadens* (L.) [9], *Lens phaseoloides* L. [10] and is commonly known as Matchbox Bean, Vine, Gogo, Elva Climber, etc. [11].

Corresponding author: Chandana Choudhury Barua, Ph.D., professor, research fields: Pharmacology and toxicology. E-mail: chanaicn@gmail.com.

In India, the species is widely distributed in the eastern Himalayas, East Bengal, Tirupati (Andhra Pradesh) etc. [12]. In the folklore of Indian medicine, the herb has been used traditionally in various diseases as analgesic, counter irritant, hair growth stimulant, emetic and remedy for cerebral haemorrhage. This comprehensive review summarizes our current knowledge of the major bioactivities and clinical efficacy of *Entada phaseoloides* as one of the currently used popular herbal plant. The popularity of *Entada phaseoloides* as a medicinal plant can be best determined by the number of papers published per year over a period of time which is presented in Fig. 1 [13-41]. We aim to derive an impressive and convenient review; scientifically beneficial for both investigators and readers who are interested in the pharmaceutical aspects of medicinally active herbs. However, it was not the intention of this review to go beyond the field of phytochemistry and ethnobotany.

2. Morphology

The woody creeper *Entada phaseoloides* with all its parts stem, leaves, leaves with flowers, flowers, fruits and fruit with seed are presented in Figs. 2a-2f, respectively [8].

Stem diameters measures up to 18 cm, laterally compressed or flattened and twisted like a corkscrew. Vessels are large, readily visible to the naked eye in transverse sections. Pith is located eccentrically much closer to one margin than the other in stem cross sections.

Leaves are bipinnate with about 8-16 leaflets, (two to four leaflets on each secondary axis) main rhachis projecting as a branched tendril beyond the leaf. Leaflet blades measure about (4-11) × 2.5-5.5 cm, while leaflet stalks are of about 0.1-0.7 cm long and are transversely wrinkled.

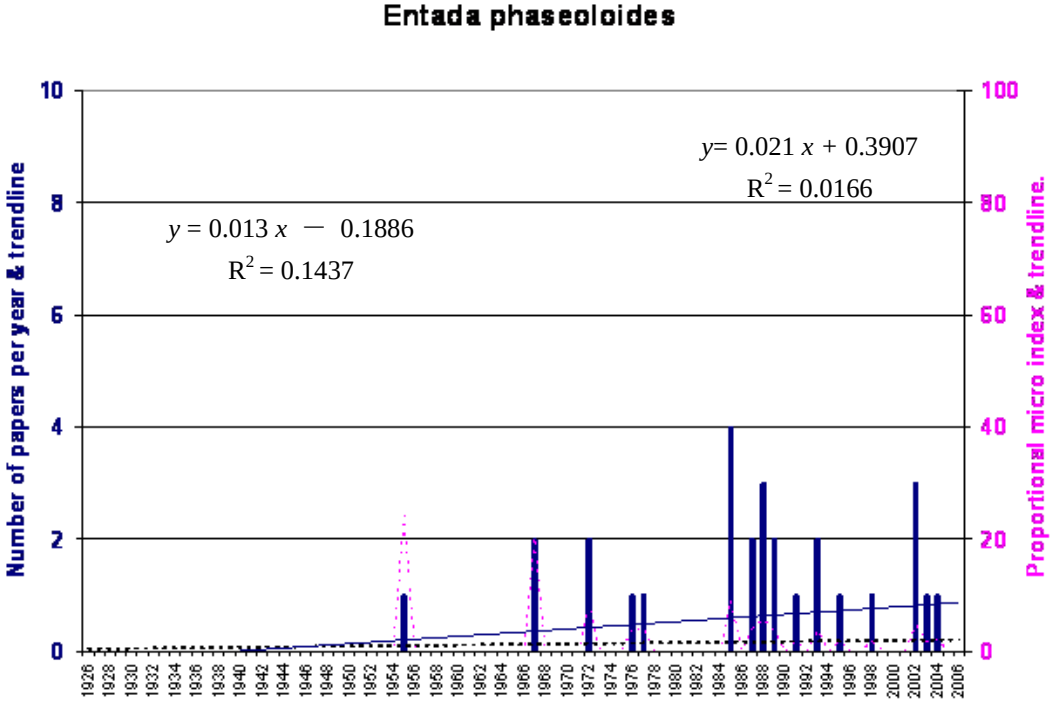

Fig. 1 Popularity of *Entada phaseoloides* over time.

Plots of numbers of papers mentioning *Entada phaseoloides* (filled column histogram and left hand axis scale) and line of best fit, 1926 to 2006 (complete line, with equation and % variation accounted for, in box on the left hand side); plots of a proportional micro index, derived from numbers of papers mentioning *Entada phaseoloides* as a proportion (scaled by multiplying by one million) of the total number of papers published for that year (broken line frequency polygon and right hand scale) and line of best fit, 1926 to 2006 (broken line, with equation and % variation accounted for, in broken line box on the right hand side).

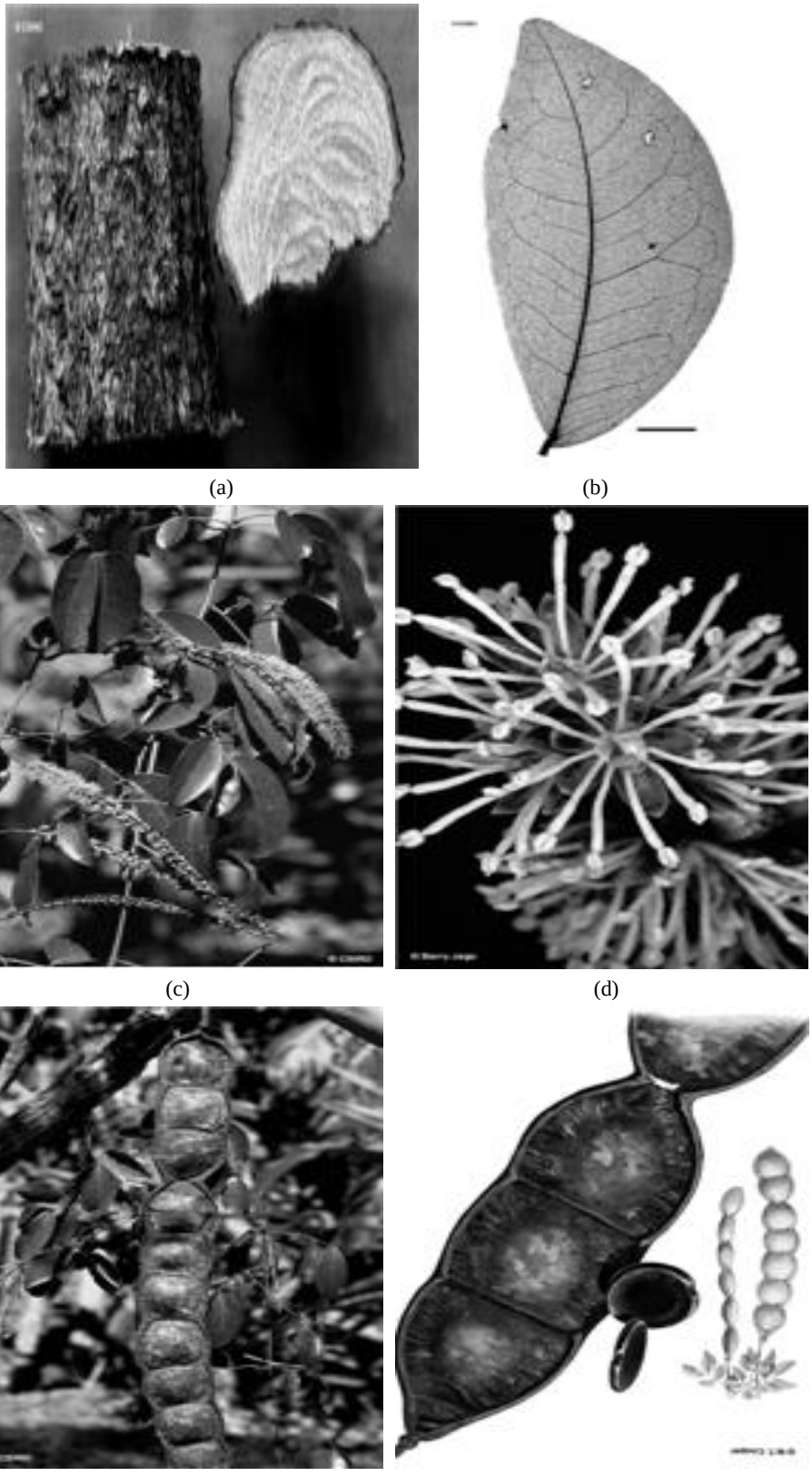

Fig. 2 (a) Stem bark & stem transverse section; (b) *Entada* leave (10 mm); (c) Entada leaves & flowers; (d) Entada fruit; (e) Entada seed; (f) Entada fruit & seeds.

Stipules are linear and falcate which measures 2-4 × 2 mm. Scattered large clear glands are visible to the naked eye in the leaflet blades, whereas numerous smaller glands can be visible with a lens.

Flowers are more or less cup-shaped, about 1.5 mm in diameter at the apex. Corolla is pink to red in colour and cream or translucent in colour on the inner surface. Petals are about 3 × (1-1.5) mm. Staminal filaments crumpled in the bud which are of about 6-7 mm long at anthesis. Style crumpled in the bud.

Fruits are flattened, about (88-100) × (9-12) cm, constricted at intervals and divided into about 12 segments, each segment measures about 7 × (9-10) cm, surrounded by endocarp and falling from the pod leaving only the sutures of the pod attached to the vine. Exocarp shed by rolling up into rolls of tissue. Endocarp is not hard but more or less leathery or like parchment.

Seeds are laterally compressed, about 5-6 cm in diameter and 1-1.5 cm thick. Testa is hard. Cotyledons are hard, about (4.5-5.5) × (4.5-5) cm in diameter which fused around the margin. Radicle measures about 4 mm long [11].

3. Distribution and Ecology

It is distributed in the altitudinal range from near sea-level to 100 m. The plant grows in beach forest, gallery forest, monsoon forest and lowland rain forest and also occurs in New Guinea and other parts of Malaysia, Asia and the Pacific islands [11]. The plant occurs throughout the sub-Himalayan tract, from Nepal eastwards ascending to 4,000 ft. in Sikkim, in Assam, Bihar and Orissa, and in the monsoon forest of western and eastern ghats; it is abundant in Andaman Islands [42]. Also found in forests at low and medium altitudes, from Northern Luzon (Cagayan) to Mindanao and Palawan [43].

4. Natural History

Entada phaseoloides is a food plant for the larval stages of the tailed green-banded blue butterfly [44]. This species may have medicinal properties and has been used as a fish poison. The species has been used medicinally in Malaysia, the Philippines and Java. The seed are considered as tonic, emetic and anthelmintic [42].

5. Properties

The seeds of *Entada phaseoloides* are slightly bitter-acrid in taste and mildly cooling in nature. It was reported as antirheumatic, relieving gastrointestinal disorders and aids circulation. The juice extracted from the bark was reportedly found to be irritating to the eyes, causing conjunctivitis. *Entada phaseoloides* was also found to exhibit detectable genotoxicity [11].

6. Utility and Edibility

Bark, seeds and vines were usually the utilized parts of *Entada phaseoloides*. The vines may be collected during any time of the year, rinse, section into slices, steamed and lastly sundried. The seeds may be collected from January to April. Seed coats are removed and roasted in a frying pan, sun-dried and pulverized. In the Dutch Indies, young leaves are eaten, raw or cooked. In Bali and Sumatra, the seeds are eaten while in South Africa, pod and seeds are used as coffee substitute [11]. The white kernels of the seeds are eaten by the poor, after soaking in water and roasting to remove toxic principles. Roasted pods are occasionally used as substitute for calabar bean. The seeds, stems and barks are poisonous. The leaves are reported to be free from the toxic saponins which are present in other parts of the plant. They are eaten by elephants [42].

7. Folkloric Uses

Dried vine materials of about 15 g to 30 g in decoction are reported to be effective in rheumatic lumbar, leg pains, sprains and contusions. Powdered seeds of about 3 g to 9 g when taken orally with water can cure jaundice and edema due to malnutrition. In abdominal pains and colic, the pound kernels of seeds

after mixing with oil can be applied as poultice onto affected area. The paste of seed is used as counterirritant and applied to glandular swellings in the axilla, loins and joints, and swollen hands and feet. It is also used as hair growth stimulant. Seeds are used as emetic. It is used as febrifuge. In South Africa, seeds are used by infants to bite on during their teething period. Also, used as remedy for cerebral hemorrhage. As a treatment of skin itches, the affected part is washed with a decoction of the bark of *Entada phaseoloides*. Stem macerated in cold water used as cleansing soap and also used as an emetic [11].

8. Local Application

The seeds of *Entada phaseoloides* used extensively in the Philippines and other oriental countries for washing the hair. Also it is an ingredient of hair tonics. The bark is soaked in water until soft, the fibers are spread, the juice is expressed by rubbing the fibers against each other until it lathers, which is then used to cleanse the scalp. Bark is used as cordage. In Europe, it is used for tinder and for making match boxes. Large pods and seeds were used by children as playthings. In Sunda Islands, a fatty oil extracted from the seeds is used as an illuminant. In Europe, seeds were reportedly used for snuff [11]. The saponins have a strong haemolytic action on human red blood cells. A sharp fall in blood pressure was observed in experimental animals after doses of saponins varying from 0.0005-0.002 g/kg of body weight; the fall was associated with an increase in the volume of the intestines and, to a lesser extent, of the kidneys; there was no fall in blood pressure in animals which had received atropine [42, 45]. The saponins are reported to have a depressant effect on the respiratory system and inhibit the movements of unstriped muscles of the intestines and the uterus. Entagenic acid has antifungal activity against phytopathogenic fungi. A glycoside of entagenic acid possesses antineoplastic activity. The oil is used in lamps for illuminating purposes. A potable watery fluid exudes from the fresh stem when cut. The bark fibre, which is coarse but durable, is used for cordage and nets. The hard and smooth-shelled seeds are used for burnishing pottery, polishing hand-made paper and crimpling linen. The seeds are hollowed out and employed in making trinkets and small receptacles e.g., snuff and tinder boxes [42].

9. Constituents and Chemistry

9.1 Saponin

Entada phaseoloides yields saponin which is reported to be abundant in the bark, less so in the wood, plentiful in the seeds, and absent from the leave [43], a crystalline saponin isolated from seed kernels of *Entada phaseoloides*, which have the tentative empirical formula $C_{45}H_{82}O_{27}$. Acid hydrolysis yields a crystalline sapogenin $C_{30}H_{48}O_5$ which appears to be identical with entagenic acid, together with arabinose and xylose [33], the chemical formula of saponin [46], sapogenin [47], entagenic acid, arabinose and xylose are presented in Figs. 3a-3e, respectively [48].

9.2 Phaseoloidin

The structure of phaseoloidin isolated from the seeds of *Entada phaseoloides* has been determined as homogentisic acid 2-O-β-D-glucopyranoside by chemical and spectral means [34], whose chemical formula is presented in Fig. 4 [48].

9.3 Amides

Entadamide A [35] and Entadamide B [36], the two new sulfur-containing amides, isolated from the seeds of *Entada phaseoloides* which were synthesized by the addition reaction of methanethiol to propiolic acid followed by condensation with ethanolamine by the use of dicyclohexylcarbodiimide. These compounds inhibited the 5-lipoxygenase activity of RBL-1 cells at 10^{-4} g/mL. This finding suggests that entadamides A and B may be examples of a new type of anti-inflammatory drug [37]. Entadamide B was characterized by spectroscopic methods as N-(2-hydroxyethyl)-3,3-bis(methylthio) propaneamide

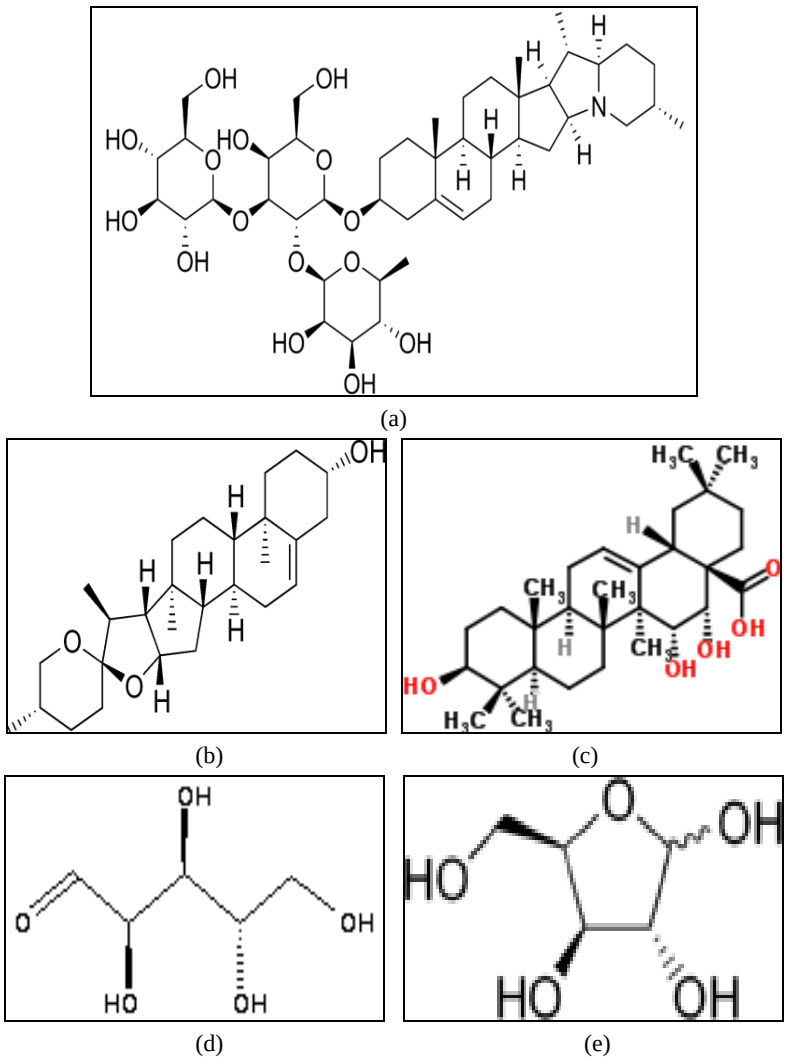

Fig. 3 (a) Chemical structure of the saponinl; (b) Chemical structure of the sapogenin; (c) Chemical structure of the entagenic acid; (d) Chemical structure of the arabinose; (e) Chemical structure of the xylose.

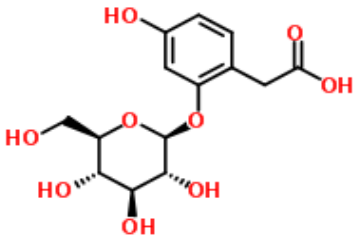

Fig. 4 Chemical structure of phaseoloidin.

and was synthesized in two steps from propiolic acid [37]. The chemical formula of Entadamide A [49] and Entadamide B [50] are presented in Figs. 5a and 5b, respectively.

Entadamide C, a third new sulphur-containing amide, has been isolated from the leaves of *Entada phaseoloides* together with entadamide A. Entadamide C, the sulphoxide form of entadamide A, is called as (*R*)-(+)-*trans*-*N*-(2-hydroxyethyl)-3-methylsulphinylpropenamide. Chemical synthesis of (±)-entadamide C was achieved in three steps from propiolic acid [21].

The chemical formula of Entadamide C is presented in Fig. 5c [51]. Again four sulfur-containing amide compounds were isolated from the n-BuOH-soluble fraction and identified as entadamide A-β-D-glucopyranosyl-(1→3)-β-D-glucopyranoside (Compound 1), which is a new compound along with and entadamide A (Compound 2), entadamide A-β-D-glucopyranoside (Compound 3) and clinacoside

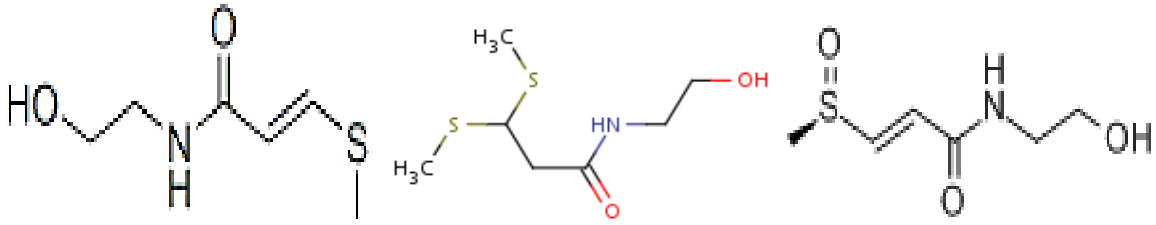

(a) (b) (c)

Fig. 5 (a) Chemical structure of entadamide A; (b) Chemical structure of entadamide B; (c) Chemical structure of the entadamide C.

C (Compound 4). Compound 4 is isolated from the genus *Entada* for the first time. The chemical formula of Compound 1, Compound 2, Compound 3 and Compound 4 are presented in Figs. 6a-6d, respectively [52].

9.4 Glycosides

Three new compounds, 2-hydroxy-5-butoxyphenylacetic acid, 2-β-D glucopyranosyloxy-5-butoxyphenylacetic acid, and entadamide A-β-D-glucopyranoside, in addition to the new natural product 2,5-dihydroxyphenylacetic acid methyl ester isolated and characterized from seeds of *Entada phaseoloides* collected in Indonesia. None of these compounds was found to demonstrate significant cytotoxicity for cultured human cancer cells, but 2-hydroxy-5-butoxyphenylacetic acid and 2,5-dihydroxyphenylacetic acid methyl ester gave ED_{50} values of 1.01.7 μg mL^{-1} and 1.7 μg mL^{-1}, respectively, with cultured P-388 cell [39].

9.5 Chalcone Glycosides

Two new chalcone glycosides4'-O-(6″-O-galloyl-β-D-glucopyranosyl)-2', 4 dihydroxychalcone (1) and 4'-O-(6″-O-galloyl-β-D-glucopyranosyl)-2'-hydroxy-4 methoxychalcone (2) together with one known chalcone glycoside 4'-O-β-d-glucopyranosyl-2'-hydroxy-4-methoxychalcone (3) isolated from the stems of *Entada phaseoloides*. The structures of the new compounds were elucidated on the basis of extensive spectroscopic analysis, including HSQC (heteronuclear single quantum correlation spectroscopy), HMBC (heteronuclear multiple bond correlation spectroscopy), ^{1}H-^{1}H COSY (^{1}H-^{1}H correlation spectroscopy), and chemical evidences. This was the first report of chalcone-type compounds isolated from the genus *Entada*. The chemical structure of three isolated compounds, i.e., Compound 1, Compound 2 and Compound 3 are presented in Fig. 7 [53].

9.6 Glucosides

The phytochemical investigation of the defatted seeds of *Entada phaseoloides* Merill. (Mimosaceae) led to the isolation of three new phenolic acid glucosides,

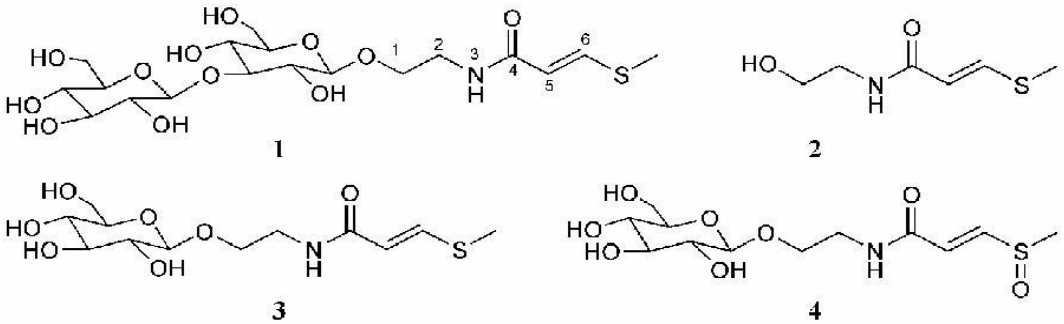

Fig. 6 The chemical structures of four sulphur containing amides, i.e., Compound 1, Compound 2, Compound 3 and Compound 4.

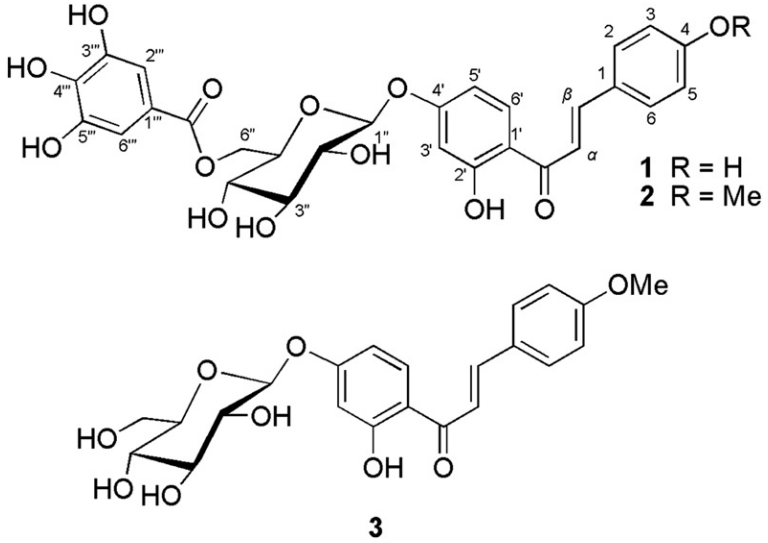

Fig. 7 The chemical structures of three chalcone glycosides, i.e., Compound 1, Compound 2 and Compound 3 .

which were characterized as 2-hydroxy-5-methylbenzoyl-β-L-glucopyranoside[p-cresotyl glucoside, 1(first phenolic acid glucosides)], 2-hydroxy-5-methylbenzoy l-β-L-glucopyranosyl (2→1)-β-glucopyranosyl(2→1)-β-L-glucopyranoside [p-cresotyltriglucoside, 2(second phenolic acid glucosides)], and 2-hydroxybenzoyl-β-Lglucopyranosyl(2→1)-β-L-glucopyranosyl(2→1)-β-L-glucopyranosyl(2→1)-β-L-glucopyranoside (salicylic acid tetraglucoside, 5(fifth phenolic acid glucosides)], along with sucrose and triglucoside. The structures of these phytoconstituents have been established on the basis of spectral data analysis and chemical reactions [54].

9.7 Sulphur-Containing Glucoside

One new and one known sulphur-containing glucoside from a MeOH extract, along with four new triterpene saponins containing *N*-acetylglucosamine in their sugar chains were isolated from the 1-BuOH-soluble fraction of a H_2O extract of kernel nuts of *Entada phaseoloides (L.) Merrill* [55].

9.8 Flavonoids

The compound 5,6,7,5'-Tetramethoxy-3', 4'-methylene dioxy flavones monohydrate (systematic name: 5,6,7-trimethoxy-2-(7-methoxy-1,3-dihydro-2-benzofuran-5-yl)-4H-chromen-4-onemonohydrate), was isolated from the popular Chinese medicinal plant *Entada phaseoloides*. In the crystal, inversion-related molecules are joined by pairs of weak C-H···O hydrogen bonds. The dimers are further interconnected by a bridging water molecule *via* weak C-H···O_{water} and pairs of (O-H)$_{water}$···O hydrogen bonds into a linear tape running parallel to the *b* axis [56].

9.9 Antioxidants

The EtOH extract of the stems of *Entada phaseoloides* displayed potent antioxidant activity when assessed by the 1,1-diphenyl-2-picrylhydrazyl(DPPH) and 2,2'-azinobis(3-ethylbenzothiazoline-6-sulfonic acid) (ABTS) radical-scavenging, reducing power, β-carotene-bleaching and superoxide radical-scavenging assays. Fractionation of the ethanol (EtOH) extracts showed that the ethyl acetate (AcOEt) fraction is the most active, which inhibited the linoleic acid oxidant to the greatest extent, had the strongest DPPH and ABTS radical-scavenging abilities, and possessed significant reducing power over other fractions followed by the H_2O fraction, while BuOH (butanol) fraction was least active. Further activity-guided fractionation studies on the active

fractions resulted in the isolation of 22 compounds, i.e., 3,4',7-trimethylquercetin (1), 5-hydroxy-3,4',7-trimethoxyflavone (2) [57], quercetin (3), (þ)-3,3',5',5,7-pentahydroxyflavanone (4) [58], luteolin (5), (þ)-dihydrokaempferol (6) [58], dehydrodicatechin A (7) [59], apigenin (8), (_)-epicatechin (9), (þ)-catechin (10) [60], 3-deoxysappanchalcone (11) [61], naringenin (12), rhamnocitrin (13), 4',7-dihydroxyflavone (14) [62], protocatechuic acid (15), vanillic acid (16), 4',5,7-trihydroxy-3'-methoxyflavonol (17) [63], galangin (18), rutin (19), 3',5,5',7-tetrahydroxyflavanone (20) [64], 2',5,5'-trihydroxy-3,4',7-trimethoxyflavone-2'-O-b-d-glucoside (21) [65] and (_)-epigallocatechin (22) [60] were confirmed by comparing their HPLC, HPTLC, and characteristic spectroscopic data with those of the standards or with those reported in the literature. The chemical structures of the isolated compounds are presented in Fig. 8. The identities of these compounds were established based on extensive spectroscopic studies. Furthermore, the antioxidant activities of the isolated compounds were evaluated by using the above-mentioned five assays. The results demonstrated that the EtOH extract of *E. phaseoloides* stems exhibit an excellent antioxidant activity and thus presents a great potential as a source of natural antioxidants. The antioxidant activity of EtOH extract and three fractions from stem of *E. phaseoloides* are presented graphically in Fig. 9. This is claimed to be the first extensive study of all compounds from *E. phaseoloides* and genus *Entada* by the author [66].

9.10 Crude and Processed Products

The chemical constituents of the *Entada phaseoloides* (L.) Merrill were studied by extracting it

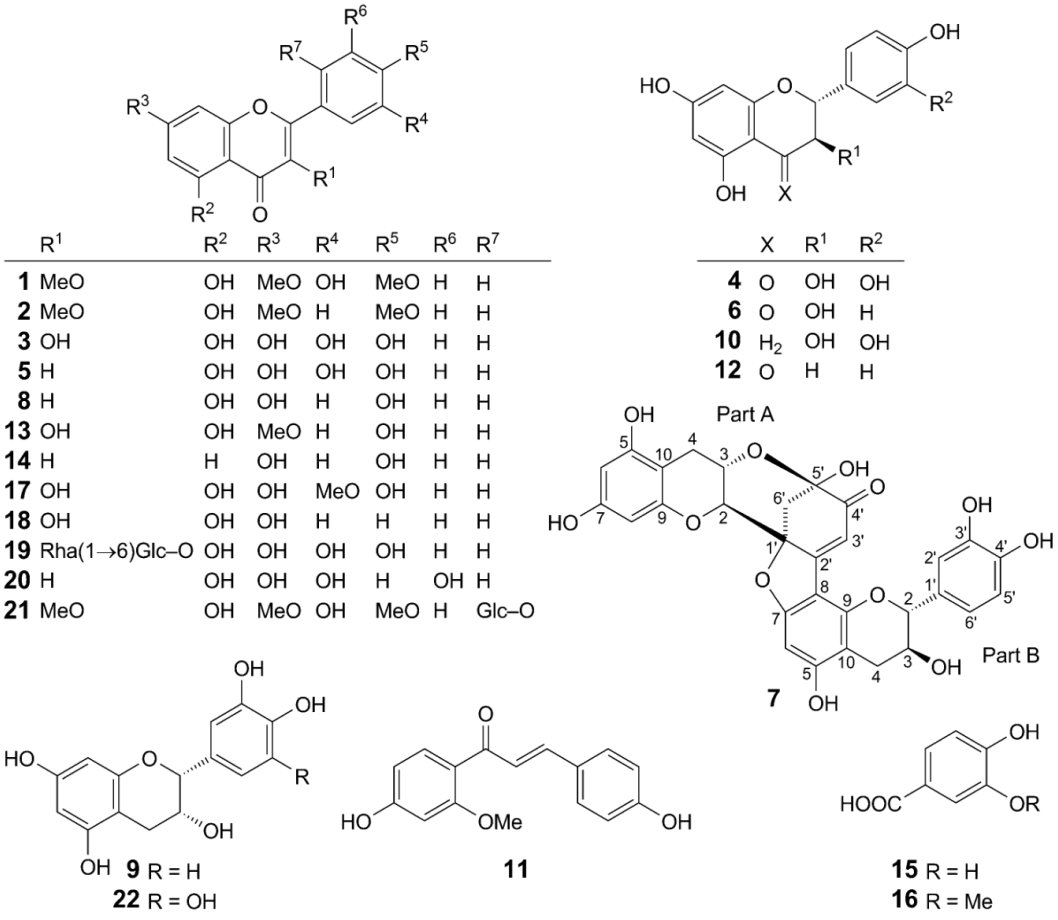

	R^1	R^2	R^3	R^4	R^5	R^6	R^7
1	MeO	OH	MeO	OH	MeO	H	H
2	MeO	OH	MeO	H	MeO	H	H
3	OH	OH	OH	OH	OH	H	H
5	H	OH	OH	OH	OH	H	H
8	H	OH	OH	H	OH	H	H
13	OH	OH	MeO	H	OH	H	H
14	H	H	OH	H	OH	H	H
17	OH	OH	OH	MeO	OH	H	H
18	OH	OH	OH	H	H	H	H
19	Rha(1→6)Glc–O	OH	OH	OH	OH	H	H
20	H	OH	OH	OH	H	OH	H
21	MeO	OH	MeO	OH	MeO	H	Glc–O

	X	R^1	R^2
4	O	OH	OH
6	O	OH	H
10	H_2	OH	OH
12	O	H	H

Fig. 8 Chemical structures of isolated compounds 1-22 from the stems of *Entada phaseoloides.*

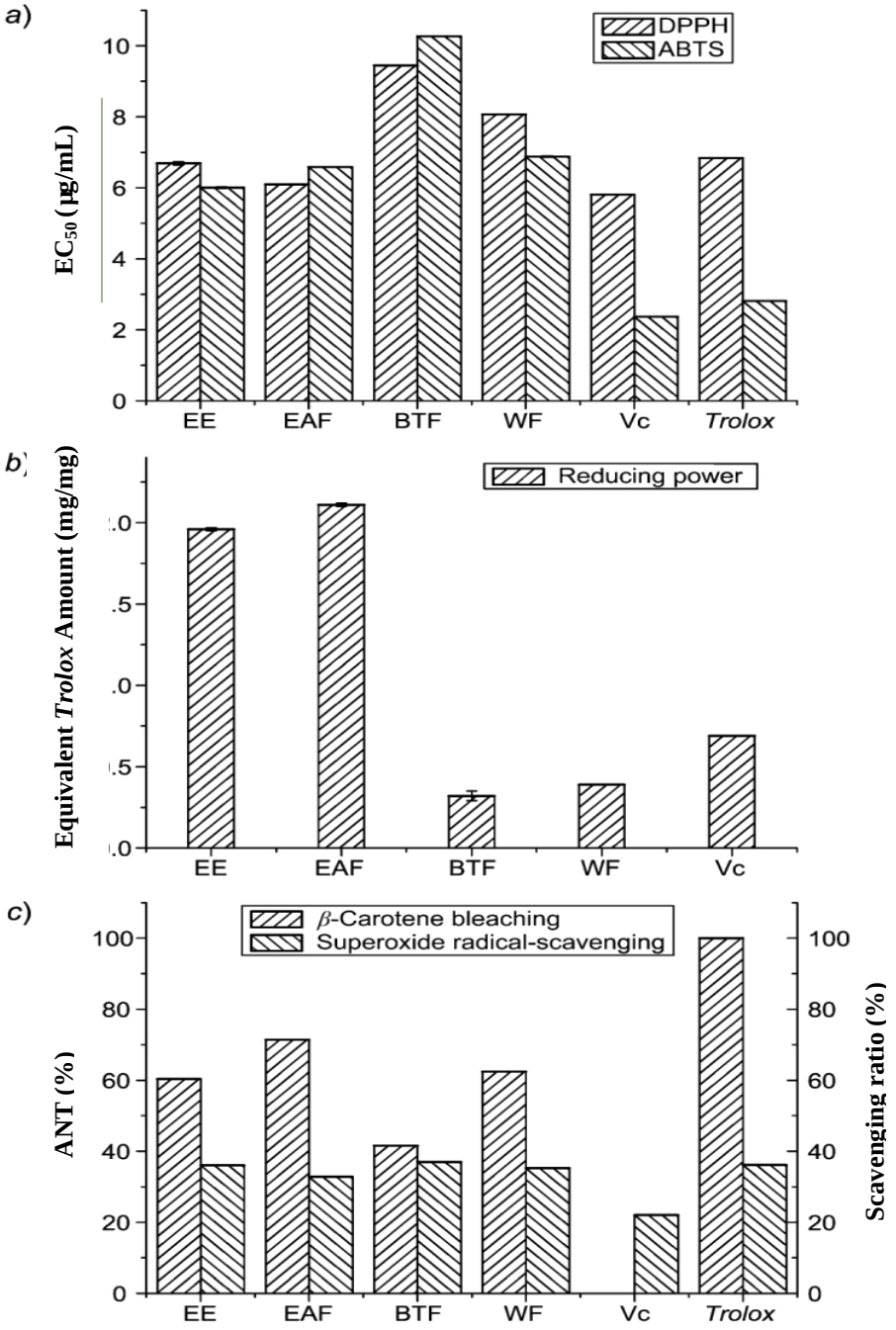

Fig. 9 The antioxidant activity of EtOH extract and three fractions from the stems of *Entada phaseoloides*. (a) DPPH and ABTS radical-scavenging assays; (b) Reducing power; (c) β-carotene-linoleate and superoxide radical-scavenging assays.

with 70% ethanol at room temperature. Isolation and purification were performed by silica gel, reversed-phase silica gel column chromatography and semi-preparative HPLC. Structures of the pure compounds were established on the basis of spectral analysis [46]. A novel method established and the results were compared for HPLC fingerprint determination of crude and processed products of *E. phaseoloides (L.) Merrill.* HPLC-ESI-MS was introduced to analyze the common peaks in each batch of crude *E. phaseoloides (L.) Merrill.* Sixteen characteristic peaks were found in crude *E.*

phaseoloides samples and twenty-one common peaks existed in processed *E.phaseoloides* samples. Nine characteristic peaks of which were identified by comparison of the retention time and their molecular weights of chemical standards, most of which were identified belong to triterpenoid saponins and glucosides. After processing, the chemical composition of the extraction with solution of 60% methanol from crude *E. phaseoloides* are found to be less or more similar to that of processed *E. phaseoloides*, and the changes in the main peaks of fingerprint chromatography suggest that HPLC can be used to reflect the difference of chemical composition of *E. phaseoloides* and their processed products. As per their report, it would be an efficient way for qualitative control of *E. phaseoloides* [67].

9.11 Nutrients

The physical characteristics of pods and seeds, proximate composition, different protein fractionation, SDS-PAGE analysis of proteins, amino acid composition, starch content, fatty acid profiles and various anti metabolic substances of *Entada phaseoloides* Merrill were also studied. The pod length and the number of seeds per pod ranged from 55 cm to 90 cm and from 5 to 11 respectively. The kernel was found to be comprised of 66.1% of the seed weight (18.41 ± 1.14 g). The seed kernels contained 256.7 g kg^{-1} crude protein, 108.1 g kg^{-1} lipid, 27.3 g kg^{-1} ash and a high content of carbohydrate (585.7 g kg^{-1}). The levels of potassium, phosphorus, zinc and iron were similar to those in conventional pulses. Among the different protein fractions of seed kernels, albumins constituted the major storage proteins (69.7%). The kernel proteins were rich in essential amino acids, particularly sulphur-containing amino acids, and their values appeared to be higher than the FAO/WHO (1990) reference protein for a 2-5-year-old growing child and soybean, and comparable to hen egg. Seed kernel lipids contained high levels of unsaturated fatty acids, oleic and linoleic acids, which accounted for 83% of the total fatty acid recovered. The kernel exhibited high trypsin and chymotrypsin inhibitor activities (96.65 mg TI g^{-1} and 30.02 CIU mg^{-1} sample respectively) in addition to containing phenolics, phytic acid, lectins and oligosaccharides. Another major toxic constituent was identified as a group of triterpenoid saponins (3.21%), which had high HeU (haemolytic activity) against cattle erythrocytes and caused high mortality in fish. The *in vitro* digestibility of the kernel protein was low (67%) [40].

10. Pharmacological Activity

10.1 Anti-inflammatory and Analgesic Activities

On the basis of various previous study models, saponins obtained from *Entada phaseoloides*, was reported to have significant anti-inflammatory activity and specifically the saponin from seed kernels of *Entada phaseoloides*, was reported to have significant activity against Walker 256 carcinosarcoma in rats [33].

Anti-inflammatory activity of saponin was explained in the study of methanolic extract of *Entada phaseoloides* seeds in animal models of inflammation where the LD_{50} was found to be more than 5,000 mg/kg in acute oral toxicity testing. Pre-treatment with the extract (400 mg/kg) reduced carrageenan induced rat paw edema at 3rd hour compared to control group of rats. Dose dependent (100, 200 and 400 mg/kg) reduction in inhibition of granuloma formation of cotton pellet granuloma, exudate volume, and total leukocyte count was observed with the extract. The extract inhibited acetic acid induced writhing dose dependently (40, 80 and 120 mg/kg) but was found inactive in reducing the pain produced by thermal injury. C-reactive proteins were absent in extract treated group. The results indicated that extract possesses weaker acute but strong sub-acute anti-inflammatory activity and strong peripheral analgesic activity. The results also suggested that the extract may act on the "proliferative phases of inflammation" [68].

In another study of anti-inflammatory effect of topical application of different formulations of seed pulp of EP (*Entada phaseoloides*), localized inflammatory reaction were developed in all the rats in 24 h. In control group, there was no resolution of swelling even in 21 days. Both EP formulations showed significant ($P < 0.001$) anti-inflammatory activity as compared to that of control. *Entada phaseoloides* ointment was equi-effective to that of diclofenac sodium on 12th day. Its paste was significantly ($P < 0.05$) found to be more effective than diclofenac sodium on 21st day. Both the formulations of *Entada phaseoloides* were found to have anti-inflammatory activity, but the paste was significantly more effective than Diclofenac sodium [69].

10.2 Anti Arthritic Activity

The effect of two formulations of *Entada phaseoloides* seeds after topical application in "monoiodoacetate-induced osteoarthritis" in rats was studied since arthritis is a very common clinical condition affecting both sexes and all ages. Most common forms of arthritis are osteoarthritis and rheumatoid arthritis. In all types of arthritis pain, inflammation and functional restriction are the presenting manifestation. Anti-inflammatory drugs like NSAIDs, corticosteroids and disease-modifying antirheumatic drugs, etc. are used for symptomatic relief, but many times they are associated with adverse effects that can often be as difficult to manage as the disease itself. Therefore, a need exists for new ways to treat these patients. The effect of topical application of two formulations of EP (*Entada phaseoloides*) seeds was studied in the MIA (monoiodoacetate-induced osteoarthritis) model in rats. Both the paste and ointment formulations of EP were tested on 32 Wistar rats weighing 150-200 g, divided into four groups as (I) vehicle, (II) EP paste, (III) EP ointment and (IV) diclofenac ointment. Osteoarthritis was induced by intra articular injection of 50 μL of MIA solution. Drug treatment was given topically according to groups for 14 days. Animals were observed for joint inflammation and gait. Joint histopathology was studied and scored. Swelling and redness of left knee was seen in all rats within 24 h which subsided gradually. Lame to gait and thickening of the joint capsule was seen only in control rats. Histopathologically, osteoarthritic changes were significantly less in drug-treated groups compared to control. As a result, both the formulations of EP were found be effective in preventing the damage to the joint [70].

10.3 Antidiabetic and Hypolipidemic Activities

On the basis of previous study, the TSEP (Total Saponin from *Entada phaseoloides*) was reported to dramatically reduce the fasting blood glucose and serum insulin levels and alleviated hyperglycemia associated oxidative stress in T2DM (type 2 Diabetes mellitus) rats. Moreover, a significantly hypolipidemic effect and an improvement in tissue steatosis were observed after TSEP administration. Further investigations revealed a possible anti-inflammation effect of TSEP by examining serum levels of IL-6 (interleukin-6), TNF-α (tumor necrosis factor-alpha) and CRP (C-reactive protein). The effects of TSEP exhibited a dose-dependent manner and were comparable to metformin. Both hypoglycemic and hypolipidemic activities of TSEP in T2DM rats supported its anti-diabetic property. TSEP exerted its therapeutic effect through repressing chronic inflammation responses [71].

In another experimental model, the anti-diabetic effects of AcOEt (Ethyl acetate), Pet ether (Petroleum-ether) and Chloroform fractions were investigated from the methanolic extract of seeds of *Entada phaseoloides* in AIDM (alloxan induced diabetic mice). The effect of these fractions (200 mg/kg body weight i.p) was observed on FBG (fasting blood glucose) level and active fraction was further investigated for its dose dependent activity (250 mg/kg

and 350 mg/kg body weight) on fasting blood glucose level and also on TC (total cholesterol), TG (triglyceride), SGOT (serum glutamate oxaloacetate transaminases) and SGPT (serum glutamate pyruvate transaminases) level in AIDM which showed significant effects. The most significant reduction of FBG level of around 72.02% was observed for Et-Ac fraction in AIDM. A significant reduction ($*p < 0.05$) in serum TC and TG level of 53.00% and 57.25% respectively was also found for Et-Ac fraction of *E. Phaseoloides*. The hypoglycemic and hypolipidemic activities were comparable to metformin HCl (150 mg/kg). In diabetic mice, SGOT and SGPT levels were significantly elevated that were further reduced after intraperitoneal administration of this fraction. These results indicated AcOEt fraction of *E. Phaseoloides* have favourable effects in bringing down the severity of diabetes together with hepatoprotectivity [72].

In another study, to observe the effect of TSEP (total saponins from *Entada phaseoloides*) on islet morphology and skeletal muscle PI3K pathway-related protein expression of type 2 diabetic rats, the type 2 diabetic rats were induced by high-fat diet and low-dose streptozotocin and then randomly divided into 5 groups, i.e., the normal control, the model group, the positive control drug (200 mg kg^{-1} metformin), the low-dose TSEP (25 mg kg^{-1}) group and the high-dose TSEP (50 mg kg^{-1}. Three weeks later, the islet morphology of rat pancreas were observed by HE (Hematoxylin and Eosin) staining, and protein expressions of IRS-1 (insulin receptor substrate-1), PI3K (phosphatidyl inositol 3-kinase), PTP-1 B (protein tyrosine phosphatase-1B) and GLUT4 (glucose transporter 4) in rat skeletal muscle were detected by Western blot. When compared with the model group, TSEP administered groups showed relatively normal structures, clear pancreatic cells and intact capsula structures in pancreatic tissue pathological sections, with the number of pancreatic islets close to the normal control group. Meanwhile, above TSEP administered groups showed increased IRS-1, PI3K and GLUT4 protein expressions in their skeletal muscle tissues and decreased PTP-1B protein expression compared with the model group. TSEP has an effect on protecting pancreatic tissues of type 2 diabetic rats and intervening in abnormal expression of proteins in skeletal muscle tissues [73].

10.4 Anti-Toxicity Activities

Entada africana, a widely used African medicinal plant of the same genus *Entada*, has been reported for various medicinal properties. When the acute toxicity of the methanolic stem bark and leaf extracts of *Entada africana* Guill. and Perr., (Mimosaceae) was assessed on mice, it revealed an average toxicity with a LD_{50} of 146.7 mg kg^{-1} and 249.9 mg kg^{-1} body weight for stem barks and leaves, respectively. The extracts showed no cytotoxicity against Human epidermoid carcinoma (KB) and African green monkey (Vero) cells. Sub-chronic toxicity was assessed in rabbits, which received orally, daily for a month, a dose corresponding to 10% of the LD_{50}. Compared to the control group, this dose caused no significant ($p > 0.05$) modification of haematological and biochemical parameters, total cholesterol, urea, creatinine and AST (aspartate amino-transferase). The extracts lowered serum glucose significantly ($p < 0.05$) by 52% at first two weeks of treatment. The stem bark and leaf extracts showed temporary decrease ($p < 0.05$) of ALT (alanine amino transferase) by 26.1 % and 39.1%, respectively. The stem bark extracts increased triglycerides significantly ($p < 0.01$) by 108% at the end of last week of treatment. These investigations seemed to indicate the safety of sub-chronic oral administration (up to 14.67 mg kg^{-1} and 24.9 mg kg^{-1} body weight) of the methanolic extracts of *Entada africana* in rabbits [74].

The impact of the crude and processed products of *Entada phaseoloides* on gastrointestinal movement in mice was studied with the methods of charcoal propulsion of small intestine and methyl orange colorimetry of gastric emptying to observe

acute-toxicity. The oral LD_{50} of crude *Entada phaseoloides,* and two processed products of *Entada phaseoloides* in mice were 27.17 g/kg, 35.13 g/kg and 42.18 g/kg body weight respectively. Crude and processed products of *Entada phaseoloides* can significantly promote the enteric propulsion of normal mice, and can significantly counteract the depressing status induced by atropine, but have no influence on the overactive status induced by neostigmine. The high, middle and low-dose of groups showed significant inhibition of the gastric emptying in normal mice. Processed *Entada phaseoloides* showed effects on the enteric propulsion of normal and depressing mice, can restrain the gastric emptying under normal mice, but its safety was better than crude *Entada phaseoloides* [75].

10.5 Antiulcer Activities

The ethanol extract of the seeds of *Entada phaseoloides* was assessed for its antiulcer activity against aspirin plus pylorus ligation induced gastric ulcers in rats, HCl- ethanol induced ulcer in mice and water immersion stress-induced ulcers in rats. A significant ($P < 0.001$) antiulcer activity was observed in all the models. The parameters taken to assess antiulcer activity were volume of gastric secretion, free acidity, total acidity and ulcer index. Preliminary phytochemical screening of the *Entada Phaseoloides* gave positive test for steroids, saponins and alkaloids. The results indicate that *Entada phaseoloides* possessed antiulcer activity [2].

10.6 Anticomplement and Antimicrobial Activities

Seventeen flavonoids isolated from the extracts of the stem of *Entada phaseoloides*, which were investigated for their anticomplement (both classic and alternative pathways) and antimicrobial activities against Gram-positive bacteria MSSA (Methicillin sensitive *Staphylococcus aureus*), MRSA (Methicillin resistant *Staphylococcus aureus*), Standard Enterococcus and *Bacillus subtilis*], Gram-negative bacteria (*Escherichia coli, Pseudomonas aeuroginosa*) and the yeast-like pathogenic fungus *Candida albicans*. The anti-complement studies revealed a dose-dependent activity among isolated quercetin, luteolin, apigenin, galangin, 5,2',5'-trihydroxy-3,7,4'-trimethoxyflavone-2'-O-β-D-glucoside(+)-3,3',5',5,7-pentahydroflavanone, (+)-dihydrokaempferol, (-)-epicatechin, (+)-catechin, naringenin, and 5,7,3',5'-tetrahydroxyflavanone, and the antimicrobial results indicated that quercetin, 5,7,4'-trihydroxy-3'-methoxyflavonol and galangin produced the inhibitory activities against MRSA, MSSA, and Standard Enterococcus, while luteolin and rhamnocitrin displayed inhibition against only MRSA and MSSA [76].

10.7 Antioxidant and Cytotoxic Activities

The methanolic crude extract of the bark and seed of *Entada phaseoloides* (L.) Merrill and its different organic soluble partitionates were screened for antioxidant, cytotoxic, membrane stabilizing and antimicrobial activities. The crude extract, carbon tetrachloride and aqueous soluble fractions of both bark and seed showed higher level of total phenolic content (TPC, 245.59, 240.22, 240.03 and 117.0 mg of Gallic acid equivalent (GAE)/gm of dried extract). In the DPPH (1,1-diphenyl-2-picrylhydrazyl) assay, the crude extract of bark and its chloroform and aqueous soluble fractions demonstrated strong antioxidant property with the IC_{50} of 3.24, 1.55 and 3.6 µg/mL, respectively, whereas, all the fractions of seed extract revealed mild antioxidant activity. The petroleum ether soluble fraction of both seed and bark exhibited significant cytotoxicity (LC_{50} = 1.54 mg/mL and 5.4 mg/mL) which confers the presence of bioactive metabolites in this plant. On the other hand, the crude extract of seed and petroleum ether soluble fraction of bark inhibited the hemolysis of RBC of rat's blood by 78.89% and 57.43%, respectively, as compared to 84.44% exerted by acetyl salicylic acid (0.10 mg/mL). In antimicrobial screening, the carbon tetrachloride soluble fraction of bark showed significant

antimicrobial activity against *Staphylococcus aureus* (zone of inhibition = 17.0 mm) with MIC (minimum inhibitory concentration) and MBC (minimum bactericidal concentration) values of 7.81 mg/mL and 125 mg/mL, respectively [77].

Apart from the above, the bark of *Entada phaseoloides* exhibits potent molluscidal activity against *Oncomelenia quadrasi*, the snail intermediate host of *Schistosoma japonicum* with LC_{50} of 3.6-5.8 ppm since *Entada phaseoloides* remained stable over a wide range of pH values, in the presence of minerals and yeast cells and after ultraviolet irradiation of solutions. Under field conditions, the Gogo bark at a dose rate of $\geq$ 40 g/m^2 was sufficient to produce a satisfactory molluscicidal effect [41] or commercial gogo bark at a dose rate of 2 g/L of water with *Oncomelenia quadrasi* can kill 100% of snail within 24 h. Thus the molluscidal effect of *Entada phaseoloides* is very much effective in controlling Schistosomiasis, a snail transmitting debilitating and fatal endemic disease which is of major public health concern [78].

11. Current Finding and Future Prospects

Natural products are promising candidates for drug discovery and they still continue to play an important role in future small organic compound drug development programs [79]. Reports on pharmacological effects of medicinal plants are growing almost exponentially. However, it was found to be very difficult to attribute the pharmacological activity in a multi-component mixture to only a single compound of an extract, as plant extracts consist of a diversity of secondary metabolites [80]. From the above review of literature, it is evident that *Entada phaseoloides* has been one of the most thoroughly studied interesting plants as reported during the last 2 decades. The body of knowledge about plants, herbs and spices, and their respective and collective roles in promoting health is modest [81, 82]. Though modern synthetic drugs are very effective in curing diseases but also cause a number of side effects; although crude drugs are less efficient in curing diseases but are relatively free from side effects [83]. Herbs have been used as food and for medicinal purpose for centuries [82]. In recent times, the use of herbal products has increased enormously in the western world as well as in developed countries [84]. But the traditional herbal medicine has simple solution which is both easier and economical. Nature keeps ready in her vast green reservoir some of those herbal remedies which can cure all human ailments and diseases that take place on this earth. The need is only to locate those miraculous herbs through trained eyes which could alleviate the pains and sufferings of mankind.

12. Prospects

Since the use of medicinal plants is a widely accepted therapeutic strategy for millions of people, further attention should be focused on the discovery of the exact modes of action of their extracts as well as the isolated pure compounds and potential combinations, so as to exploit them commercially. However, because of the diverse molecular pharmacological data, the spectrum of interpretation and speculations seem to be endless. Therefore, in future studies there is a need for thorough phytochemical, clinical and possible studies on molecular mechanism of action along with preclinical trials that are required for an integration and acceptance of many *Entada phaseoloides* extracts in conventional medicine. At the same time efforts should be made to standardise the plant extracts and formulate best alternative herbal preparations to replace or complement the synthetic drugs which are currently in use.

13. Conclusions

Entada phaseoloides offers a wide range of ethnobotanical utilizations, which are based on the diverse patterns of secondary metabolites of which most abundant are saponins, diterpenes, triterpenes and

phenolics compounds. Phenolic compounds, saponins, diterpenes as well as triterpenes were reported to contribute the pharmacological properties of *Entada phaseoloides* such as anti-inflammatory, antidiabetic, antitumour and analgesic activity (saponin); anticomplement, antimicrobial and antioxidants (phenolics); as antiulcer, anti toxic in addition to molluscicidal activities (crude and processed product of *Entada phaseoloides).*

References

[1] B.E. VanWyk, M. Wink, Medicinal Plants of the World: An Illustrated Scientific Guide to Important Medicinal Plants and Their Uses, OR: Timber Press, Portland, 2004.

[2] D. Ramakrishna, K. Pawan kumar, K. Mukkanti, K. Abdulla Khan, Antiulcer activity of the seeds of *Entada Phaseoloides*, Pharmacologyonline 3 (2008) 93-99.

[3] K. M. Madkarri's, A.K. Nadkarni, Indian Material Medica, Vol. 2, Popular Prakashan II, 1976, PP. 394-395.

[4] A. Sparreboom, M.C. Cox, M. R. Acharya, W. D. Figg, Herbal remedies in the United States: potential adverse interactions with anticancer agents, Journal of Clinical Oncology 22 (2004) 2489-2503.

[5] K.J. Gohil, J.A. Patel, A review on *Bacopa monniera*: Current research and future prospects, International Journal of Green Pharmacy 4 (2010) 1-9.

[6] R. A. Singha, Herbal remedies of street vendors for some urino-genital diseases, Ancient Science Life 1 (1992) 187-192.

[7] "Entada Adans", Germplasm Resources Information Network, United States: Department of Agriculture, 2007.

[8] E. D. Merrill, *Entada phaseoloides* (L.)Merr. Philippine Journal Science Section C Botany 9 (1914) 86.

[9] Benth, *Entada scandens* (L.) Benth. Hooker's Journal of Botany 4 (1841) 332.

[10] O. Stickman, Lens phaseoloides L. Herb. Amoin 18 (1754), National tropical botanical garden, http://ntbg.org/plants/plant_details.php?plantid=4612,2011

[11] *Entada phaseoloides*, Australian Tropical Rainforest Plant.

[12] K.M. Madkarri's, A.K. Nadkarni, Indian Material Medica, Vol. 1, 1976, PP. 485-486.

[13] Australian new crops wensite: http://newcrops.com.au/index.php?option=com_content&view=article&id=22&Itemid=54

[14] T. Acamovic, C.S. Stewart, T. W. Pennycott, Poisonous Plants and Related Toxins, CABI, 2004, pp. 377-386.

[15] A. Agarwal, A carbonized fossil seed, viz.*Entada palaeoscandens* (Awasthi & Prasad) Antal & Awasthi, from lignite deposits of Kalviwadi, Sindhudurg district, Maharashtra, India, Phytomorphology 53 (2003) 133-139.

[16] N. Bluthgen, K. Fiedler, Interactions between weaver ants *Oecophylla smaragdina*, homopterans, trees and lianas in an Australian rain forest canopy, Journal of Animal Ecology 71 (2002) 793-801.

[17] J.V.S. Rao, K.S.V. Priya, *In vitro* response of embryo axis of *Entada phaseoloides* Merrill, Phytomorphology 52 (2002) 97-102.

[18] Y. Zheng, K. Ben, S. Jin, Anti-human immunodeficiency virus activity of proteins from 17 species of plants, Virologica Sinica 13 (1998) 312-321.

[19] G. Grant, L.J. More, N.H. McKenzie, P.M. Dorward, W.C. Buchan, L. Telek, et al., Nutritional and haemagglutination properties of several tropical seeds, Journal of Agricultural Science 124 (1995) 437-445.

[20] E. Bergstrom, O. Hernal, L.A. Person, Dietary changes in Swedish adolescents, Acta Paediatrica 82 (1993) 472-480.

[21] V.R. Mohan, K. Janardhanan, Chemical and nutritional evaluation of raw seeds of the tribal pulses *Parkia roxburghii* G. Don. and *Entada phaseoloides* (L.) Merr, International Journal of Food Science and Technology 44 (1993) 47-53.

[22] Y. Okada, S. Shibata, O. Kamo, T. Okuyama, Carbon-13 NMR spectral studies of entagenic acid to establish its structure, Chemical and Pharmaceutical Bulletin 36 (1988) 5028-5030.

[23] Y. Okada, S. Shibata, A.M.J. Javellana, O. Kamo, *Entada* Saponins Es II and IV from the bark of *Entada phaseoloides*, Chemical and Pharmaceutical Bulletin 36 (1988) 1264-1269.

[24] Y. Okada, S. Shibata, T. Ikekawa, A.M.J. Javellana, O. Kamo, Entada Saponin III a saponin isolated from the bark of *Entada-phaseoloides*, Phytochemistry 26 (1987) 2789-2796.

[25] F.C. Ho, Notes on the Genus *Entada* of Taiwan, Journal of Taiwan Museum 38 (1985) 75-80.

[26] C.Y. Lim-Sylianco and W.T. Shier, Mutagenic and antimutagenic activities in Philippine medicinal and food plants, Journal of Toxicology Toxin Reviews 4 (1985) 71-105.

[27] G. Panigrahi, Proposal to amend the type citation of *Entada* conserved name and of Gigalobium rejected name *Fabaceae*. Taxon 34 (1985) 714-715.

[28] K. Yasuraok, A.T.J. Santos, M.J. Santos, K. Takamura, Y. Hosaka, Laboratory trials of 2 new molluscicides, the bark of "Gogo" (*Entada-Phaseoloides*) and Polynactin, against *Oncomelania* snails: a preliminary report, Southeast Asian Journal of Tropical Medicine and Public Health 7 (1976) 346-347.

[29] A.K. Barua, A. Basak, Chemical examination of the seeds

of *Entada-Phaseoloides*, Journal of Indian Chemical Society 49 (1972) 1199

[30] A.K. Barua, Triterpenoids: XXV. The constitution of entagenic acid: A new triterpenoid sapogenin from *Entada phaseoloides* Merrill, Tetrahedron 23 (1967) 1499-1503.

[31] A.K. Barua, P. Chakraborty, B.C. Das, Triterpenoids: XXVI. The constitution of entagenic acid, Tetrahedron 23 (1967) 1505-1508.

[32] J.P.M. Brenan, Notes on Mimosoideae: I, Kew Bulletin 1(1955) 161-192.

[33] W.C. Liu, M, kugelman, R.A. Wilson, K.V. Roa, A crystalline saponin with antitumor activity from *Entada phaseoloides*, The John L. Smith Memorial for Cancer Research 11 (1972) 171–173.

[34] A.K. Barua, M. Chakraborty, P.K. Dutta, S. Ray, Phaseoloidin, a homogentisic acid glucoside from *Entada phaseoloides*, Phytochemistry 27 (1988) 3259–3261.

[35] F. Ikegami, S. Ohmiya, N. Ruangrungsi, S.I. Sakai, I. Murakoshi, Entadamide A, a new sulphur-containing amide from *Entada phaseoloides* seeds, Chemical and Pharmaceutical Bulletin 33 (1985) 5153−5154.

[36] F. Ikegami, S. Ohmiya, N. Ruangrungsi, S.I. Sakai, I. Murakoshi, Entadamide B, a second new sulphur-containing amide from *Entada phaseoloides*, Phytochemistry 26 (1987) 1525−1526.

[37] F. Ikegami, T. Sekine, M. Aburada, Y. Fujii, Y. Komatsu, I. Murakoshi, Synthesis of entadamide A and entadamide B isolated from *Entada phaseoloides* and their inhibitory effects on 5-lipoxygenase, Chemical and Pharmaceutical Bulletin 37 (1989) 1932-1933.

[38] F. Ikegami T. Sekine, S. Duangteraprecha, N. Matsushita, N. Matsuda, N. Ruangrungsi, I. Murakoshi, Entadamide C, a sulphur-containing amide from *Entada phaseoloides*, Phytochemistry 28 (1989) 881−882.

[39] J.R. Dai, L.B.S. Kardono, S. Tsauri, K. Padmawinata, J.M. Pezzuto, A.D. Kinghorn, Phenylacetic acid derivatives and a thioamide glycoside from *Entada phaseoloides*, Phytochemistry 30 (1991) 3749−3752.

[40] P. Siddhuraju, K. Becker, H.P.S. Makkar, Chemical composition, protein fractionation, essential amino acid potential and antimetabolic constituents of an unconventional legume, Gila bean (*Entada phaseoloides* Merrill) seed kernel, Journal of the Science of Food and Agriculture 82 (2002) 192–202.

[41] K. Yasuraoka, Y. Irie, K. Takamura, H. Shimomura, J. Hashiguchi, M.J. Santos, et al., Laboratory and field assessment of the molluscicidal activity of gogo (Entada phaseoloides) against the amphibious snail intermediate host of Schistosoma japonicum, Journal of Experimental Medicine 47 (1977) 483-487.

[42] A. Kumar, *Entada phaseoloides* (Linn.) Merrill. syn. E. scandens: A glycoside of entagenic acid possesses anti-neoplastic activity, Science 2.0 Join the revolution 2009.

[43] Gogo, *Entada phaseoloides*, St Thomas Bean, Philippine Medicinal Plants.

[44] I.F.B. Common, D.F. Waterhouse, Butterflies of Australia, Angus and Robertson Publishers 2 (1981) 682.

[45] R.C. Cambie, A.A. Brewis, Anti-fertility Plants of the Pacific, CSIRO Pub., 1997, P. 115.

[46] K. Hostettmann, A. Marston, Saponins, Cambridge: Cambridge University Press, 1995.

[47] R. Hardman, E.A. Sofowora, Isolation and characterization of yamogenin from *Balanites aegyptiaca*, Phytochemistry 9 (1970) 645–649.

[48] Royal Society of Chemistry, available at internet site: www. Chem Spider. Com, 2013 (Accessed 4 November 2013).

[49] Chemical Book, 2008. Chem Spider ID: 24606073, 2013.

[50] U.S. National Library of Medicine. National Institutes of Health. Department of Health & Human Services. 8600 Rockville Pike, Bethesda, MD 20894, 2013.

[51] Available at internet site: www.ichemistry.cn 2009-2013.

[52] H. Xiong, E. Xiao, Y.H. Zhao, G.Z. Yang, Z.N. Mei, Sulfur-containing amides from *Entada phaseoloides*, Acta Pharmaceutica sinnnica 45 (2010) 624-626.

[53] Z.X. Zhao, J. Jin, C.Z. Lin, C.C. Zhu, Y.M. Liu, A.H. Lin, et al., Two new chalcone glycosides from the stems of *Entada phaseoloides*, Fitoterapia 82 (2011) 1102-1105.

[54] O. Singh, M. Ali, N. Ahktar, Phenolic acid glucosides from the seeds of *Entada phaseoloides* Merill, Journal of Asian Natural Products Research 13 (2011) 682-687.

[55] Y. Iwamoto, S. Sugimoto, L. Harinantenaina, K. Matsunami, H. Otsuka, Entadosides A–D, triterpene saponins and a glucoside of the sulphur-containing amide from the kernel nuts of *Entada phaseoloides* (L.) Merrill, Journal of Natural Medicine 66 (2012) 321-328.

[56] H.J. Li, D.L. Zhou, T.J. Xu, C.K. Lam, W.L. Lan, 5,6,7,5'-Tetramethoxy-3',4'methylenedioxyflavone monohydrate, Acta Crystallographica 68 (2012) 1390.

[57] K. Sutthanut, B. Sripanidkulchai, C. Yenjai, M. Jay, Simultaneous identification and quantitation of 11 flavonoid constituents in Kaempferia parvifloraby gas chromatography, Journal of Chromatography A 1143 (2007) 227–233.

[58] L.S. Ding, Q.L. Liang, Y.F. Teng, Study on flavonoids in seeds of Hovenia dulcis, Acta Pharmaceutica Sinica 32 (1997) 600-602.

[59] S. Sang, S. Tian, H. Wang, R.E. Stark, R.T. Rosen, C.S. Yang, et al., Chemical studies of the antioxidant mechanism of tea catechins: Radical reaction products of epicatechin with peroxyl radicals, Bioorganic Medical chemistry 11 (2003) 3371-3378.

[60] L.Y. Foo, Y. Lu, W.C. McNabb, G. Waghorn, M.J. Ulyatt, Proanthocyanidins from Lotus pedunculatus,

Phytochemistry 45 (1997) 1689.

[61] Y.P. Chen, L. Liu, Y.H. Zhou, J. Wen, Y. Jiang, P.F. Tu, Chemical constituents from *Sappan lignum*, Journal of Chinese Pharmaceutical Sciences 17 (2008) 82–86.

[62] W. Herath, J.R. Mikell, A.L. Hale, D. Ferreira, I.A. Khan, Microbial metabolism. Matabolites of 3- and 7-hydroxyflavones, Chemical and Pharmaceutical Bulletin 54 (2006) 320.

[63] E. Lee, B.H. Moon, Y. Park, S. Hong, S. Lee, Y. Lee, Y. Lim, Effects of hydroxy and methoxy substituents on NMR Data in flavonols, Bulletin Korean Chemical Society 29 (2008) 507-510.

[64] F. Nessa, Z. Ismail, N. Mohamed, M.R.H.M. Haris, Free radical-scavenging activity of organic extracts and of pure flavonoids of *Blumea balsamifera* DC leaves, Food Chemistry 88 (2004) 243-252.

[65] F.W. Collins, V. Deluca, R.K. Ibrahim, B. Voirin, M. Jay, Polymethylated flavonols of *Chrysosplenium americanum*. I. Identification and enzymatic synthesis, Zeitschrift fur. Naturforschung C 36 (1981) 730-736.

[66] D Y. Dong, H. Shi, H. Yang , Y. Peng, M. Wang, X. Li, Antioxidant phenolic compounds from the stems of *Entada phaseoloides*, Chemical Biodiversity 9 (2012) 68-79.

[67] E. Xiao, H. Xiong, X. Chen, Y. Zhao, Z. Mei, Study on HPLC fingerprint of crude and processed products of *Entada phaseoloides*, Zhongguo Zhong Yao Za Zhi 35 (2010) 3140-3143.

[68] R. Gupta, B.S. Rathi, P.A. Thakurdesai, S.L. Bodhankar, Anti-inflammatory and analgesic effects of methanolic extract of *Entada phaseoloides* seeds, Journal of Cell Tissue Research 6 (2006) 609-613.

[69] J.S. Dawane, V.A. Pandit, B.D. Rajopadhye, Experimental evaluation of anti-inflammatory effect of topical application of *Entada phaseoloides* seeds as paste and ointment, North American Journal of Medical Sciences 3 (2011) 513-517.

[70] J.S. Dawane, V.A. Pandit, B.D. Rajopadhye, M. Karandikar, The effect of two formulations of *Entada phaseoloides* seeds after topical application in 'monoiodoacetate-induced osteoarthritis' in rats, Journal of Experimental and Integrative Medicine 3 (2013) 37-41.

[71] T. Zheng, G. Shu, Z. Yang, S. Mo, Y. Zhao, Z. Mei, Antidiabetic effect of total saponins from *Entada phaseoloides* (L.)Merr. in type 2 diabetic rats, Journal of Ethnopharmacology 39 (2012) 814-821.

[72] M. Ikram, Z.M. Babar, A.M.T. Islam, M.A.U. Chowdhury, M.E. Uddin, M.R. Islam, et al., Antidiabetic and hypolipidemic effects of the different fractions of methanolic extracts of *Entada phaseoloides* (L.) Merr. in alloxan induced diabetic mice, International Journal of Pharmaceutical Sciences and Research 2 (2011) 3160-3165.

[73] T. Zheng, G. Shu, Z. Yang, S. Mo, Y. Zhao, Z. Mei, Preliminary study on mechanisms of total saponins from *Entada phaseoloides* against diabetes, Zhongguo Zhong Yao Za Zhi 37 (2012) 615-619.

[74] A. Tibiri, J.T. Banzouzi, A. Traore, G.O. Nacoulma, I.P. Guissou, B. Mbatchi, Toxicological assessment of methanolic stem bark and leaf extracts of *Entada africana* Guill. and Perr., Mimosaceae, International Journal Pharmacology 3 (2007) 393-399.

[75] E. Xiao, H. Xiong, Y.H. Zhao, X.K. Deng, Z.N. Mei, Study on acute toxicity and animal gastrointestinal activity of crude and processed products of *Entada phaseoloides*, Zhong Yao Cai 33 (2010) 1704-1707.

[76] K. Li, S. Xing, M. Wang, Y. Peng, Y. Dong, X. Li, Anticomplement and antimicrobial activities of flavonoids from *Entada phaseoloides*, Natural Product Communications 7 (2012) 867-871.

[77] F. Aktar, M.R. Kuddus, O.S. Faruque, F. Rumi, M.A. Quadir, M.A. Rashi, Antioxidant, cytotoxic, membrane stabilizing and antimicrobial activities of bark and seed of *Entada phaseoloides* (L.) Merrill: A medicinal plant from Chittagong Hill Tracts, Journal of Pharmacy and Nutrition Sciences 1 (2011) 171-176.

[78] E.C. Garcia, B.D. Cabrera, A.V. Castilla, Studies on *Schistosoma japonica* and Saponins, Science Diliman 1 (1981) 47-79.

[79] D.J. Newman, G.M. Cragg, K.M. Snader, Natural products as sources of new drugs over the period 1981-2002, Journal of Natural Product 66 (2003) 1022-1037.

[80] M. Wink, Evolutionary advantage and molecular modes of action of multicomponent mixtures used in phytomedicine, Current Drug Metabolism 9 (2008) 996-1009.

[81] A.D. Ballatine, M.C. Albano, M.G. Nair, Role of medicinal plants, herbs and spices in protecting human health, Nutritional Review 57 (1999) 41-45.

[82] A.A. Adedapo, O.O. Shabi, O.A. Adedokun, Anthelmintic efficacy of the aqueous crude extract of *Euphorbia hirta* Linn in Nigerian dogs, Veterinary Arhiv 75 (2005)39-47.

[83] R.G. Mali, A.A. Mehta, A review on anthelminthic plants, Natural Product Radiance 7 (2008) 466-475.

[84] D. Sudharani, K.L. Krishna, K. Deval, A.K. Safia, Priya, Pharmacological profiles of *Bacopa monnieri*: A review, International Journal of Pharmacy 1 (2011) 15-23.

Journal of Pharmacy and Pharmacology 2 (2014) 19-25

Management of Coagulation's Disorders in Oral Surgery: State of Art

Mauro Labanca[1], Luigi F. Rodella[2] and Paolo Brunamonti Binello[3]

1. Department of Dentistry, "S. Raffaele" Hospital, University "Vita Salute", Milan 20100, Italy

2. Department of Biomedical Sciences and Biotechnology, University of Brescia, Brescia 25100, Italy

3. Department of Specialized Surgeries, "Galliera" Hospital, University of Genoa, Genoa 16128, Italy

Received: October 30, 2013 / Accepted: December 13, 2013 / Published: February 28, 2014.

Abstract: Understanding and managing the bleeding's causes is essential for a good surgical practice in general. In fact, it is crucial to know how to manage and control this problem (sometimes simply annoying, but that may be able to cause even dangerous consequences) with a comprehensive and multidisciplinary approach, trying to use all the means is available today. The goal of this paper is to describe, even through a brief review of the literature—the State of Art about the bleeding control in oral surgery, the proper use of surgical devices and the NOACs (new oral anticoagulants) appearance.

Key words: Oral surgery, bleeding control, haemostatics, guided bone regeneration, platelet concentrates, NOACs (new oral anticoagulants).

1. Introduction

The oral surgery is the branch of dentistry in which, by definition, bleeding complications along with the septic are among the most feared and frequent, often able to delay if not prevent the success of clinical rehabilitation [1, 2].

In certain clinical situations, in fact, even a banal tooth's avulsion, may induce bleeding difficult to manage and also potentially dangerous [3].

In more severe cases, this complication, in addition to significantly interfere with the healing's process—can lead to serious systemic consequences [3, 4]. In Ref. [4], however, it shows bleeding mainly contained with favorable prognosis and is considered extremely rare massive blood's depletion (more than 2 L), such as to cause hypovolemic shock.

The different bleeding's causes can be so distinct: traumatic, iatrogenic and systemic. Among the iatrogenic hemorrhage, as well as those induced by pharmacological treatments, we recognize the pre- and post-surgical bleeding, thus, resulting to surgery [1-3].

Regarding the bleeding caused by systemic, however, in Refs. [1, 2], frequent bleeding secondary to coagulation disorders, or secondary to systemic arterial hypertension without adequate compensation pharmacological compensation are reported.

We also recognize the following different bleeding types: venous, arterial, diffused and mixed. Depending on the type of evolution pathophysiological instead, we can speak of acute hemorrhage or chronic for dripping [3, 4].

2. Clinical Evaluations

Prevention, implemented through a complete medical history and physical examination, local and systemic, plays a decisive role, in order to confirm the availability of the patient to a surgical approach [2, 3].

Corresponding author: Paolo Brunamonti Binello, professor, research fields: dentistry, oral pathology and oral surgery. E-mail: paolo.brunamonti@galliera.it.

2.1 Screening Laboratory Coagulation

The screening laboratory coagulation, then, especially if combined with a correct diagnostic imaging, is an irreplaceable aid in determining the possibility of complications and, in particular, those of hemorrhagic type [5].

For example, in the presence of a status characterized by frankly altered parameters of blood count, INR (international normalized ratio), PT (thrombin's time) and PTT (prothrombin's time), platelet count (platelets under physiologically 200.000-500.00 per mm^3) should prefer the surgical treatment exclusively in a protected environment, such as the day surgery (though with no less than 90,000 platelets per mm^3), if not, indeed, in in-patient traditional (though with a platelet count below 60,000 per mm^3) [5].

Previously defined the patient availability to surgery, in order to limit the risk of bleeding intra- and post-operatory, is appropriate to adopt the techniques properly usable, in order to achieve an adequate hemostasis intra- and post-operatory [4].

2.2 Intra-surgical Hemostasis

Intra-surgical hemostasis, in particular, makes use of traditional methods (consolidated in literature) such as: binding direct or indirect vessels, indirect or direct compression of the vessels, electrocoagulation, sutures, surgical devices (local absorbable hemostatic agents).

In the context of direct or indirect arterial ligation, it is really important to remember that this choice is sometimes the unique and the irreplaceable in case of arterial bleeding of a pot of average size (for example, the oroantral or sub-mental artery) [5, 6].

It is therefore appropriate that not only the first operator, but also his team is adequately prepared to handle this case, using a klemer immediately available to block the bleeding, and then stabilized by an adequate suture [5, 6].

In this situation the second operator's role will be fundamental, which will have to be instructed in this circumstance, and must be able to handle the opening and closing of the hemostat in perfect synchrony with the suture's execution by the first operator [6-8].

2.3 Animal Hemostatics Classification

The hemostatic animal commonly used are collagen-based (with triple helical fibrillar structure, or depolymerized collagen) and the commercially most well-known are:

- Avitene (bovine);
- Congress (equine);
- Collatamp (equine);
- Antema (equine);
- Spongostan (pig);
- Gingistat (equine);
- Hemocollagene (bovine);
- Cutanplast (pig).

2.4 Vegetable Hemostatics Classification

The hemostatic of vegetable origin, instead, consist mainly of polysaccharides, or derived from cellulose [6-8].

Among these the best known are those made from oxidized cellulose and regenerated, that is, rayon (Tabotamp), used for over 50 years in general surgery and other specialized branches (neurosurgery, orthopaedics, ENT, urology, maxillofacial, etc.) [6-8].

Tabotamp, in its four different versions currently available (snow, standard, Nu-Kit and fibrillar), is obtained by a process of regeneration of the cellulose with nitrogen dioxide (ORC).

In oral surgery, the choice is definitely more appropriate for the standard type, the characteristics of which (including packaging) make it more suitable for the purpose to be achieved, as evidenced by the images related to the case report [6-8] (Figs. 1-5).

Rayon's haemostatic action is expressed through the mechanical facilitation of the process of platelet aggregation and vasoconstriction induced by lowering the pH local tissue [8]. Coming in contact with the

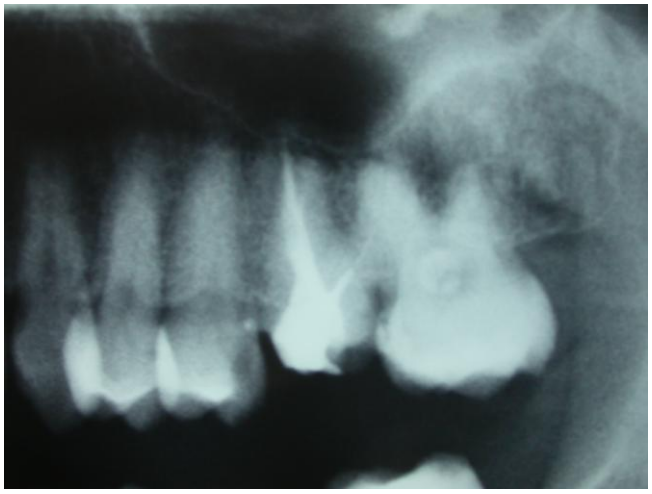

Fig. 1 Case report: Patient with coagulation's disorders and with 26 tooth irreparably compromised by mixed carious lesions and periodontal deep.

Fig. 2 On proceeds to 26 extractions and immediate fitting of a post-extractive implant, by swinging a palatine mucosal flap and putting a rayon membrane (tabotamp) in order to obtain a proper stabilization effect.

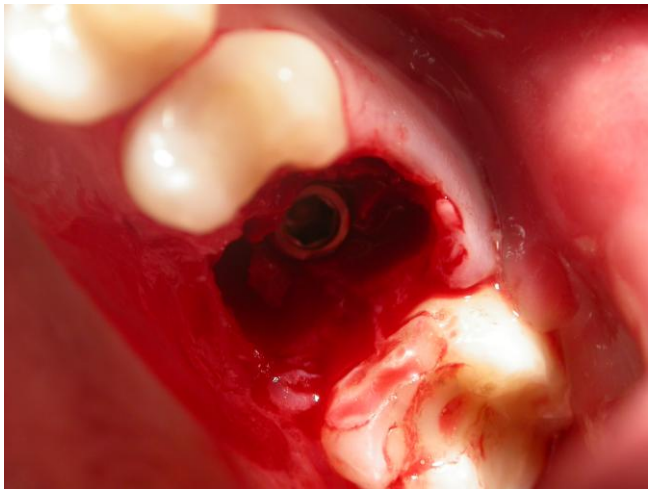

Fig. 3 Fixture's positioning in post-extractive alveolus.

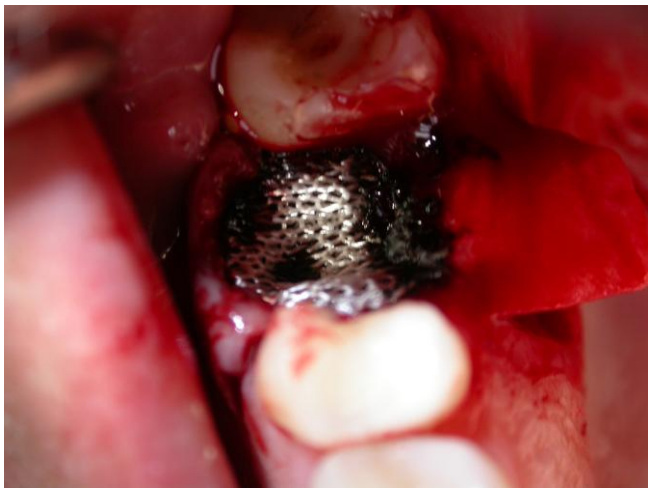

Fig. 4 Tipping of palatal flap and resorbable membrane's placement made of rayon (tabotamp).

Fig. 5 Local examination shows an excellent healing just two weeks after surgery, with a good satisfaction for the oral surgeon, but also for the patient.

blood, in fact, the cellulose fibers forming an adhesive matrix of dark red color (for hemoglobin oxidation), containing platelets and fibrinogen: during this process the platelets release certain substances (such as 5-hydroxytryptamine, thromboxane-A2 and cytokines) that promote hemostasis [6, 7].

In addition to the rapid formation of the fibrin plug, the contact between blood and oxidized cellulose produces acid , which determines a drastic lowering of local pH (< 4.4) and a consequent significant vasoconstriction [6, 7].

The acid pH, also, determines a strong bactericidal local action: numerous among the bacteria primarily responsible for the infection of the clot (*Klebsiella pneumoniae*, *Staphylococcus aureus*, etc.), in fact, become inactive or do not survive in an acidic environment (pH < 5. 0) [8].

In recent decades, moreover, to the production of traditional Tabotamp Standard have been joined three other innovative versions, in order to better satisfy the needs of the clinician in terms of speed maneuverability and versatility in addition to the already proven bactericidal properties [9, 10].

Rayon's use in its "Standard" formulation as a membrane, in order to stabilize the clot and a possible graft biomaterial, is being evaluated by a randomized and multicenter study group that involves the same authors. This could see in the near future, the application of rayon in a new context, in which they could combine the advantages described above Rayon

with those offered by a traditional membrane, even in the absence of selective permeability.

3. Discussion

In addition to the data from the literature [9, 10], showing that there are no significant differences in GBR (Guided Bone Regeneration) between the use of biomaterials animal heterologous or the use of synthetic biomaterials, the authors prefer the intra-operative hemostasis achieved using absorbable hemostatic agents (vegetable source) and in particular those based on oxidized cellulose (rayon) as tabotamp, also for the following reasons:

(1) Adaptability to a wide range of surgical procedures;

(2) Ease of use (flexibility and malleability);

(3) Simplification of the surgical;

(4) Rapid and complete absorption (within 7-14 days);

(5) Antibacterial local;

(6) Local inflammatory reaction almost absent;

(7) Possibility of prolonged storage at room temperature;

(8) Canceling the risk of cross infection (such as Creutzfeldt-Jakob disease and bovine spongiform encephalopathy);

(9) No ethical implication, cultural and religious.

About religious, moral and ethical implications, it should be noted that the question is not secondary and should not be underestimated in the current era, because the population is increasingly characterized by a strong presence of multi-ethnic and multi-religious because of increasing migration [7-9, 11]

In fact, the use of materials of bovine or porcine origin could be not only unacceptable but also a source of serious problems with individuals belonging to religious denominations that do not allow any type of contact with certain species of animals (Indians and Muslims for example) [11, 12].

In this regard, it can also be added that the main platelet concentrates (PRP, PRG and PRGF), which have long been used in various surgical specialties for regenerative purposes and also in oral surgery, have proven extremely useful to improve hemostasis and stabilize the clot's healing [10-12].

4. Conclusions

Combination of platelet concentrates (PRP, PRG and PRGF) and hemostatic agents with vegetable source would enhance the biological patient's functions in the following respects:

(1) Platelet aggregation;

(2) Production of growth factors (Cytokines, IL6, etc.);

(3) Direct action on the coagulation cascade;

(4) Prevention or reduction of septic complications;

(5) Indirect analgesy.

Finally, about the patient with coagulation disorders, an additional contribution valuable for the prevention of bleeding in oral surgery will arrive in the next future with the placing on the market of NOACs (new oral anticoagulants), as an alternative to traditional therapy with warfarin sodium [13-15]. The NOACs (Dabigatran, Rivaroxaban, etc.), in fact, represent a new group of molecules that act directly on the coagulation cascade as inhibitors of thrombin and fibrinogen [16-18]. In particular, an extensive literature with a large EBM demonstrates that the use of such molecules, which have as main indication for the prevention of stroke and thromboembolic events in patients at risk of bleeding, significantly reduces the mortality rate for bleeding complications [19, 20].

Regarding the surgery in general and in particular oral surgery—the fundamental advantage of these new drugs is constituted by the following factors:

(1) Short half-life (from 7 to 17 hours, compared with about 40 hours of Warfarin Sodium);

(2) No interactions with food substances;

(3) No interactions with other drugs.

Therefore, mainly due to the short half-life, the interruption of the treatment with NOACs for surgery

would be sufficient only from 2 days before until just 2 days after surgery, unlike warfarin, which must necessarily be suspended for about 10 days before and after surgery, to prevent the concrete risk of intra and post-operative dangerous bleeding [21, 22].

Therefore, NOACs are inevitably destined to become an irreplaceable aid for the prevention and treatment of stroke and atrial non-valvular fibrillation, as well as a considerable advantage for the prevention of bleeding in surgical all areas, including oral surgery [23, 24].

In conclusion, then, it is appropriate to say that the understanding of the possible causes of bleeding and the proper management of the patient with prevention and a right clinical approach is fundamental and essential in every good surgical practice [1, 2, 24].

It is really important, therefore, to know how to manage the "difficult patient ", with a comprehensive and multidisciplinary approach, trying to use all the means that are currently available for a more complete and safe management of bleeding complications, which may—in extremis—to create life-threatening situations [1-3].

References

[1] A. Nematullah, A. Alabousi, N. Blanas, J.D. Douketis, S.E. Sutherland, Dental Surgery for patients on anticoagulant therapy with warfarin: a systematic review and meta- analysis, J. Can. Dent. Assoc. 126 (12) (2009) 1183-1193.

[2] L. Doonquah, A.D. Mitchell, Oral surgery for patients on anticoagulant therapy: Current thougthts on patient management, Dent. Clin. North Am. 56 (1) (2012) 25-41.

[3] W. Martin, E. Lewis, A. Nicol, Local risk factors for implant therapy, Int. J. Oral Maxillofac. Implants (Suppl.) 28 (24) (2009) 28-38.

[4] U. Seligsohn, Treatment inherited platelet disorders, Haemophilia (Suppl. 4)18 (2012) 161-165.

[5] P. Sie, C.M. Sanama, Surgery and invasive procedures in patients on long -term treatment with oral direct thrombin or factor Xa inhibitors, Ann. Fr. Anesth. Réanim 30 (9) (2011) 645-650.

[6] P. Brunamonti Binello, M. Labanca, L.F. Rodella, Management of coagulation disorders in oral surgery: State of Art, in: Ann 5th International Conference on Drugs and Therapy Discovered, Dubai, UAE, 2013.

[7] J.T. Marsh, An Introduction to the Chemistry of Cellulose, Paperback Edition, Osler Press, 2007.

[8] A.J. Mangram, T.C. Horan, M.L. Pearson, Guideline for prevention of surgical site infection, Hospital Infection Control Practices Advisory Committee, Infect. Control & Hosp. Epidemiol. 20 (4) (1999) 250-278.

[9] M. Labanca, A. Leonidas, L.F. Rodella, Biomaterials natural or synthetic in Dentistry: Science and ethics as the criteria for their choice, Implantology (1) (2008) 9-23.

[10] E. Anitua, M. Sánchez, A.T. Nurden, M. Zalduendo, M. De La Fuente, J. Azofra, et al., Reciprocal actions of platelet- secreted TGF-β1 on the production of VEGF and HGF by human tendon cells, Plastic Reconstruct Surg. 119 (2007) 950-959.

[11] L.M. Bauman Kreuziger, Ct. Morton, D.J. Dries, New oral anticoagulants: A concise review, J. Trauma Surg. Acute Care 73 (4) (2012) 983-992.

[12] C. Becattini, M.C. Vedovati, G. Agnelli, Old and new oral anticoagulants for venous thromboembolism and atrial fibrillation: A review of the Literature, Thromb. Res. 129 (3) (2012) 392-400.

[13] G.A. Soff, A new generation of oral anticoagulants direct, Arterioscler Thromb. Vasc. Biol. 32 (3) (2012) 569-574.

[14] L.F. Rodella, G. Favero, M. Labanca, Biomaterials in maxillofacial surgery: membranes and grafts, International Journal of Biomedical Science 7 (2) (2011) 81-88.

[15] J. Harenberg, C. Weiss, Clinical trials with new oral anticoagulants, Additive value of indirect comparisons also named network meta-analyses, Hamostaseologie 33 (1) (2013)62-70.

[16] A.J. Greenspon, A review of oral anticoagulants in patients with atrial fibrillation, Postgrad Med. 124 (6) (2012) 7-16.

[17] Y. Guo, R. Pisters, S. Apostolakis, A.D. Blann, H. Wang, X. Zhao, et al., Stroke risk and suboptimal thromboprophylaxis in Chinese patients with atrial fibrillation: Would the novel oral anticoagulants have an impact?, Int. J. Cardiol. 168 (1) (2013) 515-522.

[18] F. Dentali, N. Riva, M. Crowther, A.G. Turpie, G.Y. Lip, W. Ageno, Efficacy and safety of the novel oral anticoagulants in atrial fibrillation: a systematic review and meta-analysis of the literature, Circulation 126 (20) (2012) 2381-2391.

[19] J. Harenberg, S. Marx, O.E. Dahl, V.J. Marder, A. Schulze, M. Wehling, et al., Interpretation of endpoints in a network meta-analysis of new oral anticoagulants following total hip or total knee replacement surgery, Thromb. Haemost. 108 (5) (2012) 903-912.

[20] S.S. Adam, J.R. McDuffie, T.L. Ortel, J.W. Williams Jr., Comparative effectiveness of warfarin and new oral

anticoagulants for the management of atrial fibrillation and venous thromboembolism: a systematic review, Ann. Intern. Med. 157 (11) (2012) 796-807.

[21] S. Haas, M. Spannagl, S.M. Schellong, Novel oral anticoagulants-key messages for the angiologist, Vasa. 41 (3) (2012) 177-191.

[22] S. Werth, K. Halbritter, J. Beyer-Westendorf, Efficacy and safety of venous thromboembolism prophylaxis with apixaban in major orthopedic surgery, Ther. Clin. Risk Manag. 8 (2012) 139-147.

[23] S.M. Schellong, S. Haas, Novel oral anticoagulants and their use in the perioperative setting, Anasthesiol Intensivmed Notfallmed Schmerzther 47 (4) (2012) 266-272.

[24] T.A. Helin, A. Pakkanen, R. Lassila, L. Joutsi-Korhonen, Laboratory assessment of novel oral anticoagulants: Method suitability and variability between coagulation laboratories, Clin. Chem. 59 (5) 807-814.

Journal of Pharmacy and Pharmacology 2 (2014) 26-37

Anti-inflammatory and Anti-oxidative Effects of the Ethanol Extract of *Cryptocarya densiflora* Blume in Lipopolysaccharide-Stimulated RAW264.7 Mouse Macrophages

Ji-Won Park[1, 2], Ok-Kyoung Kwon[1, 3], Doo-Young Kim[1], Jung-Hee Kim[1], In Sik Shin[1], Sei-Ryang Oh[1], Sang-Woo Lee[4], Jae-Hong Kim[2], Hang Jin[5], Wan Yi Lee[5] and Kyung-Seop Ahn[1]

1. Natural Medicine Research Center, Korea Research Institute of Bioscience and Biotechnology, 30 Yeongudanji-ro, Ochang-eup, Cheongwon-gun, Chungbuk 363-883, Republic of Korea

2. College of Life Sciences and Biotechnology, University of Korea, Anam-dong 5-ga, Seongbuk-gu, Seoul 136-701, Republic of Korea

3. Department of Toxicology, College of Pharmacy, University of Chungnam National, Yuseong-gu, Daejeon 305-764, Republic of Korea

4. International Biological Material Research Center, Research Institute of Bioscience and Biotechnology, Yuseong-gu, Daejeon 305-806, Republic of Korea

5. Yunnan Academy of Agricultural Sciences, Medicinal Plants Research Institute, Beijing 2238, China

Received: October 12, 2013 / Accepted: December 09, 2013 / Published: February 28, 2014.

Abstract: CD (*Cryptocarya densiflora*) Blume has traditionally been used as an herbal medicine. In this study, the effects of CDEE (CD ethanol extract) on inflammation were investigated in LPS (lipopolysaccharide)-stimulated mouse RAW264.7 macrophages. We investigated the effects of CDEE on the production of NO, PGE_2 interleukin (IL)-6, IL-1β, and tumor necrosis factor (TNF)-α in LPS-stimulated RAW264.7 cells. We measured the mRNA or protein expression of the pro-inflammatory mediators induced by CDEE in LPS-stimulated RAW264.7 cells. We explored the expression of Nrf-2, heme oxygenase (HO)-1 and NADPH-quinone oxidoreductase (NQO)-1 to elucidate the antioxidative mechanisms. CDEE significantly inhibited the production of NO, PGE_2, IL-6, IL-1β and TNF-α in LPS-stimulated RAW264.7 cells. CDEE suppressed the mRNA or protein expression of iNOS, COX-2, and the MAPKs with a reduction in the translocation of NF-κB in LPS-stimulated RAW264.7 cells. In addition, CDEE significantly increased the expression of HO-1 and NQO-1 with an increase in the translocation of Nrf-2 into the nucleus. These results indicate that CDEE inhibits the LPS-induced inflammatory and oxidative responses via suppression of NF-κB activation and the enhancement of Nrf2 activation. We suggest that CDEE may be therapeutic for treating inflammatory diseases.

Key words: *Cryptocarya densiflora*, inflammation, MAPK, NF-κB, Nrf-2.

1. Introduction

Inflammation is a biological response of living organisms to the presence of internal and external substances that are recognized by the host as being non-self or foreign invaders [1, 2]. Lipopolysaccharide (LPS), a cell wall component of gram-negative bacteria, triggers the release of pro-inflammatory mediators such cytokines, NO (nitric oxide) and prostaglandin-E$(PGE)_2$ [3]. The release of these

Corresponding author: Kyung-Seop Ahn, Ph.D., research fields: pharmacology and cell biology. E-mail: ksahn@kribb.re.kr.

mediators is influenced by several inflammatory proteins. Activated macrophages express iNOS, which catalyzes the oxidative deamination of L-arginine to produce large amounts of NO [4]. The aberrant release of NO can provoke deleterious consequences, such as septic shock and inflammatory diseases [5]. COX exists in two isoforms, COX-1 and COX-2, and is the rate-limiting enzyme in the synthesis of dienoic eicosanoids, such as PGE_2. COX-2 is induced by proinflammatory stimuli, including bacterial LPS, and produces pro-inflammatory prostaglandins at the inflammatory sites [6, 7]. iNOS and COX-2 induce NO and PGE_2 expression, which stimulates inflammatory signaling proteins, such as nuclear transcription factor-kappa B (NF-κB) and the MAPK (mitogen-activated protein kinase) members, such as p42/p44 ERKs, p38 and c-JNK (Jun N-terminal kinase) [8, 9], resulting in aggravation of an inflammatory responses.

In addition, ROS (reactive oxygen species) induces oxidative stress in bio-organisms and plays a crucial role in the inflammatory response. Previous studies have demonstrated that ROS induces the expression of proinflammatory proteins. Chen et al. [10, 11] reported that increased ROS production induced the development of inflammatory disease by increasing iNOS and COX-2 expression. Therefore, a decrease in ROS production is believed to be a critical step in attenuating an inflammatory response. As part of the defense system, Nrf-2 translocates into the nucleus as a result of oxidative stress, which induces heme oxygenase (HO)-1, and NADPH-quinone oxidoreductase (NQO)-1 expression. HO-1 is a highly inducible enzyme that degrades heme into carbon monoxide, free iron and biliverdin [12, 13]. Generally, HO-1 expression has been considered to be an adaptive cellular response against the toxicity of oxidative stress [14]. Bilirubin is well-known as a strong antioxidant. NQO-1 catalyzes the oxidation of NADH to NAD^+ by various quinones. Several activators and substrates of NQO-1 have been identified. To protect against oxidative stress, various antioxidant defense systems exist in organisms. The antioxidant defense systems include anti-oxidants and anti-inflammatory actions [15].

Cryptocarya densiflora Blume (CD) is a member of theLauraceae family [16, 17]. This species has little commercial value, as it seldom grows large enough to produce millable logs, and the peculiar structure of the wood does encourage the use of the timber. CD has traditionally been used as an herbal medicine in several countries [18, 19]. The effects, biological activities and mechanisms of action of CD on inflammation remain largely unknown.

Therefore, the aim of this study was to investigate the anti-inflammatory effects of CDEE on LPS-stimulated RAW264.7 cells. We measured the levels of NO, cytokines and PGE_2 after the CDEE treatment in LPS-stimulated RAW264.7 cells. To elucidate the protective mechanism of the CDEE, we determined the expression levels of mRNA and proteins associated with inflammation and oxidative stress.

2. Materials and Methods

2.1 Preparation of Cryptocarya densiflora Blume Extract

Preparation of *Cryptocarya densiflora* Blume Extract (Code No. YAAS 0362-2). Plant was collected from the Jing Hong Yunnan Province of China in 2008. Plant samples were identified by Shao Yun Zhang, a botanist. A voucher specimen (YAAS 0362-2) has been deposited in the herbarium of the Korea Research Institute of Bioscience and Biotechnology. Branch, Stem *Cryptocarya densiflora* (100 g) was treated with 95% EtoH and sonicated several times at room temperature for 3 days to produce an extract (2.4 g).

2.2 Cell Culture

RAW264.7 cells (American Type Culture Collection), a mouse peritoneal macrophage cell line, were maintained in a 95% air, 5% CO_2 atmosphere in

Dulbecco's modified Eagle's medium (DMEM; GibcoBRL, Grand Island, NY, USA) supplemented with 10% heat-inactivated FBS (fetal bovine serum, Hyclone, Logan, UT, USA) and 1% antibiotic-antimycotic (Invitrogen, Grand Island, N.Y., USA). The RAW264.7 cells were maintained via weekly passage, and the cells were utilized for experimentation at 60%-80% confluence. After preincubation of the RAW264.7 cells for 4 h, 0-40 μg/mL of the extract was added.

2.3 Cell Viability

The cell viability was determined by the mitochondrial-dependent reduction of 3-(4,5-dimethylthiazol-2-yl)-2,5-diphenyl tetrazolium bromide (MTT, Amnesco, OH, USA) to purple formazan. Based on the results of the cytotoxicity assay, we used nontoxic concentration of CDEE on the RAW264.7 cells in this study.

Briefly, 5 μL of a 5 mg/mL MTT solution was added to the cell supernatant and incubated for 4 h at 37 ℃. The DMSO was added after the medium was removed. The optical density of the formazan was measured using a microplate reader (Benchmark, Bio-Rad Laboratories, Hercules, CA) at 570 nm. The formazan generated by the untreated cells was taken as 100%.

2.4 Nitric Oxide Assay

The RAW264.7 cells were plated at 2.5×10^5 cells/mL in 96-well plates and then incubated with or without lipopolysaccharide (LPS, 0.5 μg/mL) in the absence or presence of various concentrations of the CD extract for 24 h. The nitrite accumulation in the supernatant was assessed by a Griess reaction. Each 100 μL of the culture supernatant was mixed with an equal volume of the Griess reagent (0.1% *N*-(1-naphthyl)-ethylenediamine, 1% sulfanilamide in 5% phosphoric acid) and incubated at room temperature for 10 min. The absorbance at 540 nm was measured in a microplate reader and a series of known concentrations of sodium nitrite was used as a standard.

2.5 PGE_2 Assay

The PGE_2 concentration in the supernatant was determined using a commonly available PGE_2 ELISA kit (Cayman Chemical Co., Inc.), according to the manufacturer's protocols. Briefly, 50 μL of the diluted standard or sample was pipetted into a 96-well plate that had been precoated with a goat polyclonal anti-mouse IgG. Aliquots of a PGE_2 monoclonal antibody and a PGE_2 AChE (acetylcholine esterase) conjugate were added to each well and allowed to incubate at room temperature for 18 h. Subsequently, the wells were washed six times with a buffer containing 0.05% Tween 20, followed by the addition of 200 μL of Ellman's reagent containing acetylthiocholine and 5,5'-dithio-bis-(2-nitrobenzoic acid). The PGE_2 concentrations were determined by measuring the absorbance at 405 nm.

2.6 Cytokine Assays

The levels of interleukin (IL)-6, IL-1β and TNF-α were determined by commercial ELISA (enzyme-linked immunosorbence assay) kits. IL-6, IL-1β and TNF-α were purchased from R&D systems (Minneapolis, MN, USA). The assay procedure for each kit was conducted according to manufacturer's instructions. The concentrations of the mediators were determined at 450 nm using a microplate reader (Benchmark, Bio-Rad Laboratories, Hercules, CA).

2.7 Reverse Transcription (RT)-PCR Analysis

RT-PCR was performed for the detection of the mRNA expression of iNOS, COX-2, HO-1, NQO-1, IL-6, IL-1β, TNF-α and β-actin. Briefly, after LPS (0.5 μg/mL) stimulation of the RAW264.7 cells for 6 h, the total RNA was isolated using Trizol™ reagent (Invitrogen, Carlsbad, CA) as suggested by the manufacturer, then a reverse transcription reaction was carried out using a kit for producing cDNA (Qiagen, GmbH, Hilden, Germany). The PCR was carried out using specific forward and reverse primers

and a premix according to the manufacturer's instructions (Bioneer, Korea). The following sequence was followed for each PCR reaction: 94 ℃ for 5 min (1 cycle); 94 ℃ for 30 s, 60 ℃ for 30 s, and 72 ℃ for 45 s (for 30 cycles); and a final extension phase at 72 ℃ for 10 min. The primer sequences for the analysis of mRNA were as follows: iNOS, 5'-CAA GAG TTT GAC CAG AGG ACC-3' (sense) and 5'-TGG AAC CAC TCG TAC TTG GGA-3' (antisense); COX-2, 5'-GAA GTC TTT GGT CTG GTG CCT G-3' (sense) and 5''-GTC TGC TGG TTT GGA ATA GTT GC-3' (antisense); HO-1, 5'-TGA AGG AGG CCA CCA AGG AGG-3' (sense) and 5'-AGA GGT CAC CCA GGT AGC GGG-3' (antisense); NQO-1, 5'-ACT ACG CCA TGA AGG AGG CT-3' (sense) and 5'-TTC CAG CTT CTT GTG TTC GG-3' (antisense); IL-1β, 5'-GTG TCT TTC CCG TGG ACC TT-3' (sense) and 5'-TCG TTG CTT GGT TCT CCT TG-3' (antisense); IL-6, 5'-AAC GAT GAT GCA CTT GCA GA-3' (sense) and 5'-GAG CAT TGG AAA TTG GGG TA-3' (antisense); and β-actin, 5'-TGT TTG AGA CCT TCA ACA CC-3' (sense) and 5'-CGC TCA TTG CCG ATA GTG AT-3' (antisense). β-actin expression was included as an internal, housekeeping gene control. The reaction products were separated by electrophoresis on a 1.5% agarose gel, stained with EtBr and visualized by UV transillumination. The images were captured by an Olympus C4000 zoom camera system (Olympus AMERICA INC. C4000).

2.8 Western Blot Analysis

After the 30 min LPS (0.5 μg/mL) stimulation, the cells (5×10^5 cells/mL) were harvested. The cells were washed twice with ice-cold PBS, scraped off with a rubber policeman and centrifuged at 2,000 rpm for 5 min at 4 ℃. The cell pellets were resuspended in an appropriate volume of lysis buffer (C-3228, Sigma, USA), incubated for 10 min at room temperature and then for 20 min on ice. The lysates were centrifuged at 14,000 rpm for 10 min at 4 ℃ and collected for further analysis. The supernatant was stored at -70 ℃ until use. The protein concentrations of the samples were determined by a Bradford assay (Bio-Rad, USA) using samples equilibrated to 2 mg/mL with the lysis buffer. The total protein (20 μg) was separated on a 10% SDS polyacrylamide gel and transferred to a PVDF membrane (Millipore, MA, USA). Each membrane was incubated for 1 h in 5% skim milk in TBS-T buffer (0.1 M Tris–HCl, pH 7.4, 0.9% NaCl, 0.1% Tween-20) to block non-specific binding and was then incubated with primary antibodies that recognized iNOS (1:1,000, Stressgen, Assay Designs), COX-2 (1:1,000, Santa Cruz, CA, USA), β-actin (1:2,000, Cell Signaling Technology), the total forms of ERK2, p38 MAPK, JNK1/3 (1:1,000, Santa Cruz, CA, USA), the phospho forms of p38 MAPK, JNK1/2 (1:1,000, Stressgen, Assay Designs), the phospho forms of ERK (1:1,000, Cell Signaling Technology), and Nrf2 (1:1,000, Novus Biological). Each protein was detected by using a chemiluminescence detection system according to the instructions of the manufacturer (ECL, Amersham, Berkshire, UK).

2.9 Immunocytochemistry

The RAW264.7 cells were cultured on Permanox plastic chamber slides (Nunc, Rochester, USA) and fixed with ethanol at 4 ℃ for 30 min. The slides were washed three times with 1 × PBS and blocked with 3% BSA in PBS for 30 min. The slides were incubated for 24 h at 4 ℃ with anti-NF-κB p65 subunit (rabbit polyclonal IgG, 1:500 dilution, Assay Designs) antibodies. After washing, to remove excess primary antibody, the slides were incubated with an anti-rabbit-Texas Red conjugated secondary antibody (Santa Cruz Biotechnology) for 2 h at room temperature. The slides were washed with PBS and mounted using ProLong Gold Antifade reagent containing DAPI (4',6-diamidino-2-phenylindole) (Invitrogen, USA) for 5 min for the localization and quantification of the nuclei. Subsequently, the slides were covered with coverslips and visualized under a laser scanning confocal microscope (LSM510 m, Carl

Zeiss, Germany). The same exposure was used for photographing all the samples, and the nuclei were quantified using the images.

2.10 Statistics

For the statistical analyses, the values are expressed as the means ±S.E.M of the sample determinations. The statistical significance was determined using a two-tailed Student's *t*-test for independent means. *P* values of less than 0.05 were considered to be statistically significant.

3. Results

3.1 Evaluation of the Cytotoxicity of CDEE on RAW264.7 Cells

A prerequisite to studying the biological activity of CDEE is to ensure that it does not have a detrimental effect on cell metabolism. To determine whether CDEE affects cell viability, the RAW264.7 cells were incubated for 24 h with the extract at a wide range of concentrations (0-40 μg/mL), and the cell viability was evaluated by an MTT assay. A statistically significant decrease in the cell survival was observed at concentrations higher than 40 μg/mL (Fig. 1).

3.2 CDEE Reduces the Production of NO by Suppressing iNOS Expression in LPS-Stimulated RAW264.7 Cells

Unstimulated RAW264.7 cells secrete basal levels of NO, while an LPS stimulation resulted in an increase in NO production. The CDEE significantly inhibited the production of LPS-induced NO in a concentration-dependent manner. At 40 μg/mL of the CD extract, the NO production was reduced to approximately basal levels (Fig. 2a). The LPS-stimulated RAW264.7 cells overexpressed iNOS mRNA, whereas this was suppressed by the CDEE (Fig. 2b). The expression of the iNOS protein was consistent with the mRNA results. The CDEE inhibited the expression of the iNOS protein in the RAW264.7 cells stimulated with LPS.

3.3 CDEE Decreases the Production of PGE_2 by Suppressing COX-2 Expression in LPS-Stimulated RAW264.7 Cells

Unstimulated RAW264.7 cells secrete basal levels of PGE2, while LPS stimulation induces an increase in PGE2 production. The CDEE significantly decreased the LPS stimulated PGE_2 production in a concentration-dependent manner (Fig. 2c). The LPS-stimulated RAW264.7 cells overexpressed COX2 mRNA, whereas the CDEE treated RAW264.7 cells stimulated with LPS had suppressed expression of COX2 mRNA (Fig. 2d). The expression of the iNOS protein was consistent with the mRNA results. The CDEE inhibited the expression of the iNOS protein in the RAW264.7 cells stimulated with LPS.

3.4 CDEE Reduces the Release of Proinflammatory Cytokines in LPS-Stimulated RAW264.7 Cells

LPS stimulation induces an increase in TNF-α, IL-6 and IL-1β in RAW264.7 cells. In contrast, the CDEE significantly reduced the release of these mediators in a concentration-dependent manner (Figs. 3a, 3b and 3c). Similar to these results, the mRNA expression of TNF-α, IL-6 and IL-1β was increased in the LPS stimulated RAW264.7 cells, whereas the CDEE suppressed this (Fig. 3d).

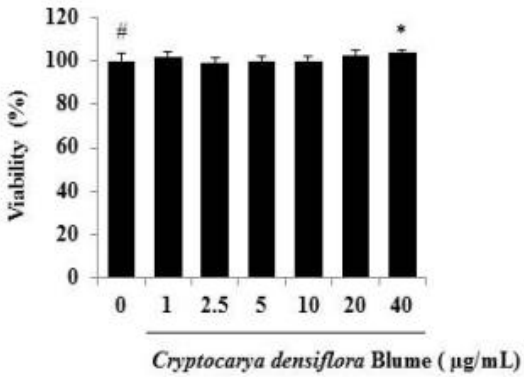

Fig. 1 Effect of the CDEE on cell viability. RAW264.7 cells were incubated in the presence or absence of 0-40 μM of CDEE, and the cell viability was determined using the MTT assay. The data are the means ±SDs of three independent experiments.

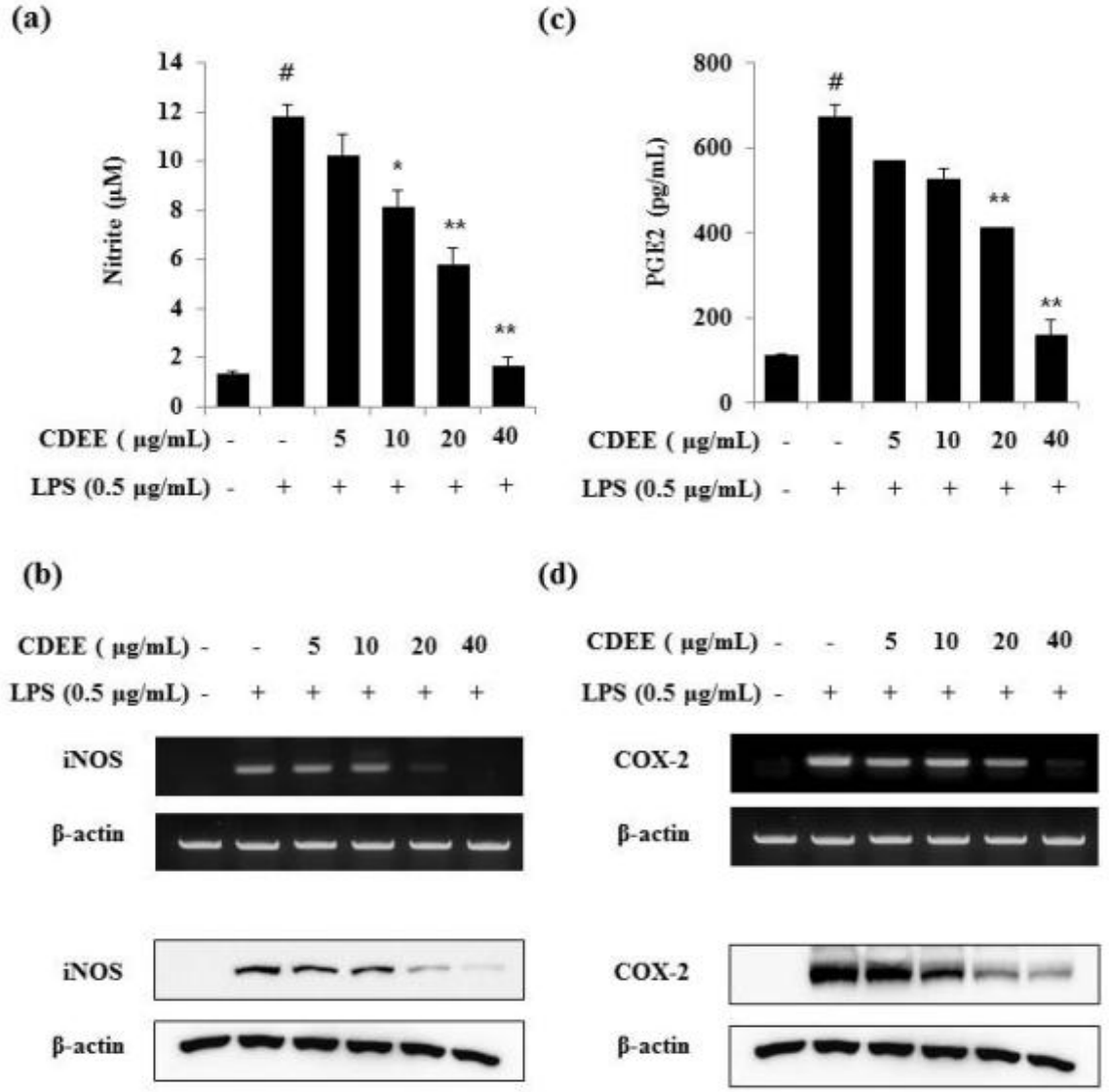

Fig. 2 The CDEE inhibits LPS-induced NO and PGE_2 production and iNOS and COX-2 expression in RAW264.7 cells. (a) RAW264.7 cells were pretreated with the CDEE (5, 10, 20 or 40 μg/mL) for 1 h, and then stimulated with LPS (0.5 μg/mL). The culture media were collected at 24 h, and the NO concentrations were measured using a Griess reaction. Three independent experiments were performed, and the data are presented as the means ± SEMs; (b) The total RNA was isolated, and the iNOS mRNA levels were measured by RT-PCR. The results representative of three independent experiments are shown. β-actin expression was used as an internal control for the RT-PCR; (c) The PGE_2 concentrations using an enzyme immunoassay, and the data are presented as the means ± SEMs; (d) The cell lysates were obtained, and the COX-2 protein levels were analyzed via Western blotting. The results representative of four independent experiments are shown. β-actin expression was used as an internal control for the western blotting. *P < 0.05, **P < 0.01 and ***P < 0.001, compared with cells treated with LPS alone.

3.5 CDEE Inhibits the Phosphorylation of the MAPKs and the Activation of NF-κB in LPS-Stimulated RAW264.7 Cells

The LPS-stimulated RAW264.7 cells exhibited an increased in the phosphorylation of p38, ERK and JNK1/2. In contrast, the CDEE treated RAW264.7 cells stimulated with LPS had suppressed phosphorylation of the MAPKs (Fig. 4). In addition, the LPS stimulation induced an increase in the

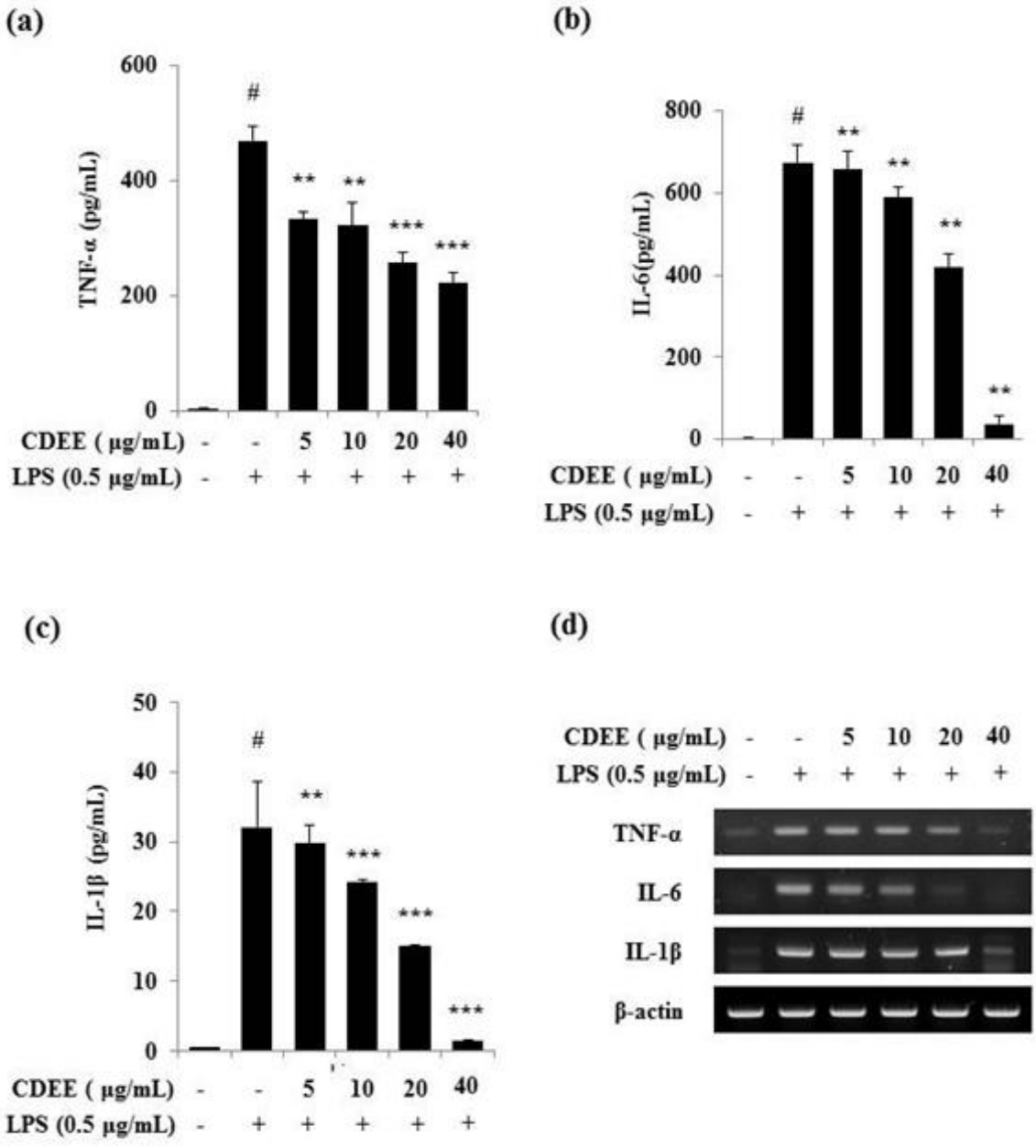

Fig. 3 The CDEE inhibits IL-6, IL-1β and TNF-α production in LPS-stimulated RAW264.7 cells. The cytokines were measured using an ELISA (enzyme-linked immunosorbence assays) in the culture supernatants collected from the treated cells. (a) IL-6; (b) IL-1β and (c) TNF-α levels in the culture media. The total RNA was isolated, and the mRNA levels encoding IL-6, IL-1β and TNF-α were measured by RT-PCR; (d) the data are presented as the means ± SEMs of three samples. Statistically significant differences (*$P < 0.05$, **$P < 0.01$ and ***$P < 0.001$) between the treatment groups are indicated using different lettering.

activation of NF-κB, whereas the CDEE inhibited the NF-κB activation in the RAW264.7 cells stimulated with LPS. This activation is consistent with the ICH results for NF-κB (Fig. 5a). The LPS stimulation caused the translocation of NF-κB into the nucleus (Fig. 5b). However, the CDEE treated RAW264.7 cells showed a reduction in the translocation of NF-κB into the nucleus.

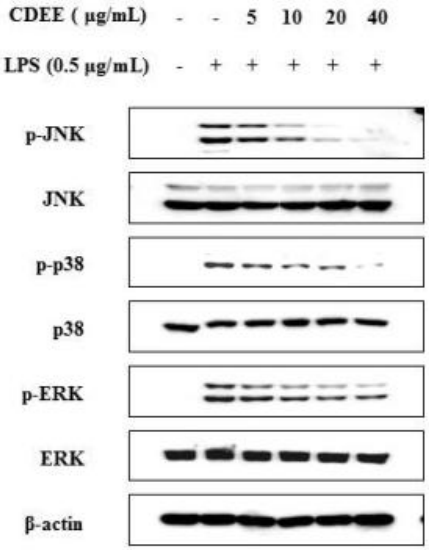

Fig. 4 The CDEE suppresses phosphorylation of MAPK molecules in the LPS-stimulated RAW264.7 cells. The cellular proteins were evaluated for the detection of the phosphorylated form or all forms of the MAPK molecules; ERK, JNK1/2 and p38 MAPK. The results representative of three independent experiments are shown.

3.6 CDEE Increases the Expression of Antioxidant Proteins and the Activation of Nrf-2

HO-1 and NQO-1 expression was not observed in the unstimulated RAW264.7 cells. However, the unstimulated RAW264.7 cells treated with SFN expressed the HO-1 and NQO-1 proteins. The unstimulated RAW264.7 cells treated with the CDEE exhibited the expression of HO-1 and NQO-1 proteins similar to those that result after SFN treatment (Fig. 6a). In addition, the CDEE increased the translocation of Nrf-2 into the nucleus in the unstimulated RAW264.7 cells (Fig. 6b).

4. Discussion

Herbal medicines are becoming increasingly attractive therapies for the treatment of various inflammatory disorders. CD has traditionally been used as an herbal medicine in several countries [18].

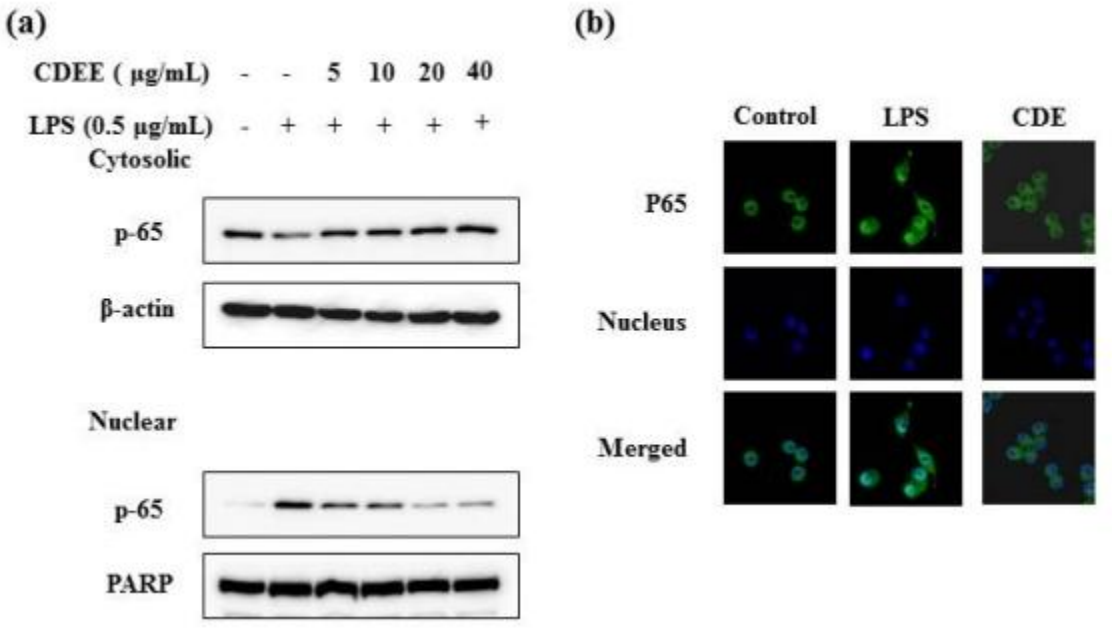

Fig. 5 The inhibitory effects of CDEE on the nuclear translocation of NF-κB. (a) The cells were pretreated with increasing concentrations of the CDEE (5, 10, 20 and 40 μg/mL) for 1 h and then with LPS (0.5 μg/mL) for 30 min. PARP and β-actin were used as internal controls; (b) the cells were treated with the CDEE for 1 h, and then stimulated with LPS for a further 1 h. The cellular localization of NF-κB was determined by immunocytochemistry. After fixation, the cells were stained with a red color. The nuclei were visualized using DAPI (blue color), and observed at 400× magnification. Control: untreated cells; LPS: LPS only (0.5 μg/mL); CDEE: CDEE (20 μg/mL) and LPS.

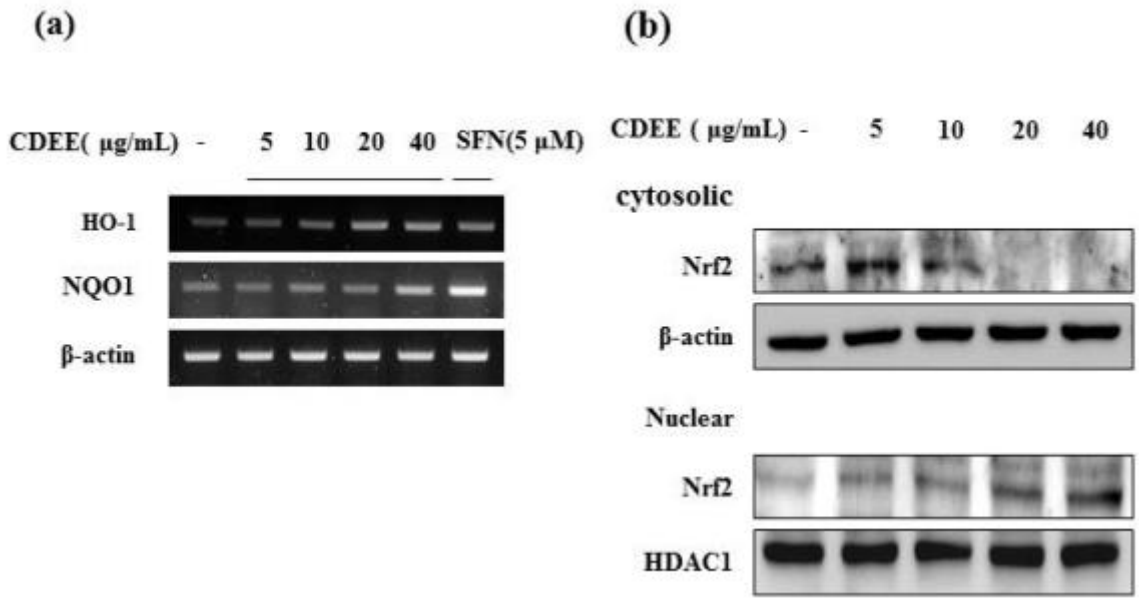

Fig. 6 The CDEE activates Nrf2 in RAW264.7 cells. (a) The total RNA was isolated, and the mRNA levels encoding HO-1 an NQO-1 were measured by RT-PCR. The results representative of three independent experiments are shown. The β-actin expression was used as an internal control for the RT-PCR; (b) the RAW264.7 cells were treated with the CDEE for 30 min and the cytosolic and nuclear extracts were prepared. A Western blot analysis was conducted using an anti-Nrf2 antibody. These results are representative of similar findings from at least three separate experiments.

In this study, the CDEE significantly inhibited the production of NO, PGE_2, IL-6, IL-1β and TNF-α in LPS stimulated RAW264.7 cells. The CDEE suppressed the mRNA or protein expression of iNOS, COX-2, and MAPKs (p38 MAPK, JNK and ERK) with a reduction in the translocation of NF-κB to the nucleus in the LPS-stimulated RAW264.7 cells. In addition, the CDEE significantly increased the expression of HO-1 and NQO-1 with an elevation in the Nrf-2 nuclear translocation.

NO, a strong stimuli, is implicated in the pathogenesis of a variety of inflammatory diseases and is synthesized from L-arginine by iNOS [20]. iNOS expression is stimulated by various mediators including proinflammatory cytokines such as IL-1β, IL-6 and TNF-α and bacterial products [21, 22]. iNOS expression induces NO overproduction, resulting in the aggravation of inflammatory responses by activating cellular inflammatory signaling [23]. Therefore, a reduction in the NO level through inhibiting iNOS expression provides a method to assess the efficacy of new therapeutics for treating inflammatory diseases [24, 25]. In this study, the CDEE induced significant reductions in proinflammatory cytokines including IL-1β, IL-6 and TNF-α in the LPS-stimulated RAW264.7 cells as shown in Fig. 3. With these reductions, the CDEE meaningfully decreased the NO production in a concentration-dependent manner with a reduction in iNOS expression in LPS-stimulated RAW264.7 cells (Fig. 2). These findings indicate that the CDEE may effectively attenuate inflammatory responses via the inhibition of the NO production associated with a reduction in iNOS and proinflammatory cytokines.

The MAP kinases are a group of signaling molecules that also appear to play a critical role in inflammatory processes [9]. Several studies have shown that the activation of MAP kinases is important in the regulation of NO production via activation of NF-κB [26]. NF-κB is an important factor that regulates the expression of inflammation-associated mediators, including iNOS, COX-2 and TNF-α that

contain NF-κB binding motifs within their promoters. Many anti-inflammatory agents exhibit their potency by suppressing NF-κB signaling [27]. In particular, NF-κB-targeted herbal remedies are considered to be more effective in treating inflammatory diseases because they inhibit one or more activation steps in the signaling pathway. In agreement with these previous observations, the LPS stimulation of RAW264.7 cells caused phosphorylation of the ERK, JNK and p38 kinases, whereas the CDEE significantly inhibited ERK and p38 phosphorylation in these same cells. With the reduction in MAPKs phosphorylation, the CDEE suppresses NF-κB translocation into the nucleus. These findings indicate that the anti-inflammatory effects of the CDEE may be closely related to blocking NF-κB translocation into the nucleus caused by the reduction in MAPKs phosphorylation as shown in Figs. 4 and 5.

Oxidative stress is caused by ROS (reactive oxygen species) and is important to the progression of many inflammatory diseases. In an inflammatory response, the ROS act both as signaling molecules and inflammatory mediators. The ROS can combine with NO to form RNS (reactive nitrogen species) [28]. The RNS in turn induce nitrosative stress, which causes the production of proinflammatory mediators [29]. Bio-organisms contain various antioxidant systems to protect themselves from oxidative stress. Nrf2 is one of the antioxidant systems and a key transcription factor related to the production of antioxidant mediators such as HO-1, NQO-1 and GST [30]. The importance of Nrf-2 in the progression of inflammatory responses has been elucidated by many experiments [31-33]. Nrf-2 dissociates from Keap1 in the response to oxidative stress and is then translocated into the nucleus. Nrf-2 in turn binds directly to the promoter region of the antioxidant response element, resulting in the elevation of antioxidant mediators including HO-1 and NQO-1 [34]. In this study, the CDEE treatment induced increases in HO-1 and NQO-1 expression (Fig. 6). These results were associated with the increased Nrf-2 translocation into the nucleus induced by the CDEE treatment. Therefore, these findings indicate that the anti-inflammatory effects of the CDEE may be partially related to the antioxidant property of elevating HO-1 and NQO-1 expression via increasing Nrf-2 translocation into the nucleus.

5. Conclusions

These results indicated that the CDEE inhibits the LPS-induced inflammatory and oxidative responses. These effects were considered to be closely related to the suppression of NF-κB activation and the enhancement of Nrf2 activation. We suggest that CDEE may be a therapeutic for treating inflammatory diseases.

Acknowledgments

This study was supported by the grants FGC 1011123 and KGM 1221312 from the Korea Research Institute of Bioscience and Biotechnology (KRIBB) of the Republic of Korea.

References

[1] J.K. Kim, G.M. Park, Indirubin-3-monoxime exhibits anti-inflammatory properties by down-regulating NF-kappaB and JNK signaling pathways in lipopolysaccharide-treated RAW264.7 cells, Inflamm. Res. 61 (4) (2012) 319-325.

[2] K.M. Boje, D. Jr. Jaworowicz, J.J. Raybon, Neuroinflammatory role of prostaglandins during experimental meningitis: Evidence suggestive of an *in vivo* relationship between nitric oxide and prostaglandins, J. Pharmacol. Exp. Ther. 304 (1) (2003) 319-325.

[3] V.D. Raykova, M. Glibetic, J.P. Ofenstein, J.V. Aranda, Nitric oxide-dependent regulation of pro-inflammatory cytokines in group B streptococcal inflammation of rat lung, Ann. Clin. Lab. Sci. 33 (1) (2003) 62-67.

[4] A. Conforti, S. Lussignoli, S. Bertani, R. Ortolani, L. Cuzzolin, G. Benoni, et al., Cytokine and nitric oxide levels in a rat model of immunologic protection from adjuvant-induced arthritis, Int. J. Immunopathol. Pharmacol. 14 (3) (2001) 153-160.

[5] R. Zamora, Y. Vodovotz, T.R. Billiar, Inducible nitric oxide synthase and inflammatory diseases, Mol. Med. 6 (5) (2000) 347-373.

[6] G. Eibl, D. Bruemmer, Y. Okada, J.P. Duffy, R.E. Law, H.A. Reber, et al., PGE(2) is generated by specific COX-2 activity and increases VEGF production in COX-2-expressing human pancreatic cancer cells, Biochem. Biophys. Res. Commun. 306 (4) (2003) 887-897.

[7] Y. Kitase, L. Barragan, H. Qing, S. Kondoh, J.X. Jiang, M.L. Johnson, et al., Mechanical induction of PGE2 in osteocytes blocks glucocorticoid-induced apoptosis through both the beta-catenin and PKA pathways, J. Bone. Miner. Res. 25 (12) (2010) 2657-2668.

[8] E.J. Cho, H.J. An, J.S. Shin, H.E. Choi, J. Ko, Y.W. Cho, et al., Roxatidine suppresses inflammatory responses via inhibition of NF-kappaB and p38 MAPK activation in LPS-induced RAW 264.7 macrophages, J. Cell Biochem. 112 (12) (2011) 3648-3659.

[9] J.Y. Kim, H.J. Kim, S.M. Kim, K.R. Park, H.J. Jang, E.H. Lee, et al., Methylene chloride fraction of the leaves of Thuja orientalis inhibits in vitro inflammatory biomarkers by blocking NF-kappaB and p38 MAPK signaling and protects mice from lethal endotoxemia, J. Ethnopharmacol. 133 (2) (2011) 687-695.

[10] A. Mouithys-Mickalad, G. Deby-Dupont, J.M. Dogne, X. De Leval, S. Kohnen, R. Navet, et al., Effects of COX-2 inhibitors on ROS produced by Chlamydia pneumoniae-primed human promonocytic cells (THP-1), Biochem. Biophys. Res. Commun. 325 (4) (2004) 1122-1130.

[11] H.W. Chen, C.T. Chien, S.L. Yu, Y.T. Lee, W.J. Chen, Cyclosporine A regulate oxidative stress-induced apoptosis in cardiomyocytes: Mechanisms via ROS generation, iNOS and Hsp70, Br. J. Pharmacol. 137 (6) (2002) 771-781.

[12] H.P. Kim, H.O. Pae, S.H. Back, S.W. Chung, J.M. Woo, Y. Son, et al., Heme oxygenase-1 comes back to endoplasmic reticulum, Biochem. Biophys. Res. Commun. 404 (1) (2011) 1-5.

[13] A.A. Shahat, M.S. Alsaid, M.A. Alyahya, M. Higgins, A.T. Dinkova-Kostova, NAD(P)H: Quinone oxidoreductase 1 inducer activity of some Saudi Arabian medicinal plants, Planta. Med. 79 (6) (2013) 459-464.

[14] H.O. Pae, Y.C. Lee, E.K. Jo, H.T. Chung, Subtle interplay of endogenous bioactive gases (NO, CO and H(2)S) in inflammation, Arch. Pharm. Res. 32 (8) (2009) 1155-1162.

[15] P. Di Mascio, M.E. Murphy, H. Sies, Antioxidant defense systems: The role of carotenoids, tocopherols, and thiols, Am. J. Clin. Nutr. 53 (1 Suppl) (1991) 194S-200S.

[16] X. Fu, T. Sevenet, F. Remy, M. Pais, A. Hamid, A. Hadi, et al., Flavonone and chalcone derivatives from Cryptocarya kurzii, J. Nat. Prod. 56 (7) (1993) 1153-1163.

[17] M. Montes, L. Valenzuela, T. Wilkomirsky, A. Sanguinetti, D. Von Baer, Chemical composition of the essential oil of Cryptocarya alba (Mol.) Looser (Lauraceae) in Chile, Ann. Pharm. Fr. 46 (1) (1988) 41-47.

[18] B. Melillo, A.B. Smith, 3rd, A unified synthetic strategy to the Cryptocarya family of natural products exploiting Anion Relay Chemistry (ARC), Org. Lett. 15 (9) (2013) 2282-2285.

[19] C.J. Nehme, W.L. Bastos, A.J. De Araujo, A.J. Cavalheiro, An HPLC-PAD method to analyse flavonoid glycosides and styrylpyrones from Cryptocarya species (Lauraceae), Phytochem. Anal. 16 (2) (2005) 93-97.

[20] J.B. Weinberg, M.A. Misukonis, P.J. Shami, S.N. Mason, D.L. Sauls, W.A. Dittman, et al., Human mononuclear phagocyte inducible nitric oxide synthase (iNOS): Analysis of iNOS mRNA, iNOS protein, biopterin, and nitric oxide production by blood monocytes and peritoneal macrophages, Blood 86 (3) (1995) 1184-1195.

[21] T. Taniguchi, Regulation of cytokine gene expression, Annu. Rev. Immunol. 6 (1988) 439-464.

[22] T.K. Hughes, T.A. Kaspar, D.H. Coppenhaver, Synergy of antiviral actions of TNF and IFN-gamma: Evidence for a major role of TNF-induced IFN-beta, Antiviral. Res. 10 (1-3) (1988) 1-9.

[23] C. Knott, G. Stern, G.P. Wilkin, Inflammatory regulators in Parkinson's disease: iNOS, lipocortin-1, and cyclooxygenases-1 and -2, Mol. Cell Neurosci. 16 (6) (2000) 724-739.

[24] S. Golde, A. Coles, J.A. Lindquist, A. Compston, Decreased iNOS synthesis mediates dexamethasone-induced protection of neurons from inflammatory injury in vitro, Eur. J. Neurosci. 18 (9) (2003) 2527-2537.

[25] S.H. Lee, S.A. Park, S.H. Ko, H.W. Yim, Y.B. Ahn, K.H. Yoon, Insulin resistance and inflammation may have an additional role in the link between cystatin C and cardiovascular disease in type 2 diabetes mellitus patients, Metabolism 59 (2) (2010) 241-246.

[26] O.K. Kwon, K.S. Ahn, J.W. Park, H.Y. Jang, H. Joung, H.K. Lee, et al., Ethanol extract of Elaeocarpus petiolatus inhibits lipopolysaccharide-induced inflammation in macrophage cells, Inflammation. 35 (2) (2012) 535-544.

[27] J.W. Park, O.K. Kwon, H.Y. Jang, H. Jeong, S.R. Oh, H.K. Lee, et al., A leaf methanolic extract of Wercklea insignis attenuates the lipopolysaccharide-induced inflammatory response by blocking the NF-kappaB signaling pathway in RAW 264.7 macrophages, Inflammation 35 (1) (2012) 321-331.

[28] C. Mccabe, A. Samali, T. O'brien, Beta cell cytoprotective strategies: Establishing the relative roles for iNOS and ROS, Biochem. Biophys. Res. Commun. 342 (4) (2006) 1240-1248.

[29] J. Egea, M.D. Martin-De-Saavedra, E. Parada, A. Romero,

L. Del Barrio, A.O. Rosa, et al., Galantamine elicits neuroprotection by inhibiting iNOS, NADPH oxidase and ROS in hippocampal slices stressed with anoxia/reoxygenation, Neuropharmacology 62 (2) (2012) 1082-1090.

[30] C.M. Yang, S.M. Huang, C.L. Liu, M.L. Hu, Apo-8'-lycopenal induces expression of HO-1 and NQO-1 via the ERK/p38-Nrf2-ARE pathway in human HepG2 cells, J. Agric. Food Chem. 60 (6) (2012) 1576-1585.

[31] M.K. Kwak, K. Itoh, M. Yamamoto, T.R. Sutter, T.W. Kensler, Role of transcription factor Nrf2 in the induction of hepatic phase 2 and antioxidative enzymes *in vivo* by the cancer chemoprotective agent, 3H-1, 2-dimethiole-3-thione, Mol. Med. 7 (2) (2001) 135-145.

[32] R. Venugopal, A.K. Jaiswal, Nrf1 and Nrf2 positively and c-Fos and Fra1 negatively regulate the human antioxidant response element-mediated expression of NAD(P)H:quinone oxidoreductase1 gene, Proc. Natl. Acad. Sci. USA 93 (25) (1996) 14960-14965.

[33] K. Chan, Y.W. Kan, Nrf2 is essential for protection against acute pulmonary injury in mice, Proc. Natl. Acad. Sci. USA 96 (22) (1999) 12731-12736.

[34] A. Bassan, M.R.A. Blomberg, P.E. Siegbahn, L. Que, A density functional study on a biomimetic non-heme iron catalyst: Insights into alkane hydroxylation by a formally HO-FeV=O oxidant, Chemistry 11 (2) (2005) 692-705.

Journal of Pharmacy and Pharmacology 2 (2014) 38-49

Antiasthmatic Effect of Eugenol (4-Allyl-2-Methoxyophenol) Mediated by Both Bronchodilator and Immunomodulatory Properties

Campos Keina Maciele[1], Teixeira Tatiane Oliveira[1], Cerqueira-Lima Ana Tereza[1], Costa Ryan Santos[1], Carneiro Tamires Cana Brasil[1], Silva Darizy Flávia[1], Barreto Mauricio Lima[2], Pontes-de-Carvalho Lain Carlos[3], Alcantatara-Neves Neuza Maria[1] and Figueiredo Camila Alexandrina[1]

1. Instituto de Ciências da Saúde, Universidade Federal da Bahia, Salvador, Bahia 41110-100, Brazil

2. Instituto de Saúde Coletiva, Universidade Federal de Bahia, Rua Basilio da Gama s/n, Canela, Salvador, Bahia 41110-040, Brazil

3. Centro de pesquisa Gonçalo Moniz, Fundação Oswaldo Cruz, Salvador, Bahia 40296-710, Brazil

Received: October 19, 2013 / Accepted: January 02, 2014 / Published: February 28, 2014.

Abstract: Eugenol, an aromatic product, exhibits anti-inflammatory properties, however, little is known about its effect in allergic inflammation mediated by Th2-type cells and cytokines. We examined the pharmacological potential of this compound in a murine model of respiratory allergy to Bt (*Blomia tropicalis*). For this, AJ mice were sensitized (100 μg/animal s.c.) and challenged (10 μg/animal i.n.) with Bt mite extract. Sensitized animals were treated or not with eugenol (20, 40 or 80 mg/kg) and the following parameters were analyzed: number of total cells in BAL (bronchoalveolar lavage); EPO (eosinophil peroxidase activity) and histopathological changes in the lungs; serum level of specific IgE, IgG1 and IgG2a and; concentration of Th2 cytokines on BAL and spleen cultures. In addition, the capability of eugenol in relaxing tracheal smooth muscle was also evaluated. Our results showed that treatment with eugenol significantly reduced the airway inflammation, decreasing the cellular infiltrate, EPO and mucus in the lungs, as well as the production of Th2 cytokines. It was also demonstrated a dilator effect of eugenol observed by the relaxation of normal and hyper-reactivity isolated trachea upon carbachol stimulation. These results suggest that eugenol has potential as an anti-asthmatic drug by both bronchodilator and immunomodulatory properties.

Key words: Asthma; *Blomia tropicalis*, natural products, eugenol.

List of Abbreviations

BAL: Broncho alveolar lavage
BK: BradykininCch, carbachol
ELISA: Enzyme immunoassay test
Eug: Eugenol
EPO: Eosinophil peroxidase
Emax: Maximum relaxation
BHR: Bronchial hyper-reactivity
HBSS: Hanks' balanced salt solution
IL: Interleukin
i.n.: Intranasal
IgE: Immunoglobulin E-type
LPS: Lipopolysaccharide
NF-Kb: nuclear factor of activated B cells potentiating
OVA: Ovalbumin
PAS: Periodic Acid Schiff
PBS: Phosphate buffered solution bisódica
PWM: Pokweed (mitogen)
RPM: Revolutions per minute
s.c.: Subcutaneous
Th2: T helper lymphocyte type 2
v.o.: Oral

Corresponding author: Figueiredo Camila Alexandrina, Ph.D., professor, research field: immunopharmacology and immunoepidemiology. E-mail: cavfigueiredo@gmail.com.

1. Introduction

Atopic asthma is a chronic inflammatory disorder associated with hyperresponsiveness of the lower airways and variable airflow limitation [1-3]. It is characterized by a Th2-dominant response where interleukin-4 (IL-4), IL-5, and IL-13 are involved in the coordination, amplification and perpetuation of the inflammatory response by attracting additional inflammatory cells, mainly eosinophils, increasing mucus production and serum IgE (immunoglobulin E) Ab (antibody) levels [4-6].

Although current treatments are able to control symptoms and improve lung function in most patients, in severe asthma, acute exacerbations still occur and contribute significantly to morbidity and mortality of asthma in all age groups [2, 7]. Historically, herbal medicine has a great importance on asthma treatment. Four fifths classes of drugs currently are in use to treat asthma-namely, α2 agonists, anticholinergics, methyl xanthines and cromones-have herbal origins [8, 9].

Eugenol (4-allyl-2-methoxyphenol) is an aromatic compound, a member of the phenyl propanoids compounds. It is found in several species, especially in cloves, nutmeg [10] and *Ocimum gratissimum* whose immunomodulatory property was recently demonstrated in an experimental model of allergic asthma [11]. Eugenol is commonly used as a flavoring agent in cosmetics and food products and, in particular, in dentistry in zinc oxide-eugenol chelating cement. Its antioxidant and anti-inflammatory activities have been already investigated. Several studies have pointed out the anti-inflammatory effects of eugenol, reporting that this oil was able to modulate inflammatory markers such nitric oxide, iNOS, prostaglandin E2, mast cell degranulation and the transcription nuclear factor Kappa B (NF-kB) [12-18]. Also, it has been shown that phenolic compounds have a relaxing effect on tracheal smooth muscle from guinea pigs and may have bronchodilator effect [19]. However, little is known about the effect of eugenol in allergic inflammation mediated by cells and Th2-type cytokine.

Since eugenol exhibit anti-inflammatory properties and a possible relaxing effect on smooth muscle, we examined the pharmacological potential of eugenol in a murine model of respiratory allergy to Bt (*Blomia tropicalis*) mite.

2. Materials and Methods

2.1 Animals

Females AJ mice (20-25g) were obtained in the animal facilities from the Fundação Oswaldo Cruz, Bahia, Brazil and were used throughout the study. Animals were maintained with free access to food and water. Groups of 5 animals were used in each experiment. All the experimental procedures were approved by the Ethical Committee for Use of Experimental Animals of the Faculdade de Odontologia, Universidade Federal da Bahia, Brazil (protocol number: 02/09).

2.2 Experimental Groups and Eugenol Oral Treatment

To investigate the anti-allergic effect of eugenol, we performed an experimental model of allergy to *Blomia tropicalis* dust mite as previously described [20]. As positive control, A/J mice (n = 5) were sensitized with two subcutaneous injections (at day 0 and day 7) of Bt (100 μg of protein), adsorbed to 4 mg/mL of $Al(OH)_3$ in saline. Twenty-four hours after the second subcutaneous injection, the animals received four intranasal boosters/challenges with Bt (10 μg/instilation) every other day. One day after the last challenge, the animals were euthanized with intraperitoneal injections of xylazine and ketamine (40 mg/kg/body weight). Mice sensitized and challenged with $Al(OH)_3$ in saline alone (vehicle) were considered negative controls. The tested groups were animals sensitized as the positive control and daily treated orally with 20, 40 or 80mg/kg of eugenol, obtained commercially from Sigma-Aldrich® (St. Louis, MA, USA), dissolved in 1% of Tween 20 in saline from the 8th to the 14th day of the experimental

protocol and one hour after the intranasal challenges with Bt. The groups of animals were defined as: Non-sensitized and vehicle-treated mice (control group); Bt, Bt-sensitized mice and vehicle-treated mice (positive control group); Bt/Eug 20, Bt-sensitized and eugenol 20mg/kg treated mice; Bt/Eug 40, Bt-sensitized and eugenol 40mg/kg treated mice; Bt/Eug 80, Bt-sensitized and eugenol 80mg/kg treated mice (tested groups). To determine the *in vivo* doses of eugenol, pilot studies were carried out using doses between 80 mg/kg and 160 mg/kg (this last dose was based in previous studies evaluating anti-inflammatory effect of this compound) [18]. As 160 mg/kg and 80 mg/kg had the same effect (data not shown), we choose the effective dose of 80 mg/kg and in addition we included 40 mg/kg and 20 mg/kg doses aiming to obtain a dose-response curve.

2.3 BAL (Bronchoalveolar Lavage)

The trachea was canulated and the lungs were carefully washed with 1.5 mL of phosphate buffered saline, pH 7.4 (PBS) containing 1% of bovine serum albumin (Sigma-Aldrick St. Louis, MA, USA). The total number of leukocytes in the BAL was determined using Trypan blue. Differential cell counts were obtained by using Wright-stained cytospin preparations. Differential counts of at least 100 cells were made in a blind fashion in accordance with standard morphologic protocol. The concentrations of IL-4 and IL-10 in BAL, were quantified by sandwich-ELISA, as recommended by the manufacturer (BD Pharmingen, city, State, USA).

2.4 EPO (Eosinophil Peroxidase) Activity in Lung Cell Lysates

The EPO activity in lung cells was evaluated according to a previously described method [21]. Briefly, cell suspensions were frozen and thawed three times in liquid nitrogen. After centrifugation at 4 ^{o}C for 10 min at 1,000 g, the cell lysates were placed into wells of 96-well plates (75 μL/well), followed by the addition of the chromogen and substrate solution (1.5 mmol/L of o-phenylenediamine and 6.6 mmol/L of H_2O_2 in 0.05 mol/L Tris-HCl, pH 8.0). After 30 min, the reaction was stopped with the addition of 0.2 mol/L citric acid, and the absorbance of the sample determined at 492 nm in an ELISA reader.

2.5 Histopathological Analysis

The histopathological changes were assessed as described previously [22]. Briefly, lung tissue was fixed using 10% (v/v) formaldehyde (Sigma-Aldrich St. Louis, MA, USA). The tissue was dehydrated, embedded in paraffin and cut in 5 μm sections which were stained with hematoxylin and eosin for evaluation of cellular infiltration and with periodic acid Schiff to assess mucus, under light microscopy with 40x magnification.

2.6 Measurement of Anti-Bt IgE, IgG1 and IgG2a Antibody Levels in Serum

Anti-Bt antibody levels in the serum of mice from the different experimental groups were determined by indirect ELISA. 96-well micro titer high-binding plate (Costar, Cambridge, MA, USA) were coated with Bt (100 μg/well) overnight, at 4 ℃, and blocked during 1 hour with PBS-T containing 10% fetal calf serum (FCS, Gibco, Pisley, UK) at RT (room temperature). After this incubation period, the serum samples were added and the plates were incubated overnight at 4 ℃. Biotin-conjugated IgE, IgG1 or IgG2a anti-mouse (BD Pharmingen, San Diego, CA, USA) were added to the wells and incubated during 1 h at RT. A solution of avidin-horseradish peroxidase (BD Pharmingen, San Diego, CA, USA) was then added to each well for 30 min. Finally a solution containing 3,3',5,5'-tetramethylbenzidine and hydrogen peroxide (BD Pharmingen, San Diego, CA, USA) was added and incubated during 30 min at RT and the reaction was stopped with 4 M sulfuric acid. The absorbance of the sample was determined at 492 nm in an ELISA reader.

2.7 In vitro Cytokine Production in Spleen Cells of Bt-Sensitized Mice Cultivated in the Presence of Different Concentrations of Eugenol

In vitro estimation of cytokines concentration produced by spleen cells treated *in vitro* with eugenol was performed according to the method described by Bezerra-Santos et al. [23]. In brief, spleen cell suspensions from non-sensitized and Bt-sensitized groups were obtained and washed twice in RPMI medium by centrifugation at 200 g for 10 min. The pellet was resuspended in RPMI medium supplemented with 200 mM l-glutamine, 100 units/mL penicillin, 100 μg/mL streptomycin, 5-Mercaptoethanol and 10% FCS (Gibco, Pisley, UK). A total of 5×10^5 viable cells were placed in each well. The cells were incubated with eugenol at different non-cytotoxic concentrations (12.5-200 μm) determined by MTT test (data not shown), and Pokeweed (PWM) (Sigma, St Louis, MA, USA) at 5 μg/mL for 48 h. Supernatants from the cell culture were removed for cytokine measurement by enzymatic immunoassay with their respective antibody pairs following manufacturer's instructions (BD Pharmingen, San Diego, CA, USA).

2.8 Effect of Eugenol on Normal and Hyperresponsive Airway Smooth Muscle from AJ Mice

Normal AJ mice were euthanized by overdose of xylazine and ketamine and the tracheae were rapidly removed, cleaned of connective tissue and washed three times with Krebs-bicarbonate solution (composition in mM: NaCl 119, $NaHCO_3$ 25, $CaCl_2 \cdot H_2O$ 1.6, KCl 4.7, KH_2PO_4 1.2, $MgSO_4 \cdot 7H_2O$ 1.2 and glucose 11.1). Following, the tracheae were sectioned into rings of 2 mm, containing on average three to four cartilage bands. The rings were suspended on metal rods, attached to a force transducer (FORT10 WPI, Sarasota, USA) and placed in tanks for isolated organ, maintained at 37 ℃ and aerated with a carbogen mixture (95% O_2 and 5% CO_2). The rings were subjected to stabilization for a period of 1 h at 0.5 g. After the stabilization period, the rings were contracted with 10 μM of carbachol (Cch; Sigma, St Louis, MA, USA) to assess the contractile state of the tissue. To evaluate the presence of functional epithelium, the rings were stimulated with bradykinin (Bk; Sigma, St Louis, MA, USA) (10^{-6} M). After stabilization and assessment of the presence of functional epithelium, the rings were washed, again contracted with carbachol (10 μM) and were added cumulatively and increasing concentrations of eugenol. Concentration response curve was constructed and the data analyzed.

To assess the effects of eugenol on the hyper-responsive airway smooth muscle, tracheal rings were previously exposed in culture to IL-13 as previously described [24]. Tissues were placed individually in multiwell plates containing Dulbecco's modified Eagle's medium (containing 25 mM D-glucose, 1 mM sodium pyruvate, 100 U/mL penicillin, 100 μg/mL streptomycin, 0.2 M L-glutamine, 2.5 μg/mL Fungizone, and 0.1% w/v bovine serum albumin) (Sigma, St Louis, MA, USA). Tracheal segments were incubated at 37 ℃ in a humidified CO_2 gassed incubator in the presence or absence of IL-13 (10 ng/mL, 24 h; BD Pharmingen, San Diego, CA, USA). Cumulative concentration-response curves to CCh after incubation in the absence or presence of IL-13 was built to analyze the hyper reactivity of smooth muscle. After that, concentration-response curve for eugenol was built.

2.9 Statistical Analysis

The ANOVA (one-way analysis of variance) and Tukey's post-test (for data with normal distribution by Kolmogorov-Smirnov test) were used to determine the statistical significance between the experimental groups. Differences in P values ≤ 0.05 were considered statistically significant. Each experiment was repeated at least two times. Concentration response curve for isolated organ experiments and all

the graphs included in this study were performed using GraphPad Prisma 5.

3. Results

3.1 Treatment with Eugenol Reduces the Rosinophilic Cellular Infiltration in BAL of Bt Sensitized Mice

To assess the effects of eugenol on the inflammatory cell infiltration in BAL of the Bt-sensitized and challenged mice, the BAL cellularity was assessed 24 hours after the last challenge. Bt-sensitized mice displayed a significant increase of total cells and eosinophils in relation to the control group ($P < 0.001$; Fig. 1). Oral daily administration of 40 mg/kg or 80 mg/kg of eugenol significantly suppressed the number of total inflammatory cells (Fig. 1a) and eosinophils (Fig. 1b), in relation to the untreated Bt-sensitized mice. No effect was observed on eosinophil count in mice treated with 20 mg/kg of eugenol.

3.2 Treatment with Eugenol Reduces Eosinophil Peroxidase Levels in Lungs of Bt Sensitized Mice

Bt sensitization led to an increase of EPO activity in the lungs ($P < 0.001$) when compared to the control group (Fig. 1c). Treatment with 40 and 80 mg/kg of eugenol decreased EPO activity in lung tissue ($P < 0.001$) of Bt-immunized and challenged mice (Fig. 1c). No effect was observed on eosinophil peroxidase in lungs from mice treated with 20 mg/kg of eugenol.

3.3 Treatment with Eugenol Decreases the Inflammatory Cell Infiltration and Amount of Mucus in Lungs of Bt-immunized Animals

The Fig. 2 shows the typical pathologic features of allergic asthma in lung tissue from Bt-sensitized mice, characterized by the infiltration of numerous inflammatory cells in the peribronchiolar and perivascular regions (Fig. 2b) and airway mucus hypersecretion (Fig. 2f). Treatment with both doses of eugenol (40 mg/kg and 80 mg/kg) markedly reduced the inflammatory cell infiltration around the bronchioles (Figs. 2c and 2d) as well as suppressed mucus secretion in the lung tissue (Fig. 2g and 4h). No effect was observed on leukocyte infiltration and mucus hyper-secretion in lungs from mice treated with 20 mg/kg of eugenol (data not shown).

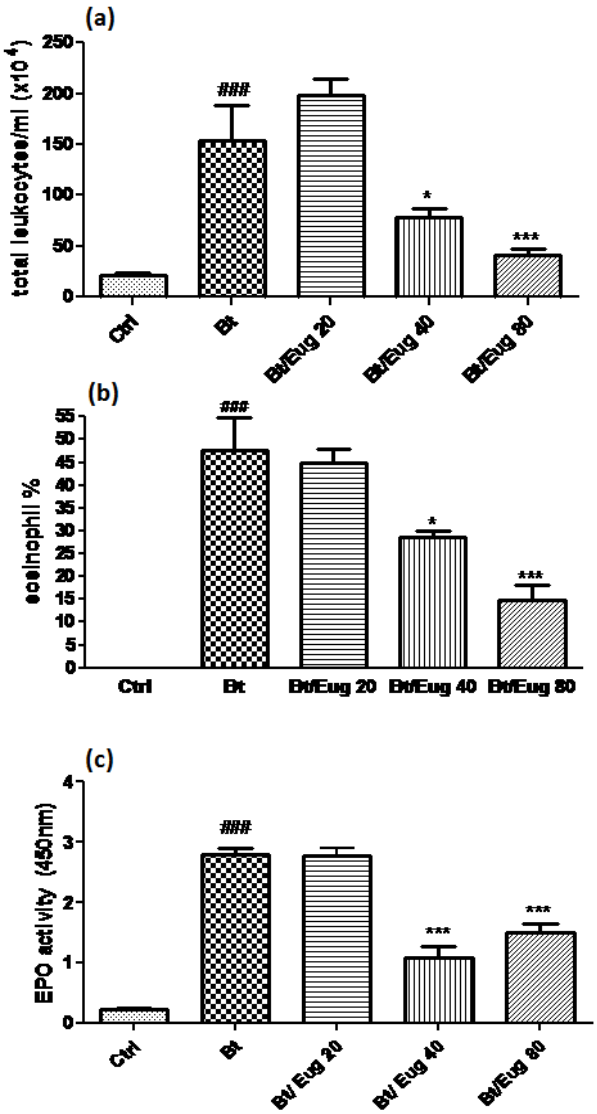

Fig. 1 Effect of Eugenol on leukocytes and EPO activity of Bt sensitized and challenged mouse. (a) Number of total cells; (b) eosinophilia in the BAL and (c) kinetics of EPO (eosinophil peroxidase) activity in lung tissue from Bt-sensitized animals.

Non-sensitized, normal controls mice (Control), Bt-sensitized and challenged animals (Bt), Bt-sensitized and challenged, Eugenol (20 mg/kg, 40 mg/kg or 80 mg/kg) treated mice (Bt/Eug20, Bt/Eug40 or Bt/Eug80). Columns represent the mean values of the results obtained from five animals, and error bars represent the standard error from the means. #$P < 0.05$; ###$P < 0.001$ vs. Control; *$P < 0.05$; ***$P < 0.001$ vs. Bt group.

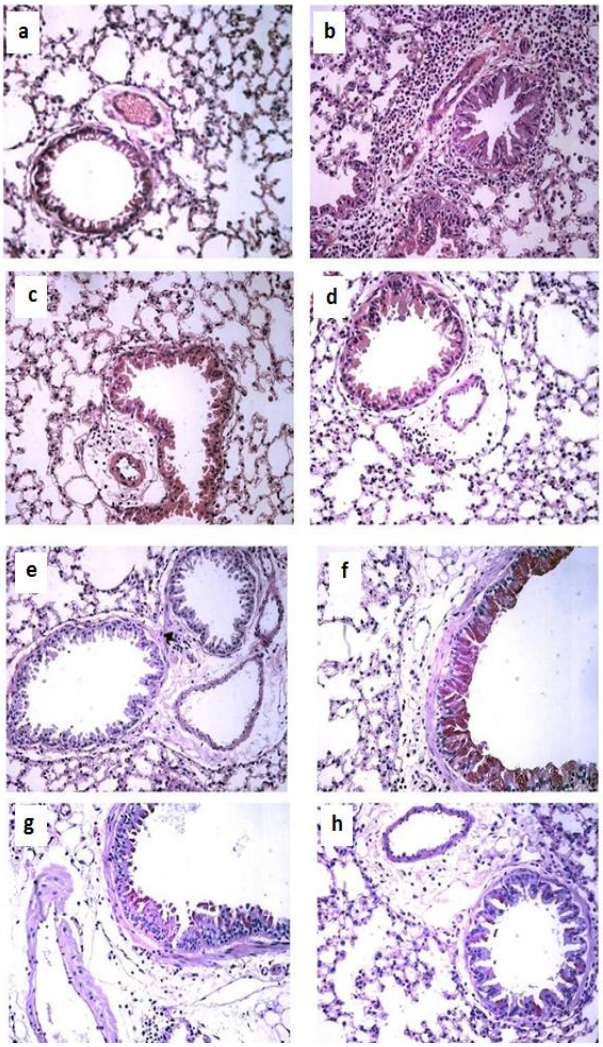

Fig. 2 Effect of Eug (Eugenol) treatment on leukocyte infiltration and mucus production in lung tissues. Sections were stained with hematoxylin-eosin (magnification ×400) (a-d) and sections were stained with periodic acid-Schiff (magnification ×400) (e-h). (a) and (e) Lung section from a control, saline-treated mice; (b) and (f) Lung section from a Bt-immunized and challenged, saline-treated mice; (c) and (g) Lung section from a Bt-immunized and challenged, Eug 40 mg/kg-treated mice; (d) and (h) Lung section from a Bt-immunized and challenged, Eug 80 mg/kg treated mice.

3.4 Treatment with Eugenol Does not Decrease the Levels of Bt-specific IgE, IgG1 and IgG2a Antibodies in the Sera of Bt-sensitized Mice

To assess if eugenol affects anti-*B. tropicalis* specific antibody levels, we evaluated the effect of eugenol on anti-*B. tropicalis* antibody response in Bt-sensitized animals. Bt-sensitized mice produced high levels of specific IgE, IgG1 and IgG2a antibodies than non-sensitized animals ($P < 0.001$). Treatment with eugenol did not reduce significantly serum immunoglobulins levels (Fig. 3).

3.5 Treatement with Eugenol Decreases Levels of Th2-type Cytokines in BAL and Spleen Cells Culture

To determine the possible mechanisms whereby eugenol exerts its modulatory activity in airways from Bt-sensitized animals, levels of the Th (T-helper) type 2 cytokine, typically found during allergic inflammation, were evaluated. Levels of IL-4 in the BAL were higher in Bt-sensitized mice than in the control group ($P < 0.001$) (Fig. 4a). Bt-sensitized animals treated with eugenol had lower levels of this Th2 cytokine in the BAL compared to those untreated mice ($P < 0.01$) (Fig. 4a). However, the oral treatment with eugenol did not affect the levels of regulatory cytokine IL-10 in the BAL (Fig. 4b) of Bt-sensitized mice.

An increased production of Th2 cytokines IL-4, IL-5 and IL-13 was observed in spleen cells stimulated with PWM from Bt-sensitized animals compared with non-stimulated splenocytes. *In vitro* treatment with eugenol (12.5-200 μM) significantly reduced Th2 cytokines (Figs. 5a-5c) in spleen cells culture from Bt-sensitized mice. The concentrations of eugenol herein studied showed 100% cell viability evaluated by MTT assay (data not shown).

3.6 Eugenol Demonstrated a Relaxing Effect o Tracheal Smooth Muscle from Normal Mice

Eugenol (10^{-9}-10^{-3} M), in a concentration-dependent manner, relaxed tracheal smooth muscle isolated from mice without functional epithelium, pre-contracted with the muscarinic agonist carbachol (10 μM). The dataset can be seen in Fig. 6a which shows the concentration-response curve of eugenol where the percentage of maximum relaxation (E_{max}) induced by eugenol was $E_{max} = 112 \pm 3.9$ and $pEC_{50} = 3.7 \pm 0.2$.

In our *in vitro* model of hyper-reactivity using IL-13, tissues that were incubated overnight with IL-13

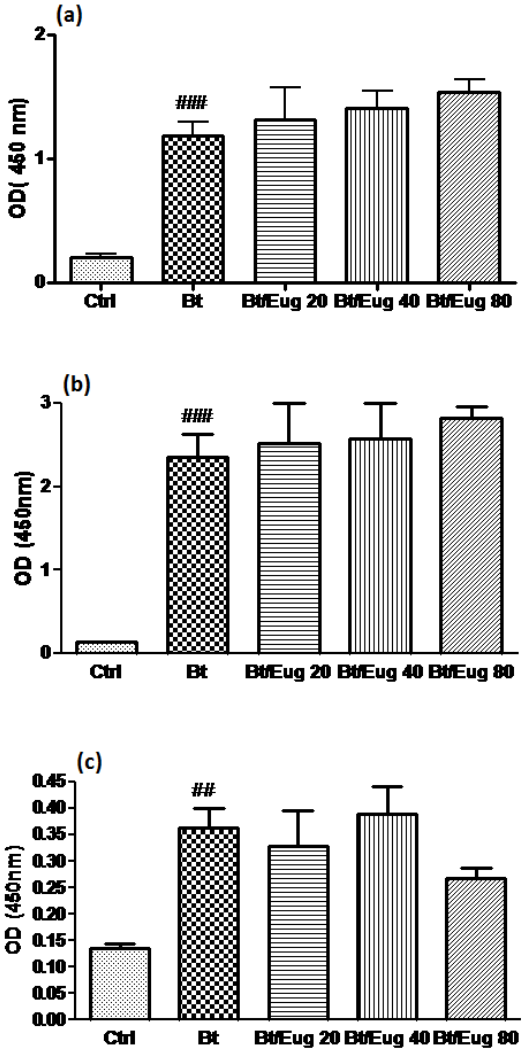

Fig. 3 Effect of Eugenol (Eug) on the levels of (a) IgE, (b) IgG1 and (c) IgG2a anti-*Blomia tropicalis*.

Vehicle-treated and sensitized mice (Control), Bt-sensitized and challenged animals (Bt) and Bt-sensitized and challenged, Eug (20 mg/kg, 40 mg/kg or 80 mg/kg) treated mice (Bt/Eug20, Bt/Eug40 or Bt/Eug80). Antibody levels were measured by indirect ELISA. Columns represent the mean values of the results obtained from five animals, and error bars represent the error deviations from the means. ###$P < 0.001$ vs. Control.

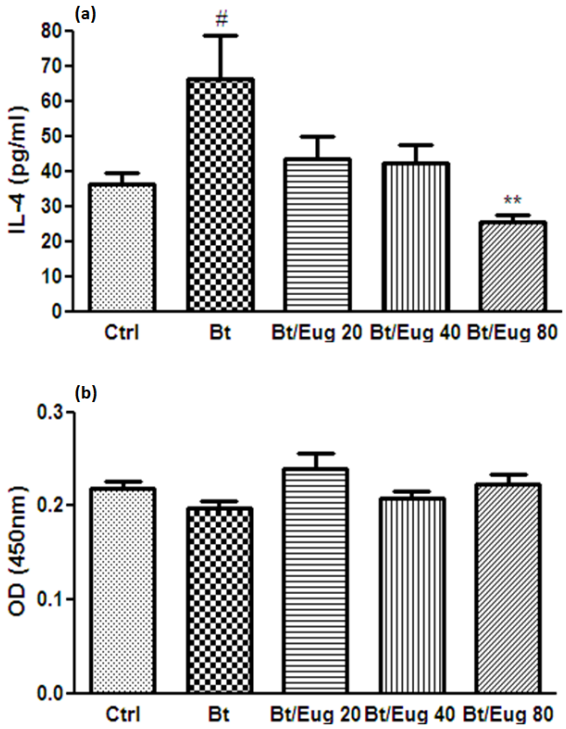

Fig. 4 Effect of Eug (Eugenol) in the cytokines production in BAL. Effect of the treatment with Eug on the levels of (a) IL-4 and (b) IL-10 in the BAL of vehicle-treated and sensitized mice (Control), Bt-sensitized and challenged animals (Bt) and Bt-sensitized and challenged, Eug (20, 40 or 80mg/kg) treated mice (Bt/Eug20, Bt/Eug40 or Bt/Eug80).

Columns represent the mean values of the results obtained from six animals, and error bars represent the standard error from the means. #$P < 0.05$ vs. Control; ###$P < 0.001$ vs control; ** $P <$ 0.01 vs. Bt group and ***$P < 0.001$ vs. Bt group, ANOVA-Tukey.

had a greater constrictor response to CCh (Emax = 0.84 ± 0.09 g), however, without changes in pharmacological potency (pEC_{50} = 6.62 ± 0.14), when compared with non-treated rings (E_{max} = 0.57 ± 0.04 g, pEC_{50} = 6.59 ± 0.08), demonstrating a typical hyper-reactivity in tracheal smooth muscle upon a contracting agent (CCh) (Fig. 6b). The efficacy and potency of eugenol in hyper-reactive tracheal rings sensitized with IL-13 (pEC_{50} = 3.81; E_{max} = 106.70 ± 1.60), were not altered when compared to normal rings, not exposed to IL-13 (pEC_{50} = 3.80; E_{max} = 108.65 ± 1.97) (Fig. 6c).

4. Discussion

The inflammatory response to allergens in the atopic asthmatic lung is a consequence of infiltration on the airway by inflammatory cells, especially eosinophils and is associated with an increased expression of several inflammatory proteins in lung tissue, including cytokines, such as IL-4, IL-5 and IL-13 [25]. The resolution of inflammation is an essential process for the establishment of appropriate host responses and the return to homeostasis [26].

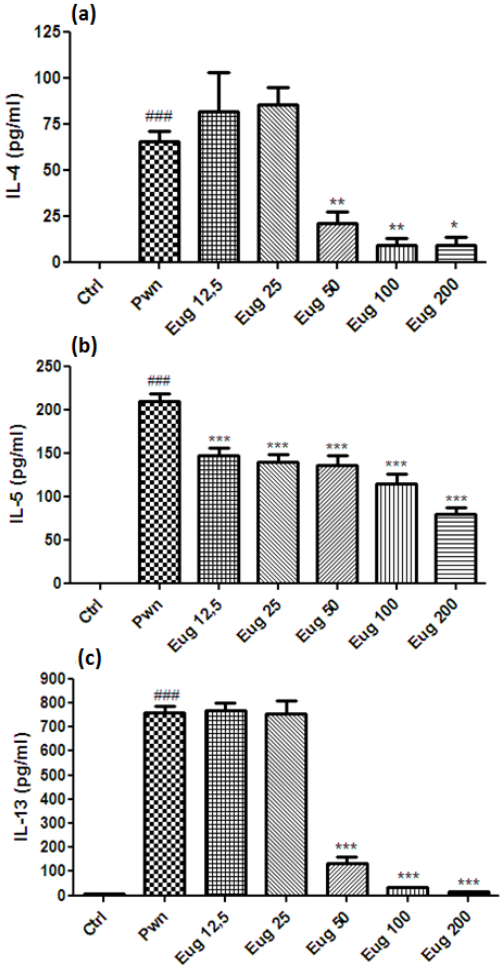

Fig. 5 Effect of Eugenol in the cytokines production in spleen. *In vitro* effect of treatment with eugenol on the levels of: (a) IL-4, (b) IL-5, and (c) IL-13 in spleen cells culture from Bt-sensitized animals. Without stimulation (Control), stimulated with PWM and stimulated with PWM + Eug treatment (12.5-200 µM).

#*P* < 0.05 vs. Control; ###*P* <0.001 vs. Control; **P < 0.01 vs. Bt group and ***P < 0.001 vs. Bt group, ANOVA-Tukey.

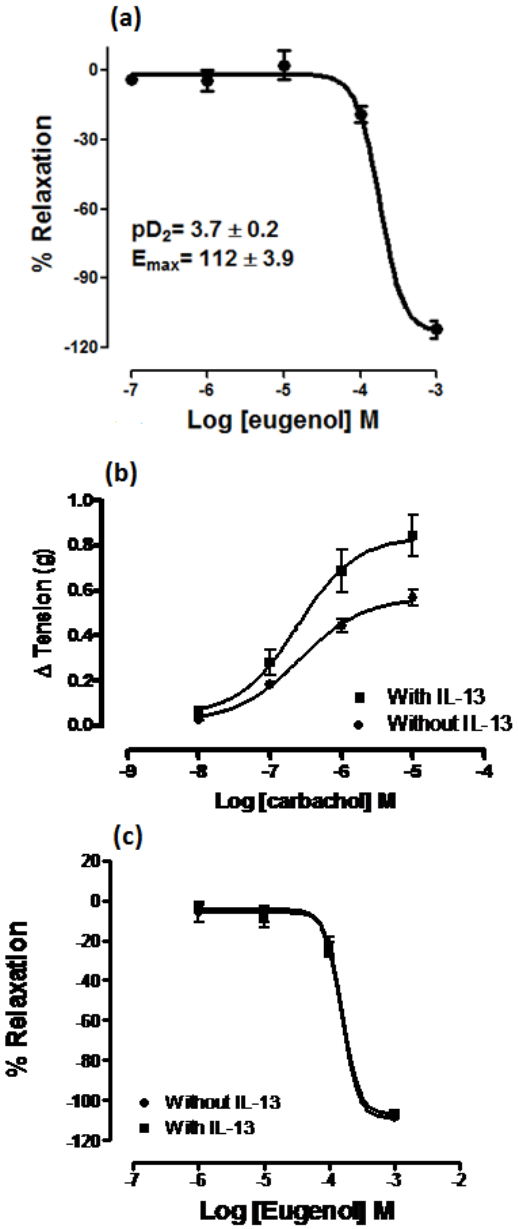

Fig. 6 Effects of Eug (Eugenol) in mice airway smooth muscle. (a) Logarithmic concentration-response curve of relaxant response of eugenol on tracheal rings pre-contracted with 10 µM carbachol, in the absence of functional epithelium (*n* = 6). (b) Concentration response curve showing contracturante effect of the CCh on smooth muscle sensitized or not with IL-13 (*n* = 8) and (c) Concentration response curve showing relaxant effect of the Eug on smooth muscle sensitized or not with IL-13 (*n* = 6). ###*P* < 0,001, ANOVA-Bonferroni.

The use of biologically active natural products is increasing popularity day by day over conventional medicine as an outstanding alternative approach for the treatment of several diseases. However, limited scientific evidence regarding the effectiveness of these natural derivatives, and lack of mechanistic understanding has prevented their incorporation into mainstream medicine and their application in human therapy. Eugenol, an o-methoxyphenol, is of interest for many researchers due to its anti-inflammatory and chemo-preventive effects based on the antioxidant capability of its phenolic group. However, little is known about the effect of eugenol in allergic inflammation mediated by Th2-type cytokines.

The present study was conducted using a murine model of allergic airway disease induced by the sensitization to a common allergen, the *Blomia tropicalis* mite, which was previously characterized by our group as a massive eosinophilic inflammation in the lungs mediated mainly by Th2 cytokines leading to airway luminal narrowing [20]. Using this model, we were able to explore the effect of eugenol on an allergic inflammation induced by a clinically relevant aeroallergen.

As we previously described, sensitization with 100 μg of Bt produced inflammatory cells influx, high levels of EPO and Bt-specific IgE, as well as Th2-type cytokines such as IL-4 in BAL [20]. The treatment with eugenol of Bt-sensitized mice resulted in a great inhibition of airway and lung tissue inflammation, characterized by reduction in: (1) numbers of total inflammatory cells and eosinophils in BAL; (2) inflammatory cell infiltration in the peribronchiolar and perivascular pulmonary region; (3) presence of mucus inside lower airways; (4) levels of EPO in the lung; but did not alter Bt-specific antibodies (IgE, IgG1 and IgG2a) in serum.

Several studies attribute the anti-allergic property of natural products to their ability to reduce the inflammatory cell infiltrate [27-31]. The eosinophilic infiltrate stimulates the production of pro-inflammatory chemokines, cytokines and cytolytic enzymes, including eosinophil cationic protein and major basic protein that degrades integrity of airway epithelium [32]. Accordingly, the increased presence of inflammatory cells and their secreted products in the asthmatic lung often correlates with severity and exacerbation of disease [33]. Reducing eosinophil numbers, when animals are treated with eugenol, may be of relevance to the improvement of inflammation and/or tissue remodeling in allergic asthma. Our results have shown that Eugenol suppresses EPO activity and those results are correlated to the reduction of eosinophilic infiltration observed during the treatment with eugenol.

In order to explore the mechanism whereby eugenol modulates eosinophils infiltration we investigated the effect of this drug on IL-4, IL-5, IL-13 and IL-10 production. Eugenol treatment decreased Th2 cytokines levels of in both *in vitro* (spleen) and *in vivo* (BAL) models. We observed the presence of IL-5 and IL-13 *in vitro* only, probably due to lower levels of these cytokines in BAL in comparison to IL-4. The reduction of IL-4 (*in vitro* and *in vivo*) and IL-5 (*in vitro*) explains, at least in part, modulated inflammation in the lung as well reduced EPO levels in treated animals, since IL-4 is the main cytokine involved in inflammatory Th2-driven response and IL-5 is the principal cytokine involved in the maturation, activation and migration of eosinophils. A study in nasal polyps showed that treatment of the eosinophil-infiltrated tissue with neutralizing anti-IL-5 induced eosinophil apoptosis and decreased tissue eosinophilia [34]. IL-4 is also related to production of IgE, the main immunoglobulin associated with allergic diseases [35], however, no reduction was observed on IgE production. The lack of modulation on IgE despite the decrease in IL-4 and IL-13 could be related to the short-term treatment and the short-term murine model of respiratory disease like ours. IL-13 and IL-4 play an important role in the production of mucus as well. Increased mucus production by goblet cells in the airway epithelium is associated with airway inflammation and asthma. Thus, the reduced production of IL-13 may reflect the decreased production of mucus and improve lung function, as was observed in animals treated with eugenol. The mechanism whereby eugenol inhibits the production of Th2 cytokines is not clear yet. It seems that it was not trough a regulatory mechanism since no alteration was found in IL-10 levels *in vivo* (and *in vitro*, data not shown). Previous studies have shown that eugenol reduces the production of inflammatory cytokines by inhibiting the activation of factor NFkB, an important transcriptional factor that regulates inflammatory response and the expression of inflammatory

cytokines [18, 36]. This may be one of the probable mechanisms of the anti-allergic effect of eugenol.

In addition to anti-inflammatory effect, the experiments with the isolated trachea showed that the eugenol induced a relaxing effect in tracheal smooth muscle pre-contracted with the muscarinic agonist, carbachol, demonstrating a potential as bronchodilator. These results are consistent with studies showing that phenolic compounds are able to relax smooth muscle and improve lung function [19]. Additionally, we evaluated the bronchodilator effect of eugenol in hyperreactive smooth muscle. As a result of inflammation, airway smooth muscle in individuals with asthma becomes hyperresponsive and narrow easily in response to numerous stimuli. This hyperreactivity is non-specific and can occur face to endogenous or exogenous factors [37]. Within the factors involved in hyperreactivity, interleukin-13 (IL-13) has been implicated as a key cytokine [38, 39]. Our study supports these findings. We demonstrated the increased contractility in response to CCh in airway smooth muscle induced by IL-13. The effects of IL-13 on contractility were principally to increase Emax, and no significant changes in EC50 were observed, indicating that IL-13 seemed to increase smooth-muscle contractility rather than induce increased sensitivity to contractile agents (at least CCh), thus demonstrating hyper-reactivity. The effect of eugenol was not altered in hyper-reactive smooth muscle (sensitized with IL-13) when compared to its effect on normal smooth muscle, showing that the bronchodilatory potential of eugenol is not selective for hyperactivity induced by IL-13 pathway. More studies are needed to verify if eugenol may have a selective effect on other mechanisms involved in the hyper-reactivity.

5. Conclusions

The results of the present study, obtained in an experimental model strongly support the potential usefulness of eugenol as antiinflammatory and bronchodilator agent for the treatment of allergic asthma. Additional studies are in progress in our laboratory in order to further elucidate the mechanisms of action whereby eugenol exerts its anti-inflammatory effects.

Acknowledgements

The authors want to thank the Brazilian agencies CNPq, FAPESB and CAPES for financial support. This study was mainly supported by INCT/CNPq Programme, Brazil, Ref 610011/2009-0. We thank also CAPES for KMC's scholarship.

References

[1] M. Kudo, Y. Ishigatsubo, I. Aoki, Pathology of asthma, Front Microbiol 4 (2013) 263.

[2] S. Hashimoto, E.H. Bel, Current treatment of severe asthma, Clin. Exp. Allergy 42 (5) (2012) 693-705.

[3] P.M. O'Byrne, Allergen-induced airway inflammation and its therapeutic intervention, Allergy Asthma Immunol. Res. 1 (1) (2009) 3-9.

[4] P.J. Barnes, How corticosteroids control inflammation: Quintiles Prize Lecture, Br. J. Pharmacol. 148 (3) (2006) 245-254.

[5] S.T. Holgate, Innate and adaptive immune responses in asthma, Nat. Med. 18 (5) (2012) 673-683.

[6] A.B. Kay, The role of T lymphocytes in asthma, Chem. Immunol. Allergy 91 (2006) 59-75.

[7] W. Busse, Asthma diagnosis and treatment: Filling in the information gaps, J. Allergy Clin. Immunol. 128 (2011) 740-750.

[8] L. Bielory, K. Lupoli, Review article: Herbal interventions in asthma and allergy, J. Asthma 36 (1) (1999) 1-65.

[9] C.R. Bezerra-Santos, A. Vieira-de-Abreu, J.M. Barbosa-Filho, C. Bandeira-Melo, M.R. Piuvezam, P.T. Bozza, Anti-allergic properties of Cissampelos sympodialis and its isolated alkaloid warifteine, Int. Immunopharmacol. 6 (7) (2006) 1152-1160.

[10] M.D. Bhuiyan, J. Begum, N.C. Nandi, F. Akter, Constituents of the essential oil from leaves and buds of clove (Syzigiumcaryophyllatum (L.) Alston), African Journal of Plant Science 4 (2010) 451-454.

[11] R.S. Costa, T.C. Carneiro, A.T. Cerqueira-Lima, N.V. Queiroz, N.M. Alcântara-Neves, L.C. Pontes-de-Carvalho, et al., *Ocimum gratissimum* Linn. and rosmarinic acid, attenuate eosinophilic airway inflammation in an experimental model of respiratory

allergy to Blomia tropicalis, Int. Immunopharmacol. 13 (1) (2012) 126-134.

[12] S. Kar Mahapatra, S. Bhattacharjee, S.P. Chakraborty, S. Majumdar, S. Roy, Alteration of immune functions and Th1/Th2 cytokine balance in nicotine-induced murine macrophages: Immunomodulatory role of eugenol and N-acetylcysteine, Int. Immunopharmacol. 11 (4) (2011) 485-495.

[13] Q. Ma, K. Kinneer, Chemoprotection by phenolic antioxidants, Inhibition of tumor necrosis factor alpha induction in macrophages, J. Biol. Chem. 277 (4) (2002) 2477-2484.

[14] Y. Murakami, M. Shoji, A. Hirata, S. Tanaka, I. Yokoe, S. Fujisawa, Dehydrodiisoeugenol, an isoeugenol dimer, inhibit lipopolysaccharide stimulated nuclear factor kappaB activation and cyclooxygenase 2 expression in macrophages, Arch. Biochem. Biophys. 434 (2) (2005) 326-332.

[15] Y.Y. Lee, S.L. Hung, S.F. Pai, Y.H. Lee, S.F. Yang, Eugenol suppressed the expression of lipopolysaccharide-induced proinflammatory mediators in human macrophages, J. Endod. 33 (6) (2007) 698-702.

[16] H.M. Kim, H.E. Lee, C.Y. Kim, J.G. Chung, S.H. Kim, J.P. Lim, et al., Antianaphylactic properties of eugenol, Pharmacol. Res. 36 (6) (1997) 475-480.

[17] T.F. Bachiega, J.P. de Sousa, J.K. Bastos, J.M. Sforcin, Clove and eugenol in noncytotoxic concentrations exert immunomodulatory/anti-inflammatory action on cytokine production by murine macrophages, J. Pharm. Pharmacol. 64 (2012) 610-616.

[18] C.B. Magalhães, D.R. Riva, L.J. DePaula, A. Brando-Lima, V.L. Koatz, J.H. Leal-Cardoso, et al., *In vivo* anti-inflammatory action of eugenol on lipopolysaccharide-induced lung injury, J. Appl. Physiol. 108 (4) (2010) 845-851.

[19] Y.T. Lin, B.N. Wu, C.F. Horng, Y.C. Huang, S.J. Hong, Y.C. Lo, et al., Isoeugenol: A selective beta1-adrenergic antagonist with tracheal and vascular smooth muscle relaxant properties, Jpn. J. Pharmacol. 80 (2) (1999) 127-136.

[20] T. Baqueiro, M. Russo, V.M. Silva, T. Meirelles, P.R. Oliveira, E. Gomes, et al., Respiratory allergy to *Blomia tropicalis*: Immune response in four syngeneic mouse strains and assessment of a low allergen-dose, short-term experimental model, Respir. Res. 11 (2010) 51-59.

[21] J.R. Choi, C.M. Lee, I.D. Jung, J.S. Lee, Y.I. Jeong, J.H. Chang, et al., Apigenin protects ovalbumin-induced asthma through the regulation of GATA-3 gene, Int. Immunopharmacol. 9 (7-8) (2009) 918-924.

[22] H. Takano, N. Osakabe, C. Sanbongi, R. Yanagisawa, K. Inoue, A. Yasuda, et al., Extract of Perillaf rutescens enriched for rosmarinic acid, a polyphenolic phytochemical, Inhibits seasonal allergic rhinoconjunctivitis in Humans, Exp. Biol. Med. 229 (3) (2004) 247-254.

[23] C.R. Bezerra-Santos, F.M. Balestieri, B. Rossi-Bergmann, L.M. Peçanha, M.R. Piuvezam, Cissampelos sympodial is Eichl. (Menispermaceae): Oral treatment decreases IgE levels and induces a Th1-skewed cytokine production in ovalbumin-sensitized mice, J. Ethnopharmacol. 95 (2-3) (2004) 191-197.

[24] H.S. Farghaly, I.S. Blagbrough, D.A. Medina-Tato, M.L. Watson, Interleukin 13 increases contractility of murine tracheal smooth muscle by a phosphoinositide 3-kinase p110 delta-dependent mechanism, Mol. Pharmacol. 73 (5) (2008) 1530-1537.

[25] M.Y. Lee, N.H. Lee, D. Jung, J.A. Lee, C.S. Seo, H. Lee, et al., Protective effects of allantoin against ovalbumin (OVA)-induced lung inflammation in a murine model of asthma, Int. Immunopharmacol. 10 (4) (2010) 474-480.

[26] M.Y. Lee, N.H. Lee, D. Jung, J.A. Lee, C.S. Seo, H. Lee, et al., Anti-inflammatory and anti-asthmatic effects of resveratrol, a polyphenolic stilbene, in a mouse model of allergic asthma, Int. Immunopharmacol. 9 (4) (2009) 418-424.

[27] A.T. Cerqueira-Lima, N.M. Alcântara-Neves, L.C. de Carvalho, R.S. Costa, J.M. Barbosa-Filho, M. Piuvezam, et al., Effects of *Cissampelos sympodialis* Eichl. and its Alkaloid, Warifteine, in an Experimental Model of Respiratory Allergy to Blomia tropicalis, Curr. Drug Targets 11 (11) (2010) 1458-1467.

[28] W.K. Jung, D.Y. Lee, Y.H. Choi, S.S. Yea, I. Choi, S.G. Park, et al., Caffeic acid phenethyl ester attenuates allergic airway inflammation and hyperresponsiveness in murine model of ovalbumin-induced asthma, Life Sci. 82 (13-14) (2008) 797-805.

[29] M. El Gazzar, R. El Mezayen, J.C. Marecki, M.R. Nicolls, A. Canastar, S.C. Dreskin, Anti-inflammatory effect of thymoquinone in a mouse model of allergic lung inflammation, Int. Immunopharmacol. 6 (7) (2006) 1135-1142.

[30] P. Bradding, Asthma: Eosinophil disease, mast cell disease, or both?, Allergy Asthma Clin. Immunol. 4 (2) (2008) 84-90.

[31] K.C. Medeiros, C.A. Figueiredo, T.B. Figueredo, K.R. Freire, F.A. Santos, N.M. Alcantara-Neves, et al., Anti-allergic effect of bee pollen phenolic extract and myricetin in ovalbumin-sensitized mice, J. Ethnopharmacol. 119 (1) (2008) 41-46.

[32] A. Todo-Bom, A.M. Pinto, Fisiopatologia da asma grave, Rev. Bras. Alerg. Imunopatol. 29 (2006) 113-116.

[33] K. Fujimoto, K. Kubo, Y. Matsuzawa, M. Sekiguchi, Eosinophil cationic protein levels in induced sputum correlate with the severity of bronchial asthma, Chest 112

(5) (1997) 1241-1247.

[34] H.U. Simon, S. Yousefi, C. Schranz, A. Schapowal, C. Bachert, K. Blaser, Direct demonstration of delayed eosinophil apoptosis as a mechanism causing tissue eosinophilia, J. Immunol. 158 (8) (1997) 3902-3908.

[35] H. Turner, J.P. Kinet, Signalling through the high-affinity IgE receptor FcεRI, Nature 402 (1999) 24–30.

[36] G. Kaur, M. Athar, M.S. Alam, Eugenol Precludes cutaneous chemical carcinogenesis in mouse by preventing oxidative stress and inflammation and by inducing apoptosis, Mol. Carcinog. 49 (3) (2010) 290-301.

[37] D.C. Doeing, J. Solway, Airway Smooth muscle in the pathophysiology and treatment of asthma, J. Appl. Physiol. 114 (7) (2013) 834-843.

[38] D.M. Walter, J.J. McIntire, G. Berry, A.N. McKenzie, D.D. Donaldson, R.H. DeKruyff, et al., Critical role for IL-13 in the development of allergen-induced airway hyperreactivity, J. Immunol. 167 (8) (2001) 4668-4675.

[39] M. Wills-Karp, Interleukin-13 in asthma pathogenesis, Immunol. Rev. 202 (2004) 175-190.

Journal of Pharmacy and Pharmacology 2 (2014) 50-58

Pandemic A/H1N1 2009 Influenza Virus-like Particles Elicited Higher and Broader Immune Responses than the Commercial *Panenza* Vaccine

Naru Zhang[1,*], Yongping Lin[1,*], Min Chen[1,*], Ho Chuen Leung[1], Chung Sing Chan[1], Kwok Man Poon[1], Jie Zhou[1], Chung Yan Cheung[1], Liwei Lu[2] and Bojian Zheng[1]

1. Department of Microbiology, Li Ka Shing Faculty of Medicine, University of Hong, Hong Kong, China.

2. Department of Pathology, Li Ka Shing Faculty of Medicine, University of Hong, Hong Kong, China.

Received: October 14, 2013 / Accepted: December 03, 2013 / Published: February 28, 2014.

Abstract: Objectives: The aim was to construct 2009 pandemic A/H1N1 influenza VLPs (virus-like particles) and compare the immunogenicity and protection efficacy with the commercial *Panenza* vaccine in BALB/c mouse model. Methods: VLPs derived from influenza A/Hong Kong/01/2009 (H1N1) virus were constructed by Bac-to-Bac baculovirus expression system. VLPs were purified by sucrose density gradient ultracentrifugation and then characterized by Western blotting analysis and transmission electron microscopy. After single dose vaccination with 3 μg of VLPs and equal amount of *Panenza* vaccine, the immune responses and efficacy of protection induced by VLPs were compared with those elicited by the *Panenza* vaccine in 6-8 weeks old female BALB/c mice. Key findings: VLPs could induce higher antibody titer as determined by hemagglutinin inhibition and microneutralization assay. Furthermore, we demonstrated that VLPs induced better antibody response to neuraminidase. In addition, VLP vaccinated mice had stronger cell-mediated immune response. As a result, our VLPs conferred 100% protection while the *Panenza* vaccine only conferred 67% protection. Conclusion: From the results, we concluded that influenza VLPs are highly immunogenic and they are promising to be developed as an alternative strategy to vaccine production in order to control the spread of influenza viruses.

Key words: Influenza virus, virus-like particle, *Panenza* vaccine, BALB/c mice.

1. Introduction

Influenza A virus belongs to the Orthomyxoviridae family and its genome contains 8 negative-sense, single stranded RNA segments encoding 11 viral proteins. On the viral surface, there are two glycoproteins named HA (hemagglutinin) and NA (neuraminidase). The structural matrix protein (M1) is the most abundant which is found underneath the lipid membrane. In April, 2009 CDC of the United States of America announced the detection of a novel strain of influenza virus in humans [1]. This novel virus transmitted rapidly among humans throughout the world, and on May 1st, Hong Kong declared a state of health emergency following the first confirmed case of swine influenza A H1N1 flu in the territory. On June 11th, the World Health Organization raised the worldwide pandemic alert level into phase 6 [2].

Vaccination is widely considered to be one of the most effective preventive strategies for the control of seasonal as well as pandemic influenza viruses. The current influenza vaccine is usually prepared from virus that is grown in embryonated chicken eggs. The virus is isolated from the allantoic fluids and then inactivated with formaldehyde or ß-propiolactone. Alternatively, the purified virus is treated with detergent for "split" or "subunit" vaccine formulation

* Equal contribution.

Corresponding author: Bojian Zheng, Ph.D., professor, research fields: virology and immunology. E-mail: bzheng@hkucc.hku.hk.

[3]. VLPs (Influenza virus like particles) are being developed as a new generation of non-egg based cell culture-derived vaccine against influenza infection during a pandemic threat [4]. This new generation vaccine has several advantages over the traditional egg-based strategies, especially in its high yield and short production time [5]. Several laboratories have successfully constructed influenza VLPs [6-13], however, there has been no report comparing the immunogenicity between VLPs with the commercially available vaccine. To afford a better understanding of VLPs' immunogenic efficacy, we constructed VLPs derived from an influenza A (H1N1) 2009 virus and then made a comparison on induction of immune responses and protection efficacy with the commercial *Panenza* inactivated vaccine for the first time in mice.

2. Materials and Methods

2.1 Recombinant Plasmid Construction

Viral RNA was extracted from influenza A/Hong Kong/01/2009 (H1N1) (HK/01) virus isolate according to the manufacturer's instructions (RNeasy Mini Handbook, QIAGEN) and cDNA was synthesized by influenza unit 12 primer and superscript II reverse transcriptase (Invitrogen). Segment PCR of HA and NA and full length of M1 PCR were then conducted using primers for the synthesis of the HA, NA, and M1 listed in Tables 1−3, respectively and cDNA fragments were then cloned into PCR2.1-TOPO vector (Invitrogen). The nucleotide sequences of the HA, NA, and M1 genes were identical to the online published sequences (GenBank GQ168606.1, GQ457486.1 and FJ966954).

The full length of HA gene was cloned as a SalI-NotI DNA fragment downstream of the AcMNPV polyhedrin promoter within pFastBac1 transfer vector (Invitrogen). The full length of NA and M1 genes were cloned as EcoRI-XhoI DNA fragments into the same enzyme digested pFastBac1 plasmid. The three resulting baculovirus transfer plasmids were designated pHA, pNA, and pM1, located downstream of the AcMNPV polyhedrin promoter and upstream of the SV40 polyadenylation signal. Then pNA was digested with SnaBI and HpaI, and the fragment was ligated into the HpaI site of pHA, which resulted the

Table 1 Primers used for HA gene amplification.

Primer name	Sequence (5'--3')
F-VLP-HA-F	ACGCGTCGACATGAAGGCAATACTAGTAG
F-VLP-HA-MR	TCTAGAAGGTTTACAGAGTGTG
F-VLP-HA-MF	CACACTCTGTAAACCTTCTAGA
F-VLP-HA-R	ACGCGCGGCCGCTTAAATACATATTCTACACTG

The underlined nucleotides indicate recognition sites of SalI and NotI.

Table 2 Primers used for NA gene amplification.

Primer name	Sequence (5'--3')
F-VLP-NA-F	CCGGAATTCATGAATCCAAACCAAAAGAT
F-VLP-NA-MR	GCTGATGTTTACATATGTCTG
F-VLP-NA-MF	CAGACATATGTAAACATCAGC
F-VLP-NA-R	CGCCGCTCGAGTTACTTGTCAATGGTAAATGGCA

The underlined nucleotides indicate recognition sites of EcoRI and XhoI.

Table 3 Primers used for M1 gene amplification.

Primer name	Sequence (5'--3')
F-VLP-M1-F	CCGGAATTCATGAGTCTTCTAACCGAGG
F-VLP-M1-R	CCGCCGCTCGAGTCACTTGAATCGCTGCATCTGCAC

The underlined nucleotides indicated recognition sites of EcoRI and XhoI.

pHANA recombinant DNA. Then the fragment of pM1 digested with SnaBI and AvrII was ligated into pHANA fragment digested with HpaI and AvrII, thus yielding the recombinant plasmid pHANAM1.

2.2 Generation of Recombinant Baculoviruses

The recombinant baculoviruses were generated by Bac-to-Bac baculovirus expression system (Invitrogen). Briefly, the plasmid pHANAM1 was transformed into *E. coli* DH10Bac competent cells (Invitrogen). The recombinant bacmid DNA was extracted and transfected into Spodoptera frugiperda (Sf9) insect cells for recombinant baculovirus packaging with Lipofectamine 2000 reagent (Invitrogen). After 3 days, the recombinant baculovirus in the supernatant was collected as P1 viral stock and further amplified into P2 and P3 viral stock. The virus titer of P3 viral stock was determined by plaque assay using Sf9 insect cells.

2.3 VLP Production and Purification

The Sf9 insect cells were infected with P3 recombinant baculoviruses (MOI = 3) at a cell density of 2×10^6/mL in 200 mL suspension culture. The culture supernatant was harvested at 72 h post-infection and the VLPs were pelleted by ultracentrifugation (Rotor-SW32Ti) and resuspended in phosphate-buffered saline (PBS) solution (pH 7.2), loaded onto a 20%-60% (*w*/*v*) discontinuous sucrose in NTE buffer (100 mM NaCl, 10 mM Tris-Cl pH 7.4, 1 mM EDTA) and ultracentrifuged (Rotor-SW41Ti). Fractions were collected and analyzed by 10% polyacrylamide gel electrophoresis and Western blot using anti-HA, anti-NA and anti-M1 rabbit polyclonal antibodies (Immune technology). Bovine serum albumin was used as a standard to quantitate the amount of HA protein [14]. Quantitative densitometry of proteins stained with coomassie blue was performed using the Odyssey application software version 3.1 (Li-Cor Bioscience).

2.4 Transmission Electron Microscopy

The fractions containing influenza VLPs were collected, negatively stained and then examined by transmission electron microscope. For negative staining, VLPs were loaded onto plastic carbon-coated 400-mesh copper grids for 2 min, stained with 1% uranyl acetate (pH 6.5) for 2 min and then rinsed gently with a few drops of distilled water. The grids were wicked dry with filter paper and then observed by transmission electron microscope (Philips EM 208s).

2.5 BALB/c Mice Immunization and Influenza Virus Challenge

Female BALB/c mice at the age of 6-8 weeks were used in this study. All of the mice were housed in the animal facility in accordance with the animal care protocol. The animal studies have been approved by the CULATR (Committee on the Use of Live Animals in Teaching and Research) of the University of Hong Kong. Three groups each consisting of fifteen mice were vaccinated on day 0. Mice were anesthetized with Phenobarbital and then group 1 were inoculated intramuscularly (i.m.) with 3 μg (based on HA content) of the commercial *Panenza* vaccine. Group 2 were inoculated with 100 μL VLPs containing the same amount of HA protein. The negative control group 3 received equal volume of PBS. Serum samples were taken before inoculation as well as on day 21. On day 21, 3 mice in each group were sacrificed for spleen extraction and the remaining mice were challenged intranasally with $10LD_{50}$ of mouse adapted influenza HK/01 virus [15]. Animals are monitored for daily activity after viral challenge. On day 5 post-viral challenge, 3 mice in each group were sacrificed for lung tissue extraction. Half of the lung was fixed in 10% formaldehyde for histological analysis and the other half was homogenized for virus titer titration in MDCK (Madin-Darby canine kidney) cells by plaque assay. The remaining 9 mice in each group were used for the calculation of the survival rate.

2.6 Histopathologic Examination

For microscopic evaluation of the pathologic changes in the lung tissues, 3 mice in each group were sacrificed and the lungs were immediately fixed in 10% paraformaldehyde. After fixation, they were embedded in paraffin. Sections were made at 4 to 6 μm thickness and mounted on slides. Histopathological changes caused by influenza virus infection were examined by H&E (haematoxylin and eosin) staining under light microscope.

2.7 ELISA for Detection of HA Specific IgG Antibodies

ELISA was conducted to measure the levels of HA-specific IgG antibodies in immunized mouse sera. Briefly, 96-well plates were coated with 100 ng recombinant HA protein per well overnight at 4 ℃. After washing with PBST (PBS containing 0.05% Tween 20), the plates were blocked with 200 μL blocking buffer overnight at 4 ℃. After washing, sera with serial dilutions were added in triplicates and incubated at 37 ℃ for 1 h. After washing, the plates were incubated at 37 ℃ for 30 min with a secondary goat anti-mouse antibody conjugated with horseradish peroxidase (Invitrogen) diluted in diluent buffer. After washing, the plates were incubated for 10 min with TMB substrate solution. The reaction was stopped by 1M H_2SO_4 and the absorbance was then measured at 450 nm using an ELISA reader (Tecan Group Ltd., Switzerland).

2.8 HI (Hemagglutinin Inhibition) Assay

The primary assay for determining the amount of influenza-specific antibody present in vaccinated mouse sera is the HI assay [16]. To inactivate non-specific inhibitors, one part of mice sera were treated with three parts of RDE II (receptor destroying enzyme II) and incubated at 37 ℃ for 18 h. Then the RDE II was inactivated at 56 ℃ water bath for 30 min and PBS was added, creating 1:10 starting dilution of sera. RDE II-treated sera were two-fold serially diluted in triplicates in 96-well plates (Greiner bio-one, Germany). An equal volume of HK/01 virus, adjusted to 8 HAU/50 μL was added into each well. The plates were incubated at 37 ℃ for 1 h followed by the addition 50 μL per well of 0.5% turkey erythrocytes. The plates were then incubated at room temperature for 1 h. The HI titer was determined as the highest serum dilution able to completely inhibit hemagglutination [17].

2.9 Neutralization Assay

Mouse sera were tested on MDCK cells for neutralization assay according to the WHO manual. Briefly, sera were heat inactivated at 56 ℃ for 30 min and prepared at 1:10 starting dilution, followed by 2-fold dilutions. The serially diluted sera were incubated with HK/01 virus of $100TCID_{50}$/60 μL at 37 ℃ for 1 h. The 96-well plates with MDCK cells were washed with PBS and then 100 μL of neutralized samples were transferred to the cell culture plates. Virus back titration was also included during the procedure. The plates were incubated at 37 ℃ for 3 days to record cytopathic effect.

2.10 Quantification of Released Viral RNA by Quantitative Real-Time PCR

MDCK cells were infected with HK/01 virus at high MOI of 3. After 2 h infection, the cells were washed 3 times and the cell culture plates were refilled with fresh medium containing different concentrations of sera. At 6 h post-infection, both the supernatant and cell pellets were collected and viral RNA from infectious viruses was quantified by real-time PCR with SYBR green PCR Master Mix (Stratagene). Primers of real-time PCR for HA gene were: HA-Forward:
5’-CAATAAGACCCAAAGTGAGGG-3’;
HA-Reverse:
5’-AATCGTGGACTGGTGTATCTG-3’. β-actin primers which were used to detect viral RNA copies in the cell pellet were β-actin-Forward: 5’-GAGACCTTCAACACCCCGG-5’ and β-actin Reverse: 5’-ATGTCGCGCACG ATTTCCC-3’.

2.11 ELISpot Assay

Mouse spleens were extracted for ELISpot assay on day 21 before virus challenge. Diluted antibodies for IFN-γ, IL-2 and IL-4 were coated onto plates and incubated overnight at 4 ℃. The plates were washed thoroughly with PBS and blocked by RPMI-1640 containing 10% FBS and 1% P/S, and incubated at room temperature for more than 2 h. During incubation, the splenocytes were isolated and determined as previously described [5]. Splenocytes in culture medium at 1×10^6/well were stimulated with recombinant HA protein (Immune Technology) and HA, NA peptides (HAI-535: IYSTVASSL and NAI-73: CPISGWAI) (Gl Biochemistry Shanghai Ltd) in 5% CO_2; 37 ℃ humidified incubator for 36 h. Then the plates were washed thoroughly with 0.05% PBST, the diluted detection antibodies were added and the plates were incubated at room temperature for 2 h. After washing, diluted streptavidin peroxidase was added into each well and the plates were incubated at room temperature for 45 min. The plates were washed again and TMB substrate solution was added into each well. The spot development was monitored with the help of hand-held magnifier and the color development was terminated with ddH_2O. The plates were air dried and spots were counted by an ImmunoSpot ELISPOT reader (Cellular Technology Ltd., USA).

2.12 Statistical Analysis

Data are presented as the arithmetic mean values of two experiments plus SD (standard deviation). Statistical significance compared between VLP and *Panenza* vaccinated mouse samples was indicated by student's *t*-test.

3. Results and Discussion

3.1 VLP Generation and Characterization

The recombinant transfer bacmid DNA was successfully constructed containing the three genes of HA, NA and M1 and they were within their own expression cassette, downstream of the AcMNPV polyhedrin promoter and upstream of the SV40 polyadenylation signal (Fig. 1a). Bovine serum albumin was used as a standard to quantitate the amount of HA protein in VLPs (Fig. 1b). In order to confirm that the influenza HA, NA, and M1 proteins were co-expressed, the VLPs fractions were analyzed by Western blotting using polyclonal antibodies to the three proteins. As shown in Fig. 1c, the three proteins were successfully co-expressed. Aliquot of concentrated VLPs were negative stained for transmission electron microscopy and Fig. 1d shows that the three proteins were self-assembled into particles with morphology similar to the real virus particles.

3.2 VLP Vaccination Provided Complete Protection against Lethal Challenge with HK/01 Virus

The BALB/c mice were i.n. inoculated with 10 LD_{50} of influenza HK/01 virus. All the mice in the negative control group which was vaccinated with PBS did not survive beyond day 8 after virus challenge, whereas all VLP vaccinated mice survived. In contrast, *Panenza* provided incomplete protection against lethal viral challenge, in which only about 67% (8/12) mice survived (Fig. 2a). The result indicated that VLP vaccination could provide more potent protection against lethal challenge with HK/01 virus. Virus titer in lung tissues was detected by plaque assay and it was found that the virus titer in VLP vaccinated mouse lungs was significantly lower than that in *Panenza* vaccinated mouse lungs (Fig. 2b).

3.3 Absence of Histopathological Changes in Lung Tissues of Mice Vaccinated with VLPs

Histopathological changes of mouse lung sections collected at 5 days post-challenge were further examined by H&E staining (Fig. 3). Compared to the uninfected mice (Fig. 3d), lung tissues of PBS injected (unvaccinated) mice showed severe inflammation with intensive infiltration of lymphocytes and marked tissue

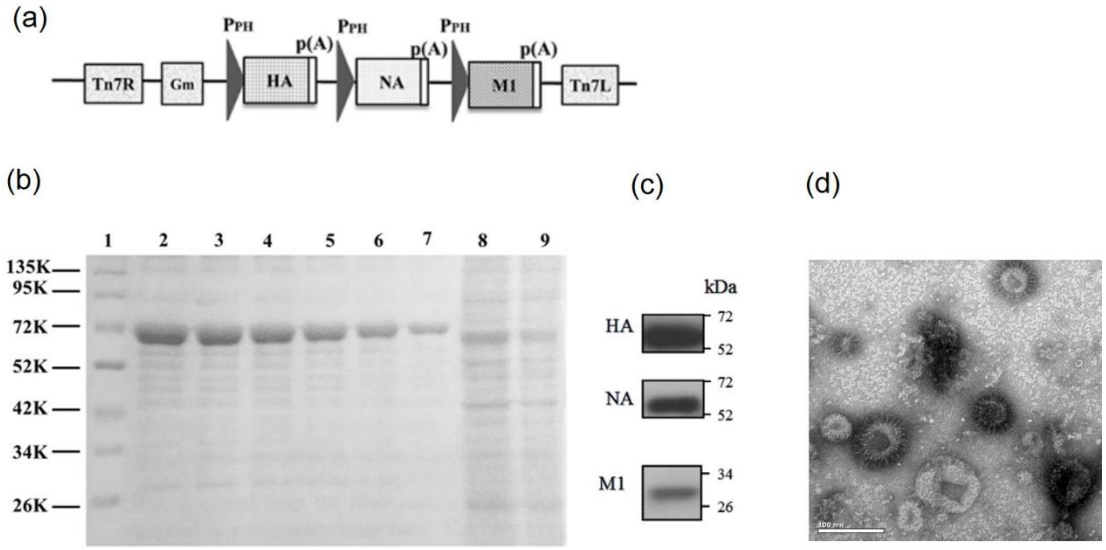

Fig. 1 (a) VLP expression cassette. Indicated are the polyhedrin promoter (P_{PH}), polyadenylation signal (p(A)), Tn7 regions, gentamicin resistance gene (Gm), and HA, hemagglutinin; NA, neuraminidase; M1, matrix 1 genes; (b) SDS-PAGE of purified VLPs stained with gel code reagent. Lane 1, Amersham full-range rainbow molecular weight marker; lanes 2-7, BSA 6 μg, 5 μg, 4 μg, 3 μg, 2 μg, 1 μg; lanes 8-9, 20 μL, 10 μL VLPs; (c) Western blot analysis of VLPs for HA, NA and M1 proteins; (d) Transmission electron micrograph of negatively stained VLPs (x 39,000).

damage (Fig. 3c). The lung sections of the mice vaccinated with *Panenza* exhibited some level of inflammatory responses, which were evidenced by lymphocyte infiltration in some area of the lung tissues, but no obvious tissue damage was observed (Fig. 3a). In contrast, no histopathological changes were found in lung tissues of the mice vaccinated with VLPs (Fig. 3b).

3.4 VLP Vaccination Induced Higher Levels of Protective Antibodies

To understand the underlined mechanism as to why VLP vaccination could provide more potent protection against the lethal challenge of the virus, serial assays were performed. As shown in Fig. 4a, the titer of HA-specific IgG antibody was much higher in VLP vaccinated group than that in *Panenza* vaccinated group. HI assay is considered to be the gold standard to evaluate the immunogenic efficiency in influenza vaccine studies, with an HI titer over 40 is considered as a representative marker for protection. While from Fig. 4b, the HI titer in *Panenza* vaccinated group was only around 20 which was not high enough to provide potent protection. It is possible that VLPs are more immunogenic over the clinical *Panenza* vaccine because VLPs contain multiple copies of HA antigens presented in an organized array, thus allowing better activation of the immune responses. Neutralization antibody plays an important role in protecting against foreign antigens. Normally, neutralizing antibody titer reaching 20-40 may provide partial protection against lethal viral challenge, while it may provide complete protection against lethal viral infection when neutralizing antibody titer is over 40. From Fig. 4c, the neutralization titer in *Panenza* vaccinated group was only 20 which was not high enough to confer complete protection. However the neutralization titer in VLP vaccinated group reached 80 which was high enough to provide potent protection in mice.

3.5 VLP Vaccination Induced Higher Levels of Antibodies which Inhibited Virus Release from Infected MDCK Cells

It has been reported that NA vaccination can induce antibodies which may inhibit influenza virus release from the infected cells [18, 19]. The presence of NA

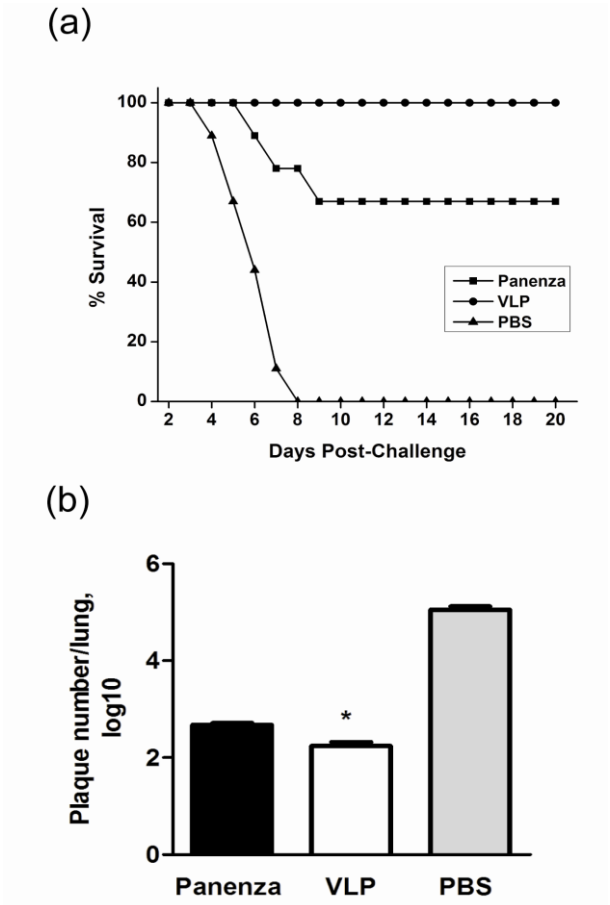

Fig. 2 Protection efficacy in BALB/c mice. On day 22 after vaccination, mice were challenged with 10LD_{50} of influenza HK/01 virus. 5 days later, three mice in each group were sacrificed and the lungs were extracted for virus titer determination. The remaining 9 mice in each group were monitored for 20 days for survival rate calculation. (a) Mouse survival rate. Virus titer in lungs was determined by (b) plaque assay 5 days after lethal virus challenge. Statistical significance compared among VLP and *Panenza* vaccinated mice was indicated by student's *t*-test.

antibodies were verified by testing whether the sera from the vaccinated mice could inhibit virus release from infected cells. The serum samples were added to the cell cultures after the cells have been infected with high MOI (MOI = 3) of virus. The culture supernatant and cell pellets were collected at 6 h post-infection and the viral RNA copies were determined by real-time PCR. Viral RNA copies in cell pellets of all cultures showed similar levels (Figure not shown). Viral RNA copies in the culture supernatant in the presence of 20 folds diluted serum samples from mice vaccinated with

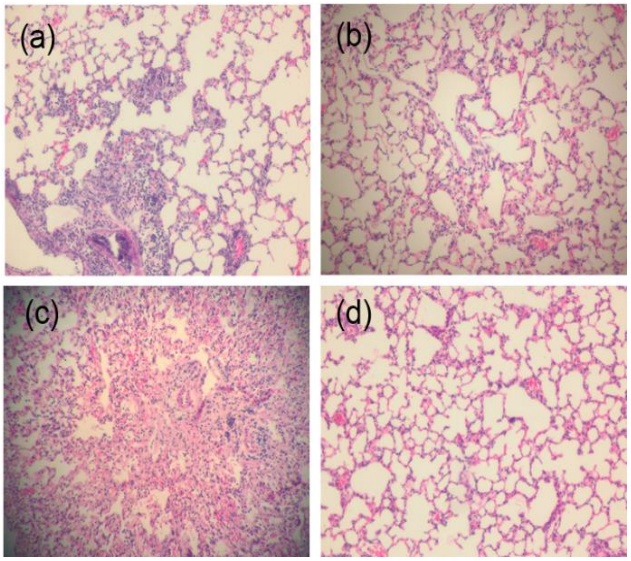

Fig. 3 Detection of histopathological changes in lung tissues after lethal challenge of HK/01 virus. On day 5 post-viral challenge, 3 mice in each group were sacrificed for lung tissue extraction. Lung tissues were collected from mice vaccinated with (a) *Panenza* vaccine; (b) VLP and (c) PBS control at 5 days post-virus challenge; (d) Lung section from uninfected normal mouse was included as control. Histopathological changes were detected by H&E staining.

VLP and *Panenza* vaccine were about 10 folds and 2 folds lower, respectively, than in the presence of sera from the mice vaccinated with the PBS control (Fig. 5). The results suggested that mice vaccinated with VLPs elicited higher levels of neutralizing NA antibodies than in those vaccinated with the *Panenza* vaccine.

3.6 VLP Vaccination Evoked Strong Cell-Mediated Immunity in Mice

The other important protective factors against viral infections that potentially induced by vaccination are cell-mediated immune responses [19, 20]. Thus, we further evaluated viral specific T help cell and CTL responses in the vaccinated mouse spleens (Fig. 6). The results showed that VLP vaccination indeed induced significantly higher levels of HA specific IL-2 and IFN-γ secreting Th1 cells than that of *Panenza* vaccination. Importantly, VLP vaccination elicited significantly higher levels of HA and NA specific CTL responses. T cell responses, particularly CTL responses, are very important in limiting viral infection and

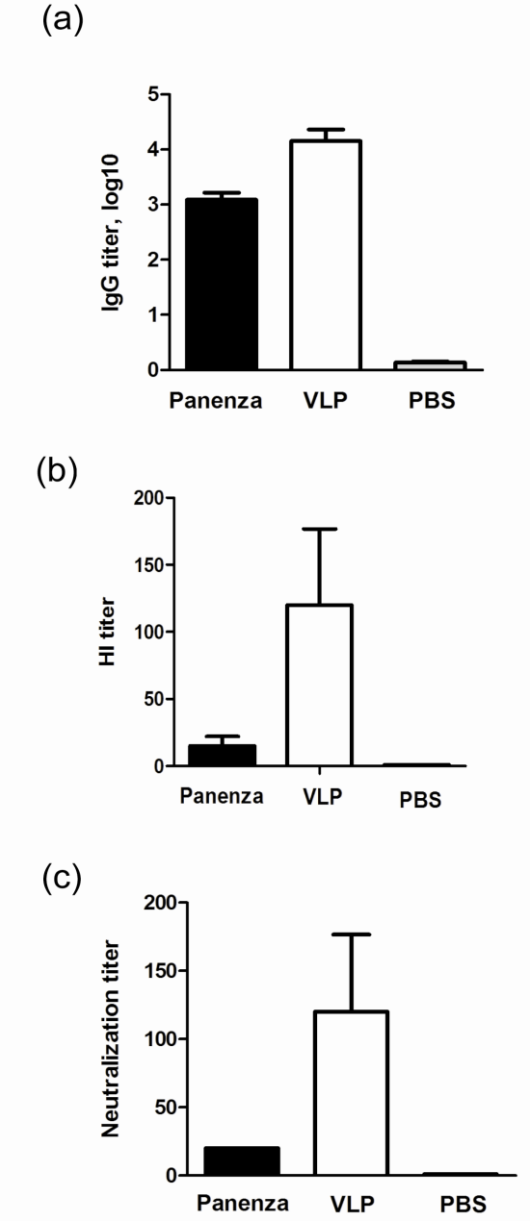

Fig. 4 Antibody responses. On day 21, mouse sera in all three groups vaccinated with *Panenza*, VLP and PBS were collected. (a) IgG titer; OD (Optical densities) were read at 450 nm; (b) HI titer and (c) Neutralization antibody titer, were determined. Results are expressed as the arithmetic means ± SD (n = 3). Statistical significance compared between samples from VLP and *Panenza* vaccinated mice was indicated by student's t-test.

response to the virus clearance [21]. Thus, the results indicated that high levels of T cell responses evoked by VLP vaccination should play a key role, at least in part, in the potent protection against lethal viral infection.

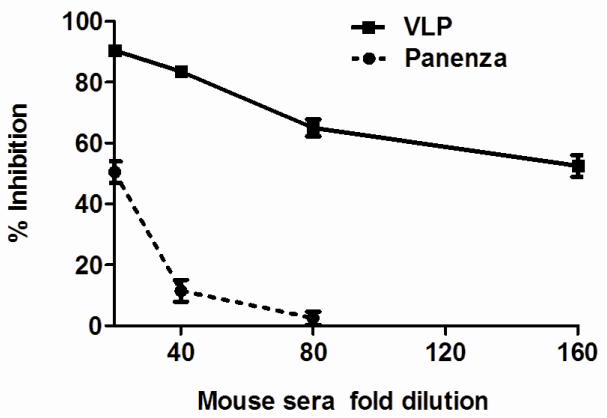

Fig. 5 Detection of inhibitory effect of vaccinated mouse sera to the virus release. MDCK cells were infected with HK/01 virus at MOI of 3. Mouse sera were added to the culture supernatants at 2 h post-infection, the supernatants were collected at 6 h post-infection and the viral RNA copies were measured by real-time PCR. The results are expressed as relative viral RNA copies ±SD.

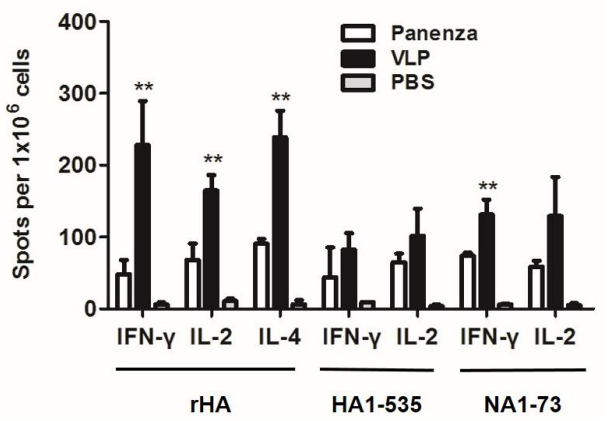

Fig. 6 Detection of specific T helper cell and CTL responses in vaccinated mice. Splenocytes were collected 21 days post-vaccination. Splenocytes (1×10^6) were stimulated with rHA (for T help cells), HA1-535 and NA1-73 (both for CTLs). Influenza HA specific IFN-γ, IL-2 and IL-4 screening T helper cells, HA1-535 and NA1-73 specific IFN-γ and IL-2 producing CTLs were detected by ELISpot. The results are presented as the mean values of two experiments ±SD. Statistical significance ($P < 0.05$) compared among VLP and *Panenza* vaccinated mice was indicated by student's t-test.**

4. Conclusions

In this study, the immune responses and efficacy of protection induced by VLPs were compared with those elicited by the commercial *Panenza* vaccine in female BALB/c mice for the first time. Our results indicate

that VLPs are highly immunogenic and they can induce higher and broader immune responses than the clinically used *Panenza* vaccine, which reinforce that influenza vaccine using VLPs is quite a promising alternative in the future.

Acknowledgments

We would like to thank Professor KY Yuen (Department of Microbiology, HKU) who kindly offered us the clinically used *Panenza* vaccine. We would also thank Mr. WS Lee (Electron Microscope Unit, HKU) for his technical assistance.

References

[1] B. Manicassamy, R.A. Medina, R. Hai, T. Tsibane, S. Stertz, E. Nistal-Villan, et al., Protection of mice against lethal challenge with 2009 H1N1 influenza A virus by 1918-like and classical swine H1N1 based vaccines, PLoS Pathog. 6 (1) (2010) e1000745.

[2] WHO, Influenza A (H1N1): Special Insights, http://www.who.int/en, 2009.

[3] T. Horimoto, Y. Kawaoka, Designing vaccines for pandemic influenza, Curr. Top Microbiol. Immunol. 333 (2009) 165-176.

[4] S.M. Kang, J.M. Song, F.S. Quan, R.W. Compans, Influenza vaccines based on virus-like particles, Virus Res. 143 (2) (2009) 140-146.

[5] T.M. Ross, K. Mahmood, C.J. Crevar, K. Schneider-Ohrum, P.M. Heaton, R.A. Bright, A trivalent virus-like particle vaccine elicits protective immune responses against seasonal influenza strains in mice and ferrets, PLoS One 4 (6) (2009) e6032.

[6] D. Matassov, A. Cupo, J.M. Galarza, A novel intranasal virus-like particle (VLP) vaccine designed to protect against the pandemic 1918 influenza A virus (H1N1), Viral Immunol 20 (3) (2007) 441-452.

[7] A. Prel, G. Le Gall-Recule, V. Jestin, Achievement of avian influenza virus-like particles that could be used as a subunit vaccine against low-pathogenic avian influenza strains in ducks, Avian Pathol. 37 (5) (2008) 513-520.

[8] R.A. Bright, D.M. Carter, C.J. Crevar, F.R. Toapanta, J.D. Steckbeck, K.S. Cole, et al., Cross-clade protective immune responses to influenza viruses with H5N1 HA and NA elicited by an influenza virus-like particle, PLoS One 3 (1) (2008) e1501.

[9] K. Mahmood, R.A. Bright, N. Mytle, D.M. Carter, C.J. Crevar, J.E. Achenbach, et al., H5N1 VLP vaccine induced protection in ferrets against lethal challenge with highly pathogenic H5N1 influenza viruses, Vaccine 26 (42) (2008) 5393-5399.

[10] P. Pushko, T.M. Tumpey, F. Bu, J. Knell, R. Robinson, G. Smith, Influenza virus-like particles comprised of the HA, NA, and M1 proteins of H9N2 influenza virus induce protective immune responses in BALB/c mice, Vaccine 23 (50) (2005) 5751-5759.

[11] S.M. Kang, D.G. Yoo, A.S. Lipatov, J.M. Song, C.T. Davis, F.S. Quan, et al., Induction of long-term protective immune responses by influenza H5N1 virus-like particles, PLoS One 4 (3) (2009) e4667.

[12] M.A. D'Aoust, P.O. Lavoie, M.M. Couture, S. Trepanier, J.M. Guay, M. Dargis, et al., Influenza virus-like particles produced by transient expression in Nicotiana benthamiana induce a protective immune response against a lethal viral challenge in mice, Plant Biotechnol. J. 6 (9) (2008) 930-940.

[13] Z. Wen, L. Ye, Y. Gao, L. Pan, K. Dong, Z. Bu, et al., Immunization by influenza virus-like particles protects aged mice against lethal influenza virus challenge, Antiviral Res. 84 (3) (2009) 215-224.

[14] J.M. Galarza, T. Latham, A. Cupo, Virus-like particle (VLP) vaccine conferred complete protection against a lethal influenza virus challenge, Viral Immunol. 18 (1) (2005) 244-251.

[15] A.L. Balish, J.M. Katz, A.I. Klimov, Influenza: Propagation, Quantification, and Storage, Current Protocols in Microbiology. (2013) 15G.1.1–15G.1.24.

[16] R.J. Russell, L.F. Haire, D.J. Stevens, P.J. Collins, Y.P. Lin, G.M. Blackburn, et al., The structure of H5N1 avian influenza neuraminidase suggests new opportunities for drug design, Nature 443 (7107) (2006) 45-49.

[17] S. Kodihalli, H. Goto, D.L. Kobasa, S. Krauss, Y. Kawaoka, R.G. Webster, DNA vaccine encoding hemagglutinin provides protective immunity against H5N1 influenza virus infection in mice, Journal of Virology 73 (3) (1999) 2094-2098.

[18] J.H. Kim, J. Jacob, DNA vaccines against influenza viruses, Vaccines for Pandemic Influenza (2009) 197-210.

[19] A. Allison, Cell-mediated immune responses to virus infection and virus-induced tumors, British Medical Bulletin 23 (1) (1967) 60-65.

[20] G. Cambridge, J. Mackenzie, D. Keast, Cell-mediated immune response to influenza virus infections in mice, Infection and immunity 13 (1) (1976) 36-43.

[21] G. Deliyannis, D.C. Jackson, N.J. Ede, W. Zeng, I. Hourdakis, E. Sakabetis, et al., Induction of long-term memory CD8+ T cells for recall of viral clearing responses against influenza virus, Journal of virology 76 (9) (2002) 4212-4221.

Journal of Pharmacy and Pharmacology 2 (2014) 59-69

Quantitative T2*-Mapping of the Knee Using a Spoiled Gradient Echo Sequence at 3 Tesla: Preliminary Results

Georg Riegler[1], Xeni Deligianni[2], Vladimir Juras[1, 3], Štefan Zbýň[1], Sebastian Apprich[1], Pavol Szomolanyi[1], Michael Weber[1], Oliver Bieri[2] and Siegfried Trattnig[1]

1. Department of Biomedical Imaging and Image-guided Therapy, MR Center of Excellence for High Field MR, Medical University of Vienna, Vienna 1090, Austria

2. Department of Radiology, Division of Radiological Physics, University of Basel Hospital, Basel 4031, Switzerland

3. Department of Imaging Methods, Institute of Measurement Science, Slovak Academy of Sciences, Bratislava 84104, Slovakia

Received: November 28, 2013 / Accepted: January 08, 2014 / Published: February 28, 2014.

Abstract: Purpose: To evaluate a me-vTE-SPGR (multi echo variable TE Spoiled Gradient Echo Sequence) approach for quantitative T2* mapping of the ME (menisci), the PT (patellar tendon), the ACL (anterior cruciate ligament), the PCL (posterior cruciate ligament) and to compare the results between normal and pathological tissue of the ME in the knee joint at 3T (3 Tesla). Methods: Eighteen consecutive knee patients (35.7 ± 11.6 years) were examined on 3T. In addition to standard morphological MRI, T2*-maps were derived from a 0.7 mm isotropic me-vTE-SPGR scan. T2*-values were assessed by two independent observers using an ROI analysis for the ME (4 different regions: posterior and anterior horn of the medial and lateral meniscus), PT, ACL and PCL. Intra-class correlation between readers was calculated. Results: On morphological MRI, the PT, ACL and PCL were diagnosed as normal in all cases. Degenerative meniscus and meniscal tears were diagnosed in 13 cases and 9 cases, respectively. T2*-values of the menisci on me-vTE-SPGR scans, in relation to morphological imaging, were normal (N = 50; 6.0 ± 0.9 ms); degenerative meniscus (N = 13; 8.0 ± 1.6 ms); meniscal tears (N = 9; 12.9 ± 3.9 ms), with significant differences between all groups ($P < 0.05$)/ significantly higher T2*-values in degenerative meniscus and meniscal tears. Mean T2* relaxation times for the PT, ACL and PCL were 2.9 ± 0.8 ms, 8.4 ± 1.6 ms and 8.9 ± 1.3 ms respectively. Intra-class correlation values between readers for the ME, PT, ACL and PCL were R^2= 0.962, R^2= 0.927, R^2= 0.594 and R^2= 0.648, respectively. Conclusion: Isotropic 3D (three-dimensional) me vTE-SPGR imaging is able to quantify T2* values of multiple tissues in the knee joint with short T2 relaxation times.

Key words: Magnetic resonance imaging, quantitative imaging, T2* imaging, connective tissue, knee.

1. Introduction

The human knee joint contains several different connective tissues, such as menisci, tendons, and ligaments, all of which are characterized by prominent short transverse relaxation times (T2) on MRI. Short T2 times are related to anatomical and biochemical properties that cannot be visualized with conventional MRI techniques [1, 2].

The structure and composition of these tissues is crucial for the integrity of the knee joint. The knee menisci consist of concentrically and radially arranged collagen fibers that play an important role in absorbing impact load [3]. Ligaments are short bands of fibrous connective tissue composed mainly of long, stringy collagen fibers, which connect with the osseous structures of a joint to afford stability [4, 5]. Tendons are tough bands of fibrous connective tissue that attach muscles to bone [6].

In the clinical routine, the most effective strategy for the diagnosis of knee diseases with MRI is the use of intermediate to long T2w (T2-weighted) imaging sequences to detect an increase in signal from abnormal tissue [7]. Standard MR sequences, however,

Corresponding author: Georg Riegler, M.D., research field: high field magnetic resonance imaging. E-mail: georg.riegler@meduniwien.ac.at.

do not provide visual information about the microstructure and biochemical composition of tissues with short T2 relaxation times. In addition, the interpretation of increased signal, especially in the meniscal tissue, can be challenging [7].

To detect MR signal from short-lived T2 tissues with relaxation times on the order of microseconds rather than milliseconds, UTE (ultrashort echo time) techniques have been developed [1, 2, 8-11]. In recent years, new quantitative imaging techniques, such as UTE-enhanced T2* (UTE-T2*) mapping [12], or UTE spectroscopic imaging (UTESI) [13, 14], have been investigated as tools with which to assess the biochemical status of tissues with short T2 relaxation times to detect microscopic alterations before gross damage occurs [12].

Quantitative T2* imaging illustrates the spatial distribution of T2* relaxation times of protons within several connective tissues that demonstrate a majority of short T2 components, and provides an estimate of tissue T2* values. However, these sequences are sensitive to gradient system imperfections, local susceptibility changes, or may be subject to blurring [15].

Alternatively, it has only recently been demonstrated that common SPGR (spoiled gradient) echo sequences can be adapted to yield sub-millisecond TE (echo times) for high-resolution MSK (musculoskeletal) imaging of short T2 components. Reportedly, sub-millisecond echo times could be achieved using a variable echo time scheme [16, 17], in combination with highly asymmetric Cartesian sampling. This variable echo time scheme exploits the fact that the image contrast is defined by the lower spatial frequencies of the k-space. The center of the k-space is sampled with a much shorter echo time, compared to the outer parts, which results in a sub-millisecond effective time echo [18]. Using a multi-echo rather than a single-echo approach, we demonstrate that this new technique allows quantitative T2* imaging of tissues with short T2 relaxation times within clinically acceptable scan times. Moreover, isotropic 3D (three-dimensional) imaging offers the possibility of multiplanar reconstructions for the different structures in the knee joint [18].

The purpose of this study was to evaluate, for the first time, an me-vTE-SPGR approach for quantitative T2* mapping of the ME (menisci), the PT (patellar tendon), the ACL (anterior cruciate ligament), and the PCL (posterior cruciate ligament) in the knee joint at 3T, and compare the results between normal and pathological tissue of the ME.

2. Materials and Methods

2.1 Patient Selection

The study was performed in compliance with the regulations of the local ethics committee. Subjects provided written, informed consent prior to enrollment in this study. Eighteen consecutive knee patients (eight female, 10 male; mean age, 35.7 ± 11.6 years) who had an MRI examination of their knee joint at our institute participated in this study (eight patients after MACT (matrix-associated autologous condrocyte transplantation), one patient after MFX (microfracture) therapy, and nine patients with chronic knee pain). Exclusion criteria were gravidity, and patients with cardiac pacemakers or any other contraindication to MRI.

2.2 Image Acquisition Methods

MR imaging was performed using a Siemens 3 Tesla TRIO scanner (Siemens, Erlangen, Germany). The protocol was identical for all patients.

2.2.1 Morphological Assessment

For morphological knee assessment, a standardized imaging protocol was used comprising a sagittal and coronal PD (proton density), fs (fat-saturated), FSE (fast spin echo) scan, an axial T2w FSE sequence, a sagittal PD FSE sequence with high in-plane resolution for cartilage imaging, a sagittal dual (PD and T2-weighted) FSE sequence, and a sagittal T1-weighted spin echo (sag T1 SE) sequence. The

detailed acquisition parameters for these sequences are summarized in Table 1.

2.2.2 Quantitative Assessment

For quantitative T2* assessment, an me-vTE-SPGR scan in the sagittal plane was obtained, as previously described [18]. With the me-vTE-SPGR, 10 echoes were acquired, with imaging parameters as follows: field of view = 118 × 180 mm; matrix size = 168 × 256; section/slice thickness = 0.7 mm; flip angle = 13 °; TR = 29 ms; TE = {0.75, 3.51, 5.87, 8.23, 10.6, 12.96, 15.33, 17.69, 20.06, 22.42} ms; and one average. Bandwidth = 320 Hz/pixel, with 144 s, and a total acquisition time of 12:16 min. The first sub-millisecond TE is optimized with the variable echo time scheme, so the first echo time differs between the center and the outside k-space. All subsequent echo times are consistent for the whole k-space [18].

2.3 Image Analysis

2.3.1 Morphological Assessment

Morphological assessment was performed on a PACS workstation by an experienced radiologist with ten years of experience in musculoskeletal imaging.

A low signal intensity on images from morphological sequences within the menisci, patellar tendon, and cruciate ligaments indicated normal tissue. A minimal, linear signal increase within the meniscus, and a globular signal replacing most of the meniscus, indicate degeneration. Abnormal signal intensity extending to the meniscus surface in more than two consecutive slices indicated a tear of the meniscus.

The cruciate ligaments were evaluated for partial or complete tears. Two patients underwent an anterior cruciate ligament reconstruction with hamstring autografts two months prior to the study.

The anterior-posterior thickness of the proximal portion of the patellar tendon, just below the inferior pole of the patella, and an abnormal intermediate signal within the tendon, indicated patellar tendinopathy. All structures with no sign of pathology were regarded as normal in this study.

2.3.2 Quantitative Assessment

For quantitative assessment of T2*, datasets were transferred to a Leonardo workstation ®. T2* values were calculated using a mono-exponential, least squares curve-fitting analysis. Two independent readers, blinded to the results of the scans, assessed the ROI (region-of-interest); one reader was a resident

Table 1 Acquisition parameters of sequences for morphological knee assessment.

	sag PD FS FSE	cor PD FS FSE	ax T2 FSE
FOV (mm)	175	150	150
Matrix size	320 ×320	384 ×384	384 ×384
Slice thickness	0.7	3	3
TR (ms)	1100	4250	2850
TE (ms)	21	27	94
Bandwith (Hz/Pixel)	381	150	178
Sections	160	36	13
Total acquisiton time (min)	09:51	02:47	02:30
	sag T2 FSE	sag T1 SE	sag PD FSE
FOV (mm)	160	150	120
Matrix size	448 ×448	448 ×448	448 ×448
Slice thickness (mm)	3	3	2
TR (ms)	5090	600	2130
TE (ms)	12.85	12	36
Bandwith (Hz/Pixel)	180	130	180
Sections	30	28	32
Total acquisiton time (min)	06:03	02:52	05:27

in radiology with two years of practice, and one researcher had four years of experience in MR imaging. ROIs were manually drawn on five consecutive, sagittal slices in the weight-bearing region for the anterior and posterior horn of the medial and lateral ME (meniscus), as well as for the PT (patellar tendon). Optimal slice orientation parallel to the course of the ACL (anterior cruciate ligament) and PCL (posterior cruciate ligament) were reconstructed using a multiplanar reconstruction tool and evaluated on three slices in the PCL and one slice in the ACL in the same way. Mean values from five consecutive ROIs of the ME and PT and from three consecutive ROIs of the ACL were calculated for comparison. In addition, the pixels of each ROI were evaluated.

2.4 Statistical Analysis

All statistical computations were performed using IBM SPSS Statistics 19.0 (SPSS Institute, Chicago, IL, USA). Metric data, such as T2* measurements, are presented using mean +/- standard deviation. Two-way random, single measures, ICC (intraclass correlation coefficients), and Bland Altman plots were used to assess rater agreement.

In order to compare the T2* values of ROIs from normal, degenerated, and torn menisci, a mixed model ANOVA with an unstructured covariance matrix was used, taking multiple measurements per patient into account. Bonferroni-corrected post hoc tests using estimated marginal means were assessed, as well. In addition, 95% confidence intervals (95% CI) were calculated. A *p*-value equal to or less than 0.05 was considered to be statistically significant.

The pixels of each ROI were described with mean values and range.

3. Results

3.1 Morphological Assessment

Fifty normal menisci, nine meniscal tears, and thirteen meniscal degenerations were assessed. The PT (N = 18) had no signs of tendinopathy, partial tear, or rupture in any of the cases. The PCL (N = 18) and ACL (N = 16) had no signs of partial tear or rupture in any of the cases. The anterior cruciate ligament ROIs of two patients, who underwent an anterior cruciate ligament reconstruction with hamstring autografts two months prior to the study, were excluded as the repair tissue did not represent original anterior cruciate ligament tissue.

3.2 Quantitative Assessment

ROIs had a mean size of 70 pixels for the ME (range, 28-181 pixels), 370 pixels for the PT (range, 218-753), 756 pixels for the ACL (range, 271-992), and 331 pixels for the PCL (range, 139-505).

T2* values for normal menisci (N = 50) were 6.0 ± 0.9 ms, with a 95% confidence interval (CI) [5.7-6.3]). Meniscal degeneration values (N = 13) were 8.0 ± 1.6 ms (95% CI [7.1-8.9]). Meniscal tear values (N = 9) were 12.9 ± 3.9 ms (95% CI [10.4-15.4]). T2* values showed significant differences between all groups (p < 0.001 each) with significantly higher T2* values in degeneration and tears compared to normal menisci. Fig. 1 presents a box plot of the T2* values for the meniscus. Fig. 2 shows a patient with meniscal degeneration. Fig. 3 shows a patient with a meniscal tear. Fig. 4 shows a me-vTE-SPGR map with manually drawn ROIs on the menisci of the same patients as shown in Figs. 2 and 3.

T2* values for the PT (N = 18) were 2.9 ± 0.8 ms (95% CI [2.54-3.33]). T2* values for the ACL (N = 16) were 8.4 ± 1.6 ms (95% CI [7.58-9.32]). T2* values for the PCL (N = 18) were 8.9 ± 1.3 ms (95% CI (8.22-9.66)). The T2* values for the ME, PT, ACL, and PCL are summarized in Table 2.

The intra-class correlation between readers for the ROI drawing in the ME, PT, ACL, and PCL yielded 0.962, 0.927, 0.594 and 0.648, respectively.

A visual presentation of the intra-class agreement between the two readers for the menisci and the patellar tendon is given with a Bland Altman diagram in Fig. 5 (meniscus) and Fig. 6 (patellar tendon).

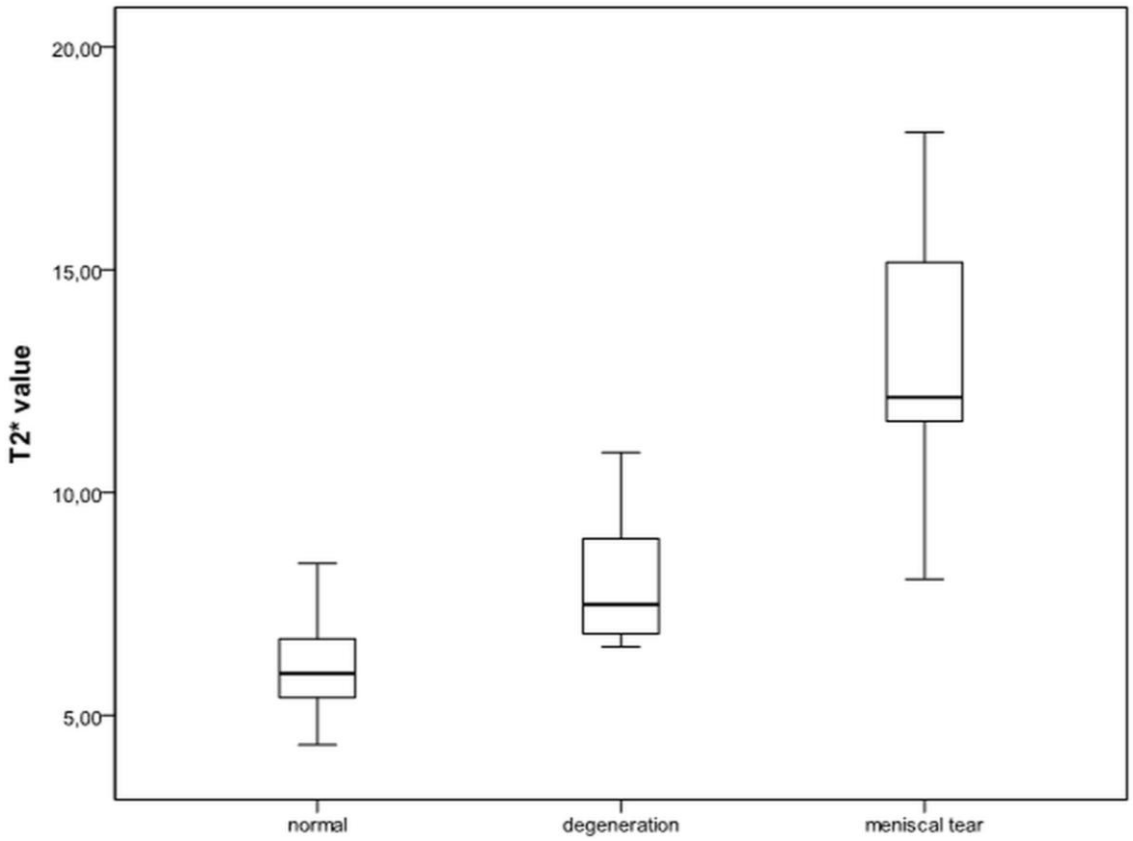

Fig. 1 Box plot of T2* values in the meniscus.

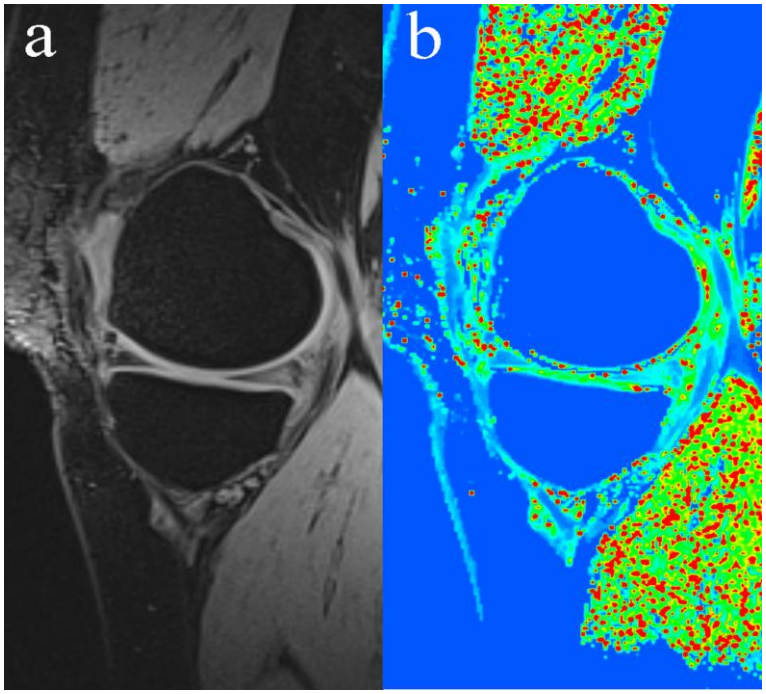

Fig. 2 A 29-year-old female referred for MRI because of ongoing knee pain. (a) and (b) show me-vTE-SPGR maps. In (b), the me-vTE-SPGR maps were converted using a color look-up table (Rainbow 16. Bit) on a Leonardo workstation ®. (a) (white) and (b) (yellow) show elevateed signal in the posterior horn of the medial meniscus. The anterior horn of the medial meniscus does not show any sign of pathology. The T2* value was 9.0 ± 3.6 ms.

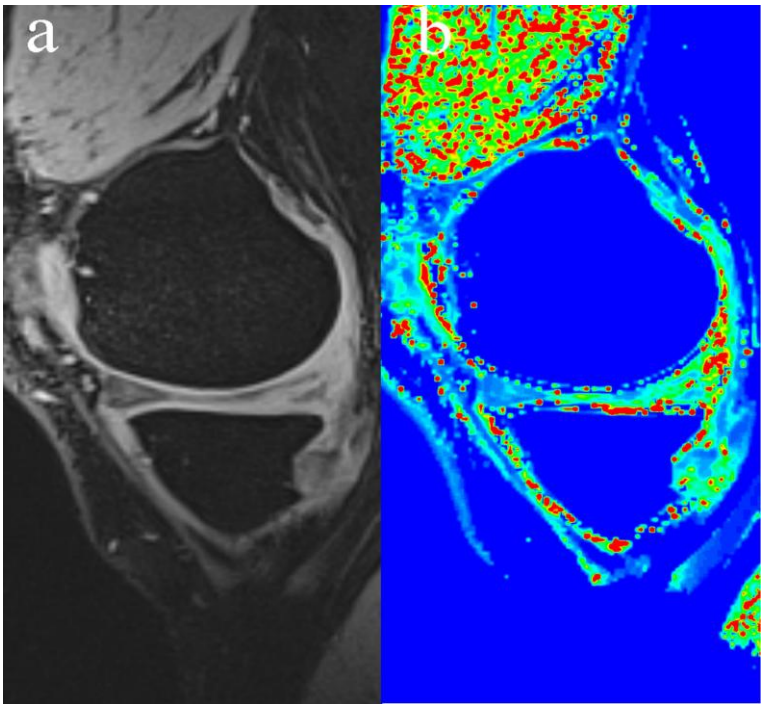

Fig. 3 A 42-year-old male referred for MRI because of ongoing knee pain. (a) and (b) show me-vTE-SPGR maps. The me-vTE-SPGR maps were converted using a color look-up table (Rainbow 16. Bit) on a Leonardo workstation®. (a) (white) and (b) (yellow and red) show elevated signal in the posterior horn of the medial meniscus. The anterior horn of the medial meniscus does not show any sign of pathology. The T2* value was 16.6 ± 6.9 ms.

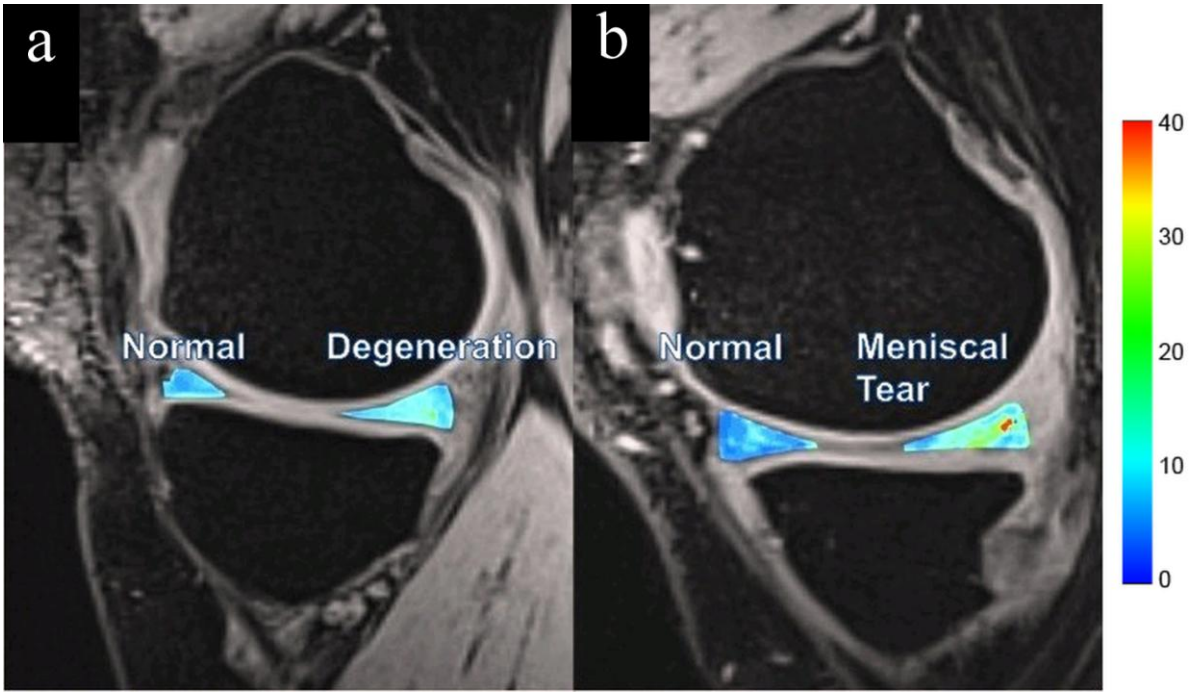

Fig. 4 (a) and (b) show me-vTE-SPGR maps with manually drawn ROIs and a color bar of T2* values on the right side. The ROIs were manually drawn on converted me-vTE-SPGR maps, as mentioned in Fig. 2 and Fig 3, and fused with the native me-vTE-SPGR maps. (a) shows the same patient as in Fig 2, and (b) shows the same patient as in Fig. 3. Note the elevated signal as a result of meniscal degeneration (a; yellow) and meniscal tear (b; red) of the posterior horn of the medial meniscus compared to the normal signal (a, b; blue) in the anterior horn of the medial meniscus.

Table 2 Mean (standard deviation) T2* values for the meniscus, the patellar tendon, and the anterior and posterior cruciate ligaments in ms (milliseconds) with a 95% CI (confidence interval).

Region and pathology	Mean T2* (SD) in ms	95% CI
Normal meniscus	6.0 ±0.9	5.7-6.3*
Meniscal degeneration	8.0 ±1.6	7.1-8.9*
Meniscal tear	12.9 ±3.9	10.4-15.4*
Patellar tendon	2.9 ±0.8	2.5-3.3
Anterior cruciate ligament	8.4 ±1.6	7.58-9.32
Posterior cruciate ligament	8.9 ±1.3	8.22-9.66

T2 values are significantly different in normal, degraded and torn meniscus tissue ($P < 0.001$ each).

4. Discussion

The biochemical composition of a tissue affects its T2 relaxation time. Tissues contain protons bound to macromolecules (with very short T2 values in the range of only a few microseconds), as well as protons in water with much longer T2 values in different proportions [2]. Moreover, collagen fiber orientation plays an important role, since strictly oriented fibers, such as those in tendons, reduce the T2 relaxation times, known as anisotropic behavior [19-21].

The menisci, the patellar tendon, and the cruciate ligaments consist of a heterogeneous network of highly organized collagen bundles, mostly of type I collagen, and different bound and free water components [22]. Tissues like tendons show higher anisotropic behavior and less free water components, compared to menisci and cruciate ligaments, and consequently, the T2 values of these tissues are lower [23, 24].

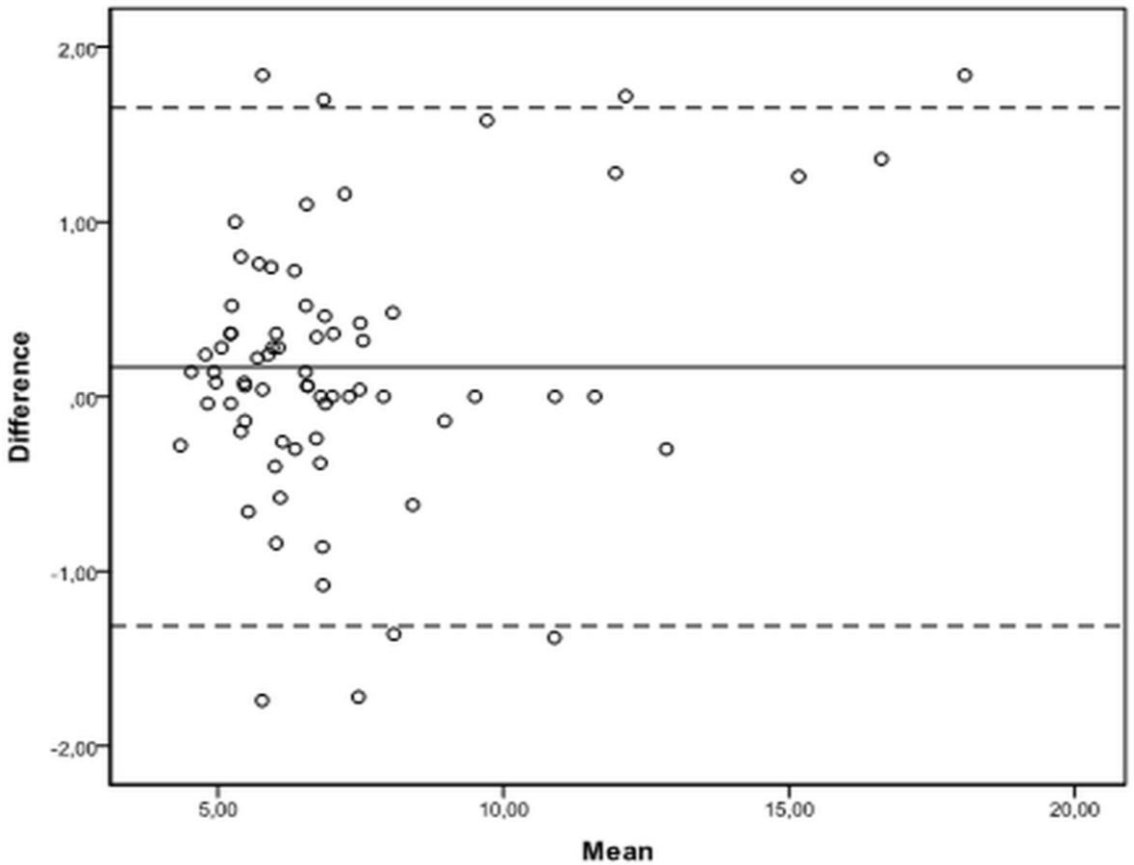

Fig. 5 Bland Altmann Diagram of the intra-class agreement between the two readers for the menisci. The intra-class correlation between readers for the ROI drawing in the ME was 0.962.

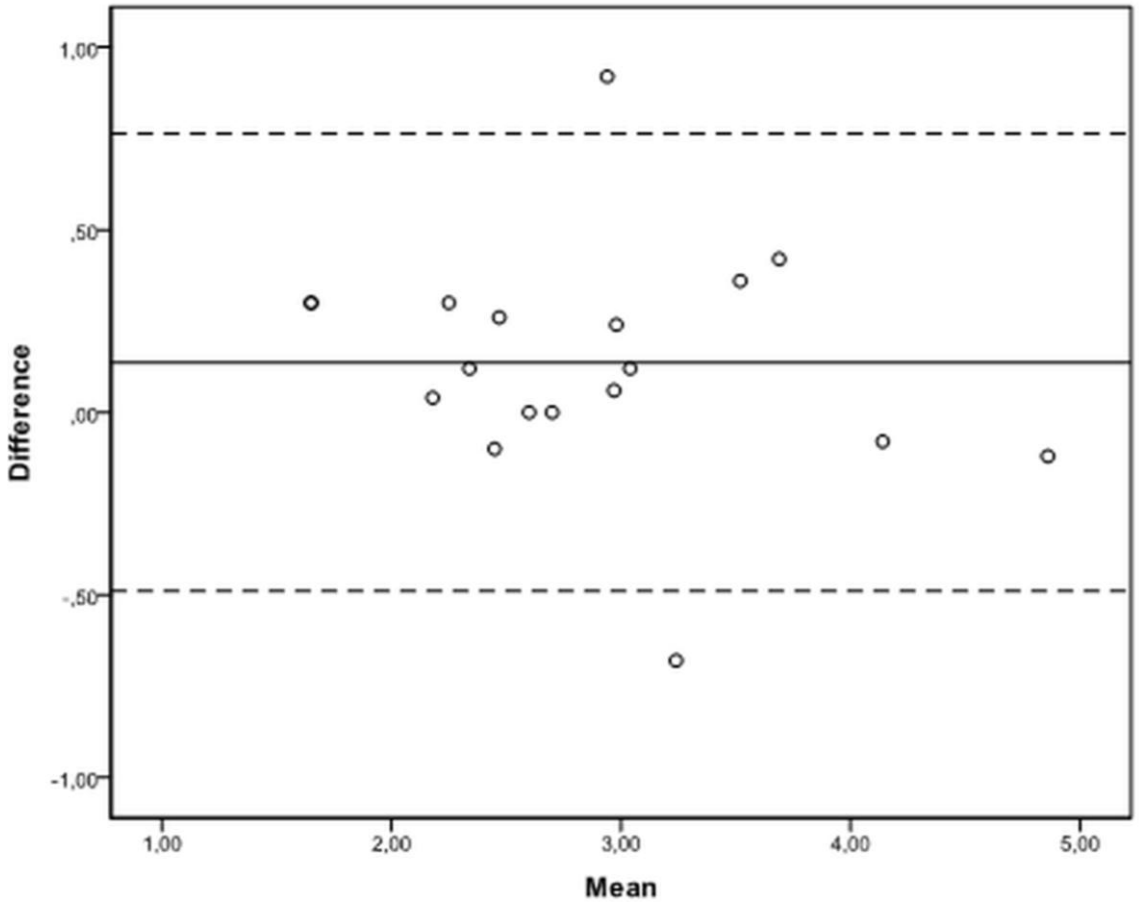

Fig. 6 Bland Altmann Diagram of the intra-class agreement between the two readers for the patellar tendon. The intra-class correlation between readers for the ROI drawing in the PT was 0.927.

The preliminary results of our study demonstrate that a reliable and fast evaluation of the T2* values for several knee joint structures can be achieved using an me-vTE-SPGR approach at 3 Tesla. Notably, we detected significant differences between normal meniscal tissue, meniscal degeneration, and meniscal tears. Since no pathologies were available in the patellar tendon and cruciate ligaments, only the T2* values of normal tissue were evaluated. The intra-class correlation between readers for the meniscus and the patellar tendon was excellent and good for the ACL and PCL.

Quantitative T2* mapping of values for the menisci, as reported in recent studies with different imaging acquisition tools, such as UTE or UTESI, range from 4.0 ms to 9.8 ms [1, 9, 13, 14, 25, 26].

In this study, the T2* values for normal menisci (6.04 ms) fell between the reported range of values, and, thus, are in very good agreement with prior studies. Nevertheless, there is a wide range of T2* values in the literature, likely influenced by different T2* acquisition methods. Thus, to interpret the T2* values of normal meniscal tissue, special attention must be paid to the imaging acquisition method. For further investigations, more attention should be focused on the zonal differences within the menisci. Some recent studies detected significant differences in T2* values between different zones of the menisci [9, 26].

The increase of T2* in pathological tissue in the menisci likely represents changes in the tissue matrix of these structures. In case of degeneration or tears, the highly structured collagen bundles in these tissues become disordered. Consequently, protons in water molecules are less tightly bound to collagen, and thus, the T2* values increase [12].

All the recent studies that have compared T2*

values of normal and pathological tissue, especially in meniscal tissue [9, 14], detected an increase of T2* in pathological tissue. Although this increase was not significant in all studies, reported results are in good agreement with the findings presented in this work.

To the best of our knowledge, this is the first study to measure the T2* values of the patellar tendon. Some work exists on T2* values of the Achilles tendon [2, 14], which has a collagen and water composition comparable to that of the patellar tendon. For further investigation, these T2* values can serve as a good standard, although histological validation is needed to verify these values.

Notably, the cruciate ligaments themselves have only been evaluated in a limited number of studies. Robson et al. [2], for example, reported T2 values of about 4-10 ms, quite similar to the results of our study (8.4 ms for the ACL and 8.9 ms for the PCL).

In the clinical routine, treatment options for patients with knee pain depend on the results of physical examination, morphological MR imaging, and, in cases of unclear diagnostic findings, invasive arthroscopic evaluation.

The MR examinations used in clinical routine practice, to date, are still limited to morphological imaging, which cannot provide information about the biochemical status of these tissues. Thus, a combination of morphological and quantitative imaging may improve the diagnostic accuracy of MRI for the evaluation of these important knee structures. Williams et al. [12], using a UTE T2* sequence, detected an increase of T2* values in histologically changed tissue in the posterior horns of the menisci in patients with an injury of the ACL, although there was no sign of pathology on conventional T2w imaging. Diaz et al. [13] were able to detect bound and free water components in different musculoskeletal tissue with UTESI sequences, using a bi-component fitting analysis. Quantitative UTE T2 imaging methods may have the potential to detect a change in tissue composition earlier than clinically used conventional MRI sequences, and consequently, improve diagnostic sensitivity and specificity.

The novel isotropic me-vTE-SPGR sequence used in the present study has several advantages: First, it is a 3D sequence, which allows isotropic imaging, and thus, enables data reformatting in every plane without loss of resolution (multiplanar reconstruction, MPR); Second, it provides sub-millisecond echo times for common Fourier-encoded spoiled gradient echo sequences (SPGR), using variable echo times in combination with a high asymmetric echo readout and a dedicated algorithm for reconstruction of undersampled data. Third, it provides positive contrast imaging of fibrous tissue components in the knee and other joints on clinical whole-body systems and within clinically feasible scan times. Overall, this results in a highly robust, flexible, and efficient method for imaging of fast relaxation components, with T_2 times in the range of several hundred microseconds at clinical field strengths.

In our study, we were able to show that, based on the proposed me-vTE-SPGR technique, quantitative T2* mapping can be performed in several knee structures within an acceptable scan time of 12:16 minutes, and that this technique has great potential to serve as a one-stop-shop method for the quantitative evaluation of various structures in the knee.

A major limitation of our study is the lack of histology or arthroscopy as a gold standard for the evaluation of pathological changes in the investigated tissues. Instead, we used the morphological evaluation by MRI for the classification of pathological tissue. For further studies, histological validation of quantitative T2* mapping in patients with different stages of disease is needed to verify this parameter as a possible marker for several important knee structures.

As previously stated, we did not perform a zonal assessment of the menisci, as performed in two other studies [9, 26], which could be a limitation for the interpretation of meniscal T2* values. For further

investigation, special attention should also be focused on the fact that the composition of the entheses of ligaments or tendons differs from other regions in these structures [8, 27], and that they are primarily involved in overuse injuries in sports. Thus, a zonal assessment of these structures could be more useful.

5. Conclusion

In conclusion, the me-vTE-SPGR sequence can quantify the T2* of multiple tissues in the knee joint, such as the menisci, the patellar tendon, and the cruciate ligaments, and can quantify pathological changes within the menisci with good spatial resolution and in acceptable scan times, using a clinical 3T MR system. This sequence might thus have the potential to serve as a one-stop-shop imaging tool for the quantitative T2* evaluation of a variety of knee joint structures.

Acknowledgements

Funding support was provided by the Austrian Science Fund P 25246 B24, the VIACLIC (Vienna Advanced Imaging Centre), and the Slovak Grant Agency VEGA; Grant number 2/0090/11. The authors thank Mary McAllister for her comments on the manuscript.

References

[1] P.D. Gatehouse, G.M. Bydder, Magnetic resonance imaging of short T2 components in tissue, Clin. Radiol. 58 (1) (2003) 1-19.

[2] M.D. Robson, P.D. Gatehouse, M. Bydder, G.M. Bydder, Magnetic resonance: An introduction to ultrashort TE (UTE) imaging, J. Comput. Assist. Tomogr. 27 (6) 2003 825-846.

[3] K. Messner, J. Gao, The menisci of the knee joint, Anatomical and functional characteristics, and a rationale for clinical treatment, J. Anat. 193 (2) (1998) 161-78.

[4] E.K. Bicer, S. Lustig, E. Servien, T.A. Selmi, P.Neyret, Current knowledge in the anatomy of the human anterior cruciate ligament, Knee Surg. Sports Traumatol. Arthrosc. 18 (8) (2010) 1075-1084.

[5] B.A. Van Dommelen, P.J. Fowler, Anatomy of the posterior cruciate ligament, A review, Am. J. Sports Med. 17 (1) 1989 24-29.

[6] M. O'Brien, Functional anatomy and physiology of tendons, Clin. Sports Med. 11 (3) (1992) 505-520.

[7] T.T. Miller, MR imaging of the knee, Sports Med. Arthrosc. 17 (1) (2009) 56-67.

[8] M. Benjamin, G.M. Bydder, Magnetic resonance imaging of entheses using ultrashort TE (UTE) pulse sequences, J. Magn. Reson. Imaging 25 (2) (2007) 381-389.

[9] P.D. Gatehouse, T. He, B.K. Puri, R.D. Thomas, D. Resnick, G.M. Bydder, Contrast-enhanced MRI of the menisci of the knee using ultrashort echo time (UTE) pulse sequences: Imaging of the red and white zones, Br. J. Radiol. 77 (920) (2004) 641-647.

[10] P.D. Gatehouse, R.W. Thomas, M.D. Robson, G. Hamilton, A.H. Herlihy, G.M. Bydder, Magnetic resonance imaging of the knee with ultrashort TE pulse sequences, Magn. Reson. Imaging 22 (8) (2004) 1061-1067.

[11] Y. Qian, A.A. Williams, C.R. Chu, F.E. Boada, High-resolution ultrashort echo time (UTE) imaging on human knee with AWSOS sequence at 3.0 T, J. Magn. Reson. Imaging 35 (1) (2012) 204-210.

[12] A. Williams, Y. Qian, S. Golla, C.R. Chu, UTE-T2* mapping detects sub-clinical meniscus injury after anterior cruciate ligament tear, Osteoarthritis Cartilage 20 (6) (2012) 486-494.

[13] E. Diaz, C.B. Chung, W.C. Bae, S. Statum, R. Znamirowski, G.M. Bydder, et al., Ultrashort echo time spectroscopic imaging (UTESI): An efficient method for quantifying bound and free water, NMR Biomed. 25 (1) (2012) 161-168.

[14] J. Du, M. Carl, E. Diaz, A. Takahashi, E. Han, N.M. Szeverenyi, et al., Ultrashort TE T1rho (UTE T1rho) imaging of the Achilles tendon and meniscus, Magn. Reson. Med. 64 (3) (2010) 834-842.

[15] I.C. Atkinson, A. Lu, K.R. Thulborn, Characterization and correction of system delays and eddy currents for MR imaging with ultrashort echo-time and time-varying gradients, Magn. Reson. Med. 62 (2) (2009) 532-537.

[16] H.K. Song, F.W. Wehrli, Variable TE gradient and spin echo sequences for *in vivo* MR microscopy of short T2 species, Magn. Reson. Med. 39 (2) (1998) 251-258.

[17] K. Ying, P. Schmalbrock, B. Clymer, Echo-time reduction for submillimeter resolution imaging with a 3D phase encode time reduced acquisition method, Magn. Reson. Med. 33 (1) (1995) 82-87.

[18] X. Deligianni, P. Bär, K. Scheffler, S. Trattnig, O. Bieri, High-resolution Fourier-encoded sub-millisecond echo time musculoskeletal imaging at 3 Tesla and 7 Tesla, Magn. Reson. Med. 70 (5) (2013) 1434-1439.

[19] Aparecida de Aro, C. Vidal Bde, E.R. Pimentel, Biochemical and anisotropical properties of tendons, Micron. 43 (2-3) (2012) 205-214.

[20] J.D. Rubenstein, J.K. Kim, I. Morova-Protzner, P.L.

Stanchev, R.M. Henkelman, Effects of collagen orientation on MR imaging characteristics of bovine articular cartilage, Radiology 188 (1) (1993) 219-226.

[21] R.M. Henkelman, G.J. Stanisz, J.K. Kim, M.J. Bronskill, Anisotropy of NMR properties of tissues, Magn. Reson. Med. 32 (5) (1994) 592-601.

[22] A.J. Fox, A. Bedi, S.A. Rodeo, The basic science of human knee menisci: Structure, composition, and function, Sports Health 4 (4) (2012) 340-351.

[23] V. Juras, S. Zbyn, C. Pressl, L.Valkovič, P. Szomolanyi, I. Frollo, et al., Regional variations of T(2)* in healthy and pathologic achilles tendon *in vivo* at 7 Tesla: Preliminary results, Magn. Reson. Med. 68 (5) (2012) 1607-1613.

[24] M.F. Koff, H.G. Potter, Noncontrast MR techniques and imaging of cartilage, Radiol. Clin. North Am. 47 (3) (2009) 495-504.

[25] M.D. Robson, G.M. Bydder, Clinical ultrashort echo time imaging of bone and other connective tissues, NMR Biomed. 19 (7) (2006) 765-780.

[26] P.H. Tasi, M.C. Chou, H.S. Lee, C.H. Lee, H.W. Chung, Y.C. Chang, et al., MR T2 values of the knee menisci in the healthy young population: Zonal and sex differences, Osteoarthritis Cartilage 17 (8) (2009) 988-994.

[27] M. Benjamin, S. Milz, G.M. Bydder, Magnetic resonance imaging of entheses, Part 1, Clin. Radiol. 63 (6) (2008) 691-703.

Journal of Pharmacy and Pharmacology 2 (2014) 70-78

Radiolabeled FMLF—a Valuable Peptide for Diagnostic Imaging

Fatemeh Keshavarzi[1] and Parviz Ashtari[2]

1. Department of Biology, Sanandaj Branch, Islamic Azad University, Sanandaj, Kurdistan 66169-35391, Iran

2. Radiation Application Research School, Nuclear Science & Technology Research Institute, Tehran 14399-51113, Iran

Received: October 14, 2013 / Accepted: December 03, 2013 / Published: February 28, 2014.

Abstract: Molecular imaging techniques are increasingly being used in the localization of disease, the staging of disease and for therapy control. The objective of current study focused on the optimization of synthesis, quality control, *in vitro* and *in vivo* evaluation of ^{123}I radiopharmaceuticals based on the chemotactic peptide N-formyl-Met-Leu-Phe. Labeling studies were done both by direct method using chloramine-T according to Khawli (1989) and indirect method using [^{125}I and ^{131}I] SIB according to Zalutsky (1987). Then, biodistribution studies were performed both in normal mice and the one bearing 50 μL turpentine for 24h, promoted inflammation in right leg. Furthermore, the ability of the labeled peptide conjugate to bind to human polymorph nuclear leukocytes was determined using *in vitro* assay. With increasing in pH, yield of labeled FMLF (N-formyl-Met-Leu-Phe) decreased perhaps because of interaction OH to carboxyl group of SIB. The maximum activity was observed in the right leg which injected with turpentine due to infection and increase in blood circulation. Also, this peptide was conjugated to PMN (Poly morph nuclear) specifically and maximum activity was 66%. The highest absorption of FLMF was seen in kidney, liver, stomach and gut. The small size of this protein causes passing through the glomerular of kidney, so high activity was observed in urine and bladder.

Key words: Molecular imaging, FLMF, radiolabeled peptide.

1. Introduction

Development of radio halogenated peptides with ^{18}F and ^{123}I for biochemical studies is one of the most active areas of radio pharmaceutical research. Compared with monoclonal antibodies and other proteins, peptides offer several potential advantages for tumor targeting [1]. Because of the considerably smaller size of peptides compared with proteins, they clear more rapidly from the blood pool and normal organs, minimizing radiation dose to these tissues [1, 2].

In addition, the penetration of peptides into tumors is significantly faster than proteins. For these reasons, peptides are ideal molecular carriers for use in tandem with short half-life radionuclide such as ^{123}I for single photon emission tomography and ^{18}F for positron emission tomography [1-3].

Because peptides and proteins are chemically similar in that both are composed of amino acids, it should be possible to adapt protein radio halogenation strategies originally developed for use with monoclonal antibodies for labeling peptides [4, 5]. However, in doing so, it is important to take into account differences between peptides and proteins with regard to aqueous solubility, knowledge of residues involved in receptor binding, effect of the acylation agent on lipophilicity and other physical properties of the carrier molecule, and sensitivity to extremes of pH [4-6].

In recent years the search for agents with specific targeting has led to a variety of molecules such as fragments, chimeric and humanized antibodies, immune adhesions and single chain antigen binding proteins and variable domain peptide molecules [7, 8]. Since the discovery of peptide receptors and the

Corresponding author: Fatemeh Keshavarzi, Ph.D., assistant professor, research field: molecular genetics. E-mail: gol.keshavarzi@gmail.com.

synthesis of small, biologically active peptides, it has been recognized that these molecules can provide new approaches for radiopharmaceutical development [9]. In many cases of cancers an over expression of receptors is observed which makes such receptors an attractive target for tumors imaging [5-10]. Many other peptides and receptor systems have been investigated in experimental animals and *in vitro* studies and have been suggested as imaging agents [11-15]. One of the outputs bacterial is N-For-MLF (N-Formyl-Met-Leu-Phe) that from the cell membrane receptors attach to a lot of immune cells in body. Binding of this peptide of many synthetic analogues initiates leukocyte chemo taxis. Further, studies developed by Zalutsky and Narula [4] and Wilbur et al. [16-19] demonstrated that antibodies can be radio iodinated using the synthesized precursor N-succinimidyl-(tri-n-butylstannyl) benzoate intermediate (ATE), that is needed for making labeled SIB (N-succinimidyliodobenzoate) [20-23]. The use of SIB reagent for protein labels significantly improve thyroid uptake of radioiodine. The objective of current study focused on the optimization of synthesis, quality control, *in vitro* and *in vivo* evaluation of ^{123}I radiopharmaceuticals based on peptides and selective labeling procedures using prosthetic groups were applied. Additionally the investigation includes on the fate of the label, stability *in vivo*, bio distribution and pharmacokinetics, rodents and also cell were made.

2. Material and Methods

2.1 Radio-Iodination of FMLF

Labeling studies were done both by direct method using chloramine-T according to Khawli et al. [8] and indirect method using [^{125}I and ^{131}I] SIB according to Zalutsky and Narula [4]. Since FMLF does not lend itself for direct radio-iodination, it was seen that, after labeling, the most unreacted radio-iodine was isolated from the reaction mixture by a column packed with Sephadex G-50 eluted with 0.01M PBS, pH7. 4. Briefly, radio-ioidination of FMLF via [^{125}I and [^{131}I] SIB was performed.

2.2. Biological Studies

According to Vaidyanathan [9] and Zalutsky and Narula [4] both in normal mice and the ones bearing 50 μL turpentine for 24h, promoted inflammation in right leg (twelve normal mice and twelve per injected turpentine ones weighting 20-28 g. Each animal was received 6-12 μCi [^{125}I] FMLF intravenously via tail vein (three mice per time point), sacrificed 0.5, 2, 4 and 24 h post injection and dissected. The tissues of interest were discarded, washed with saline, dried, weighed and counted by a gamma counter to obtain bio distribution. The tissue bio distribution results were expressed as the percentage of the injected dose, localized per gram of tissue. Because of the presence of radioactivity in urine and bladder was made the SPECT scan on the mice which were received [^{131}I] iodide and [^{131}I] FMLF. These scans confirmed the difference radioactivity localized in different organs.

2.3 Biological Evaluation of the Chemotactic-SIB Conjugate, in Vitro Studies

The ability of the labeled peptide conjugate to bind to human PMN (polymorph nuclear leukocytes) was determined using *in vitro* assays described in the literature [9, 10] with some modification taking into account the laboratory facilities. In order to determine the effect of derivatization with SIB on the potency of the peptide and in the biological activity, competitive binding to PMN and superoxide production were made.

2.4 Cell Preparation

Human PMNs were isolated using a density gradient centrifugation method as described in Ref. [9].

Isolation Procedure:

(1) Blood collect: 30-40 mL of blood from normal voluntary was used in each experiment using sodium citrate 3.8% as anticoagulant in relation blood/anticoagulant 9:1. The initial count of total leukocytes present was made in a Neuberger camera

making a dilution 1/20 of a sample of the blood with 3% acetic acid;

(2) Buffy-coat: in a 15 mL tube with 5% Dextran (PM 100,000-200,000) in PBS (phosphate-buffered saline) pH7.4 was added the blood in relation blood/dextran 1:5. It is important to add the blood slowly drop by drop in the center of the tube. The cells were allowed to settle 45 min at room temperature. In this step normally 30% of the cells are lost. The supernatant was washed in PBS or culture media (RPMI 1640, Sigma R1383), pH 7.4 and centrifuged twice at 400 × g for 10 min. The cellular pellet was re-suspended in culture media;

(3) Gradient separation: used per colldensity 1.130 ± 0.005 g/mL (Sigma P1644) and PBS to prepare two solutions of different densities (1.119 g/mL and 1.077 g/mL). The cells re-suspended in culture media (4 mL) from step (2) were layered over percoll gradients consisting of 3 mL of each of two densities (1.119 g/mL and 1.077 g/mL) in 10 mL conical tubes. PMNs were harvested from the interface between the two solutions following centrifugation at 1000 ×g for 25 min at 20 ℃. The cells were washed in culture media (RPMI 1640, Sigma R1383), pH 7.4 and centrifuged twice at 400 × g for 10 min. The cells were then re-suspended in a small volume of incubation buffer (1.7 mM KH_2PO_4, 8.0 mM Na_2HPO_4, 117.0 mM NaCl, 0.15 mM $CaCl_2$, 0.5 mM $MgCl_2$, 1 mM PMSF, pH 7.4);

(4) Cell count and determination of cell viability: a sample of isolated cells from step (3) was diluted 1:2 with 0.4% Trypan Blue and after 4 min they were count in a Neubauer camera. Viable cells counted from death cells (stained cells). Finally cell suspension was diluted at a concentration of 1 × 107 cells/mL. Cell preparation contained more than 95% PMNs as assessed by light microscopy of a sample of Giemsa-stained specimens. Cell yields of 35 × 10^6-50 ×10^6 cell from 40 mL of blood were obtained.

3. Results and Discussion

The synthesis of following intermediate products was performed:

Tri-n-butyl stannyl-3 and 4-(tri-n-buthylstannyl) benzoate in > 30% yield;

N-succinimidyl-3 and 4-(tri-n-buthylstannyl) benzoate, ATE in 70% yield;

N-succinimidyl-3 and 4-iodobenzoate, SIB in 80% yield.

Radio iodination of SIB with radioiodine 125 and 131 was performed satisfactorily in radiochemical yield more than 40%-70% (Fig. 1). Comparative HPLC analysis of IK, NCS, ATE, SIB (cold) and the elution profile of radioiodinated SIB shows a high radio chemical purity in [^{125}I and ^{131}I] SIB, 99%.

FMLF labeling was done both by direct method using chloramine-T and indirect method via radio iodinated SIB, showed that FMLF does not lent itself for direct labeling using chloramine-T (Fig. 2).

FMLF labeling via radioiodine SIB was performed at different pH 8.5, pH 9.5 and pH 10.0, disclose that radiochemical yields decrease with increasing pH (Fig. 3) and the best yield was found at pH 8.5.

Biological behavior of labeled FMLF was studied in normal mice and 24 h after the animal received 6-12 μCi [^{125}I] SIB-FMLf (Figs. 4 and 5). These results showed an accumulation in the inflamed leg. In Fig. 5, it can be seen that in the inflamed mice, in almost all the tissues, the uptake is lower than in the normal mice. The reason could be the progressive accumulation of activity by the inflammation.

A comparative SPECT scan was performed with normal mice 2 h after the animals received about 30 μCi [^{131}I] iodide and [^{131}I] SIB-FMLF to distinguish why high labeled FMLF has been localized in bladder and urine (Fig. 6). The results of bio distribution showed a very low thyroid and stomach uptake of radioiodine. These results indicate that the labeling of proteins using the ATE intermediate produced labeled proteins with a decreased rate of dehalogenation *in vivo*. This result is similar to that obtained by Zalutsky [4].

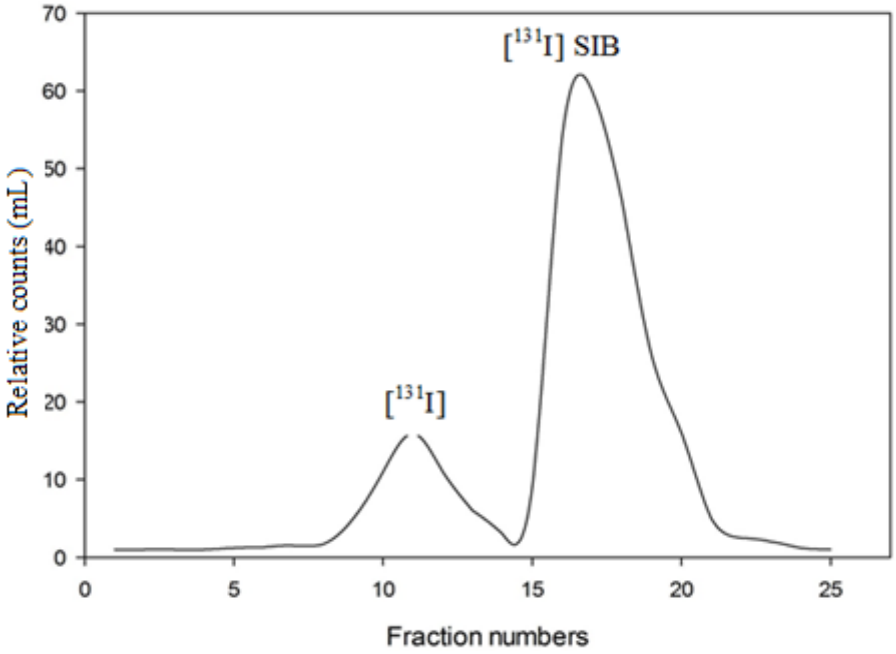

Fig. 1 Relative activity per mL of each fraction to calculate labeling yield.

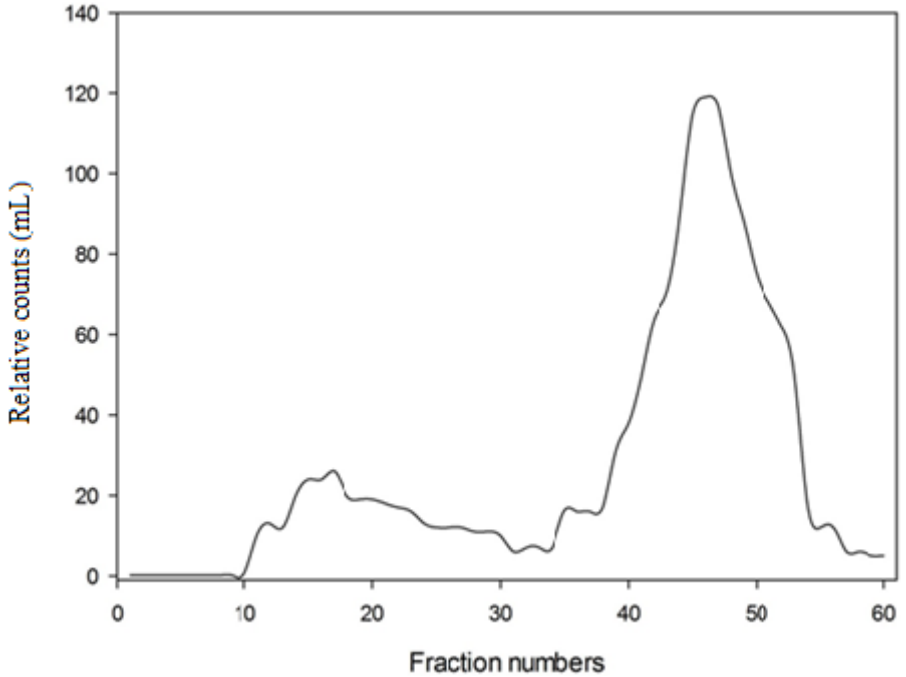

Fig. 2 Labeling studies were done both by direct method using chloramine-T and indirect method using [^{125}I and ^{131}I] SIB . Since FMLF does not lend itself for direct radioiodination, it was seen that, after labelling, the most unreacted radioiodine was isolated from the reaction mixture by a column packed with Sephadex G-50 eluted with 0.01M PBS, pH 7.4. The fractions between 20-22 mL were labelled FMLF.

The procedure for ATE synthesis and its intermediate products must be reconsidered due to low yield of intermediate products.

Protein labeling by SIB which is itself radiolabelled by "^{125}I" and "^{131}I" at pH = 8.5 was done with high yield. As pH increased, pattern of marks of FLMF decreases due to the reaction of carboxyl SIB and "OH", this causes the formation of mono Iodobenzoic acid?

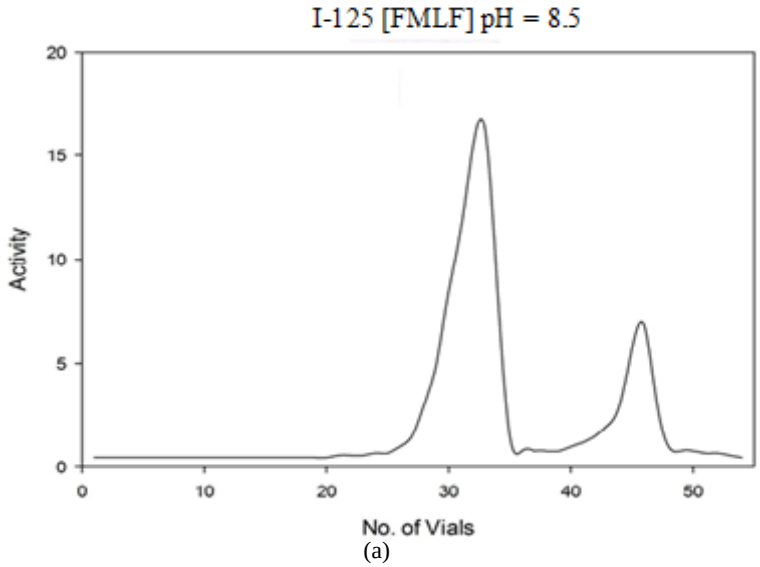

(a)

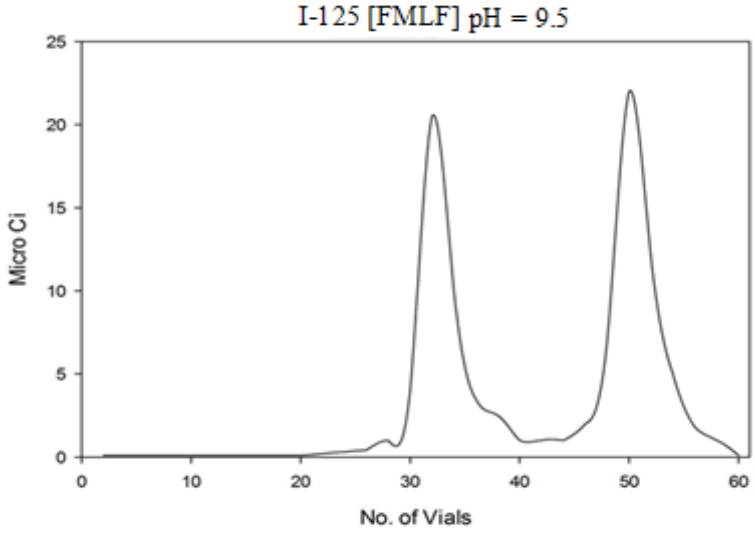

(b)

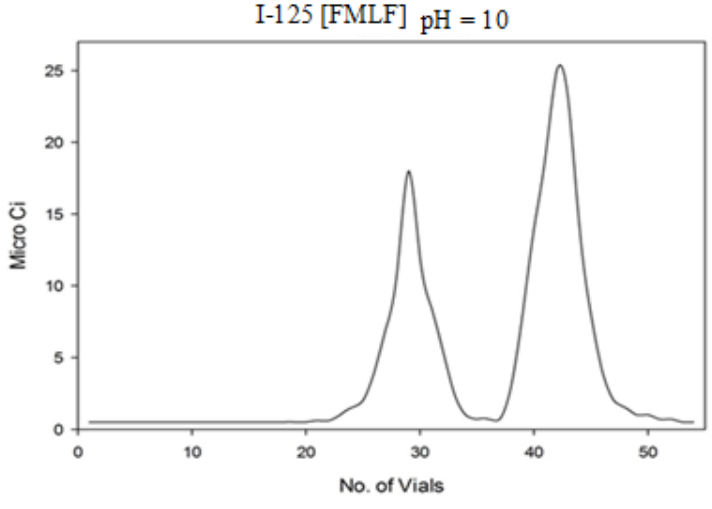

(c)

Fig. 3 FMLF labeling via radioiodine SIB was performed at different (a) pH8.5; (b) pH 9.5; (c) pH 10.0.

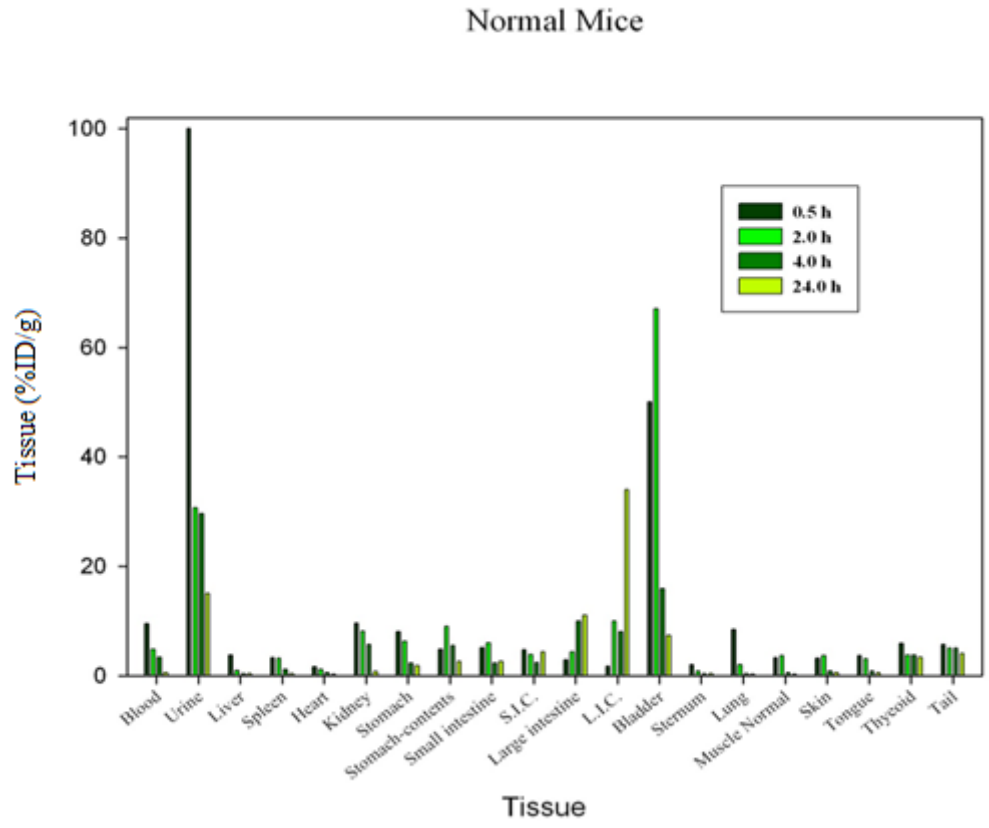

Fig. 4 Results of study of biological behavior of labelled FMLF (N-formyl-Met-Leu-Phe) in normal mice.

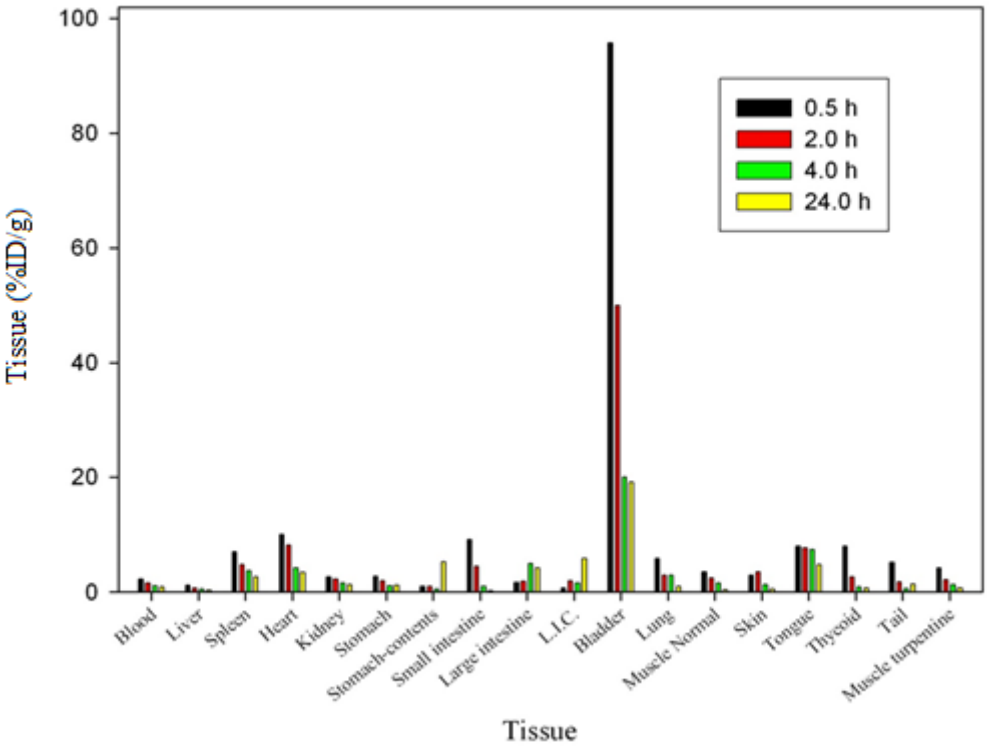

Fig. 5 Biological behavior of labelled FMLF (N-formyl-Met-Leu-Phe) in inflamed mice.

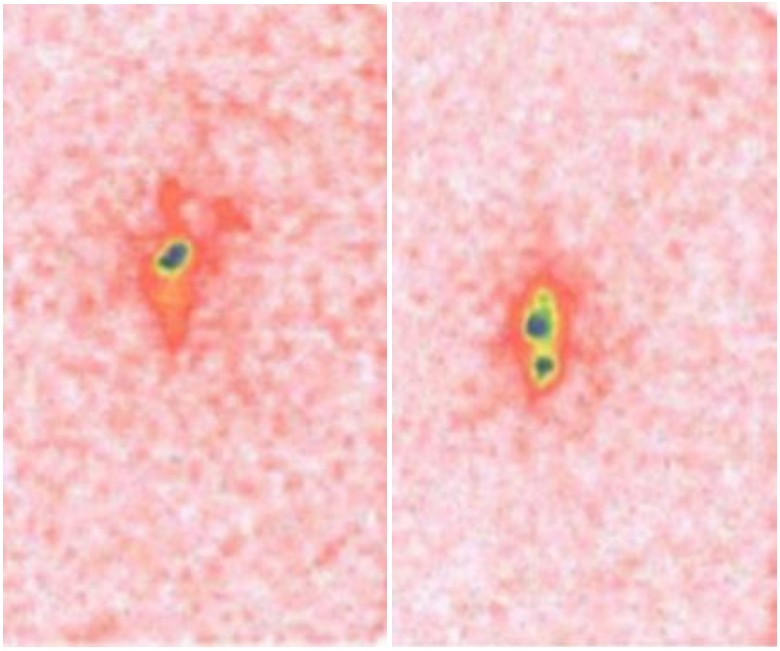

(a) (b)

Fig. 6 Comparative SPECT (single photon emission computed tomography scan) performed with normal mice 2h after the animals received about (a) 30 μCi[131I] SIB–FMLF and (b) [131I] iodide.

Chemical peptides labeled with radioactive element such as ^{131}I, ^{125}I, ^{3}H, ^{18}F, ^{99m}TC, ^{111}In is preferable method for identifying and determining infection.

While the result current experiments were 66% within 5 min while Zalatsky obtained 72% in the same experiment [4]. There are several factors which cause this difference. These are solubility of FMLF derivatives in solution compared to buffer which was used for monoclonal antibody, also apart from the positive effect of solubility of solution heterogeneous system products is better than homogenous system. In addition, since the ^{125}I ISIB is an active ester comparative hydrolysis under aqueous condition will reduce the access for conjugating of antibody. At last the reaction is dependent on the pH and the yield increased respectively.

The small size of this protein causes passing through the glomerular of kidney, so high activity was observed in urine and bladder. In this study the highest activity was observed in urine and bladder. This is not surprising since the protein is small and can pass through the glomerular of kidney. Concomitantly, in the thyroid and the abdominal region showed low activity. If $Na^{131}I^{125}I$ FMLF were injected to the same mice after two hours, the highest radio activity was observed in abdominal cavity and low uptake in thyroid. The highest absorption of FMLF was seen in kidney, liver, stomach and gut. Initial activity was high in stomach, kidney and gastrointestinal tract. Color scan showed, after injection of labeled peptides to mice, thyroid has low due to free iodine (unlabeled) is absorbed in thyroid. Then, it was concluded that the amount of unlabeled iodine is low but Fishman et al. [13] reported this differences eight times which labeling was correct. Factor such as lipophilicity, catabolism of labeled peptide must be considered in labeling of protein. Higher uptake and slow rise absorption were height in the injected right leg with turpentine compare to other organ, indicating the infection and increase influx of blood in that area.

The inflammation caused more absorption from the labeled peptide in turpentine muscle as compared to normal muscle. This peptide was conjugated to PMN specifically and maximum activity was 66%. It is possible that severe neutropenia was created by this peptide, so there is a need for more preparation for

clinical research. This can only be done by using of ^{125}I SIB with the highest activity which is achieved by using of ^{125}I with height specific activity. Using of small size protein is more preferential than antibody due to the clear more rapidly from blood pool and normal organ. The proportion of absorbed activity of labeled peptides in organs, especially gastro intestinal tract to blood is more than this proportion for the peptides which are labeled by technetium. This can be the result of more lipophilicity of peptides to iodine.

4. Conclusions

With referring to previous studies small peptides had more advantage compare with antibody due to easy penetration to tumor and so easy clearance from blood. This current biological study of labeled FMLF showed a low uptake in thyroid but a high at urine and bladder. Perhaps because of FMLF molecular weight is low in comparison to other peptides; accordingly this molecule could pass from blood to urine.

References

[1] A. Jemal, R. Siegel, E. Ward, Cancer statistics, CA Cancer J. Clin. 60 (2010) 277-300.

[2] E.T. Hawk, B. Levin, Colorectal cancer prevention, J. Clin. Oncol. 23 (2005) 378-391.

[3] Y. Yao, H. Zhao, Y.J. Sun, F. Lin, L.L. Tang, P. Chen, Combined chemotherapy of hydroxycampothecin with oxaliplatin as an adjuvant treatment for human colorectal cancer, Tohoku J. Exp. Med. 215 (2008) 267-278.

[4] M.R. Zalutsky, A.S. Narula, A method favors the radio halogenation of proteins resulting in decreased thyroid uptake of radioiodine, Appl. Radiat. Iso. 38 (12) (1987) 1051-1055.

[5] M. Langer, A.G. Beck-Sickinger, Peptides as carrier for tumor diagnosis and treatment, Curr. Med. Chem. Anticancer Agents 1 (2001) 71-93.

[6] J. Lister-James, B.R. Moyer, R.T. Dean, Small peptides radiolabelled with 99mTc, Q. J. Nucl. Med. 40 (1996) 221-233.

[7] G. Mariani, P.A. Erba, A. Signore, Receptor-mediated tumor targeting with radiolabeled peptides: There is more to it than somatostatin analogs, J. Nucl. Med. 47 (2006) 1904-1907.

[8] L.A. Khawli, A.I. Kassis, Synthesis of ^{125}I labeled N-succinimidyl p-iodobenzoate for use in radio-labeling antibodies, Nucl. Med. Biol. 16 (1989) 727-733.

[9] G. Vaidyanathan, M.R. Zalutsky, Targeted therapy using alpha emitters, Phys. Med. Biol. 41 (1996) 1915-1931.

[10] G.V. Vaidyanathan, H.S. Friedman, S.T. Keir, M.R. Zalutsky, Localisation of [^{131}I] MIBG in nude mice bearing SK-N-SH human neuroblastoma xenografts: Effect of specific activity, Br. J. Cancer 73 (1996) 1171-1179.

[11] P. Angelberger, I. Virgolini, I. Szilvasi, A. Kurtaran, Radiopharmaceutical development of 123I-vasoactive intestinalpeptide (VIP) for receptor scintigrphy in oncology, J. Label. Compd. Radioph. 37 (1995) 502-503.

[12] J.W. Babich, H. Solomon, M.C. Pike, D. Kroon, W. Graham, M.J. Abrams, et al., Technetium-99m-labelled hydrazine nicotinamide derivatized chemotactic peptide analogs for imaging focal sites of bacterial infection, J. Nucl. Med. 34 (1993) 1964-1974.

[13] A.J. Fischman, J.W. Babich, H.W. Strauss, A ticket to ride: Peptide radiopharmaceuticals, J. Nucl. Med. 34 (12) (1993) 2253-2262.

[14] R.M. Hunter, F.C. Greenwood, Preparation of iodine-^{131}I labelled human growth hormone of high specific activity, Nature 194 (1962) 495.

[15] S.M. Okarvi, Peptide-based radiopharmaceuticals: Future tools for diag-nostic imaging of cancers and other diseases, Med. Res. Rev. 24 (2004) 357-397.

[16] D.S.Wilbur, D.K. Hamlin, R.L. Vessella, J.E. Stray, K.R. Buhler, P.S. Stayton, Development of a stable radioiodinating reagent to label monoclonal antibodies for radiotherapy of cancer, J. Nucl. Med. 30 (1989) 216-226.

[17] J.C. Reubi, Peptide receptors as molecular targets for cancer diagnosis and therapy, Endocr. Rev. 24 (2003) 389-427.

[18] P.R.P. Salacinsky, Iodination of proteins, glycoproteins and peptides using a solid phase oxidizingagent, 1,3,4,6-Tetrachloro-3,6-diphenyl glycosuria (iodogen), Anal. Biochem. 117 (1981) 136-146.

[19] D. Dimitroulopoulos, A. Zisimopoulos, D. Xinopoulos, K.Tsamakidis, E. Andriotis, E. Fotopoulou, Somatostatin receptor scintigraphy with In-111 octreotidein the detection of gastroenteropancreatic carcinoidsand their metastases, Annals of gastroenterology J. 16 (4) (2003) 339-345.

[20] J.C. Reubi, H.R. Macke, E.P. Krenning, Candidates for peptide receptor radiotherapy today and in the future, J. Nucl. Med. 46 (2005) 675-755.

[21] V.D. Bossche, V.D. Wiele, Receptor imaging in oncology by means of nuclear medicine: Current status, J. Clin. Oncol. 22 (2004) 3593-3607.

[22] A.E. Bolton, W.M. Hunter, The labelling of proteins to

high specific radioactivities by conjugation to a ^{125}I-containing acylating agent, Application to the radioimmunoassay, Biochem. J. 133 (3) (1973) 529-539.

[23] I. Virgolini, B. Niederle, P. Valent, Vasoactive intestinal peptide receptor scintigraphy, J. Nucl. Med. 36 (1995) 1732-1739.

Journal of Pharmacy and Pharmacology 2 (2014) 79-86

Determination of Natural Radioactivity in Different Regions of Iran and Compared with Global Standards

Samaneh Babazadeh-Toloti, Hashem Miri-Hakimabad and Laleh Rafat-Motavalli

Physics Department, School of Sciences, Ferdowsi University of Mashhad, Mashhad 91775-1436, Iran

Received: July 08, 2013 / Accepted: December 14, 2013 / Published: February 28, 2014.

Abstract: Soils are naturally radioactive, because of their mineral content. An effective dose delivered by photon emitted from natural radioactivity in soil (^{40}K, ^{238}U and ^{232}Th and their progenies) was calculated in this work. Calculations were performed using the ORNL (Oak Ridge national laboratory) human phantom and Monte Carlo N-particle transport code MCNP-4C according to ICRP103 recommendations. Optimum dimensions of each source were determined considering the incident photon energy. Then, these dimensions were employed in the MCNP code input for calculation of conversion factors which relate the effective dose rate and activity. The obtained factors of the ^{238}U series, ^{232}Th series and the ^{40}K in soil are 0.383, 0.314 and 0.019 nSv h^{-1} per Bq kg^{-1}, respectively. These results were compared with other studies and revealed that there is a good agreement exists between two sets of data. The estimation of the effective dose rates and the annual effective dose for the adult population has been derived in different regions of Iran, considering the natural radioactivity distribution in soil samples from these regions. Finally, the obtained results in this study were compared with UNSCEAR (United Nations Scientific Committee on the Effects of Atomic Radiation) 2008 report.

Key words: Effective dose, Natural radioactivity, MCNP code, ORNL phantom.

1. Introduction

The environmental radiation is composed of the natural and artificial radiation. Natural radiation originates from the ground, and the cosmic radiation, while the artificial originates from nuclear weapons tests and accidents which, eventually, will come down to ground level. The earth is still being heated through the decay of long-lived natural radionuclide, e.g., uranium, thorium and potassium which occur in nature as a complex of oxides, hydrated oxides, carbonates, phosphates, sulfates and silicates [1].

The gamma radiation emitted from naturally occurring radioisotopes, called terrestrial background radiation, represents the main external source of irradiation of the human body [2]. Natural environmental radioactivity and the associated external exposure due to the gamma radiation depend primarily on the geological and geographical conditions and activities of naturally radioactive elements in soil of each region in the world [3]. Therefore, the assessment of gamma radiation doses from natural sources is of particular importance as natural radiation is the largest contributor to the external dose of the world population [4]. In order to provide fundamental data required for dose evaluation due to environmental exposures, the effective dose conversion factors, that is, the effective dose rate per unit activity, are calculated for natural radionuclides.

Corresponding author: Samaneh Babazadeh-Toloti, Ph.D. student, research field: nuclear physics. E-mail: babazadeh_samaneh@yahoo.com.

2. Materials and Methods

The elements of the two radioactive series, the ^{238}U and ^{232}Th, are emitting many photons with different probabilities, whereas the ^{40}K is emitting only one group of photons with an energy of 1.46 MeV in 11% of disintegrations.

The MCNP-4C Monte Carlo code has been used for simulating the photon transport from the source to

individual target organs. The absorbed dose and the effective dose obtained from natural radionuclides in soil have calculated for the ORNL adult male and female human phantoms [5]. It has been claimed that phantom is standing on the ground, while the source was represented as a volumetric geometrical body in the ground. The coordinate origin has been taken at the center of the lower base of the trunk section of the phantom. The soil composition, given in Table 1, is for conditions of 30% relative humidity and a density of 1.6 g cm^{-3}.

The dose rate at a reference point for discrete photon energy strongly depends on attenuation effects in material between the source and the reference point. The gamma ray attenuation depends primarily on emitted photon energy [6]. In other words, the effects of radiations incident on the gamma dose value are important for a specified radius and the depth of source that these dimensions for each sources consider their photon energies and mean free path, is unique. Hence, for an accurate assessment of dose value, it is essential to be determined the optimum radius and depth for each isotope.

Totally, 2×10^9 simulations were run in order to obtain "good statistic", i.e., small calculation uncertainty. The MCNP-4C energy deposition tally-f6 was used for dose calculation. It gives the absorbed doses in different cells of phantoms in MeV/g per one emitted photon which is converted in nGy per one emitted photon. For photon the radiation weighting factor is equal to one, therefore; the absorbed dose is numerically equal to equivalent dose. Then, the unit conversion was applied further to obtain equivalent doses for all organs in (nGy/h)/(Bq/kg). The effective dose in nSv, eq.1, could be calculated from the equivalent dose H_T for each organ:

$$E = \sum_T w_T H_T \quad (1)$$

W_T in Eq. 1 is the tissue-weighting factor of organ T. The values of the tissue—weighting factors recommended in the ICRP (International Commission on Radiological Protection) Publication 103 were applied to all the calculations performed in this present study. Finally, a conversion of units was performed in order to express the effective dose conversion factor in nSv/h per Bq/kg. The conversion factors of ^{238}U series, ^{232}Th series and ^{40}K in soil, calculated in this work are 0.383, 0.314 and 0.019 nSv/h per Bq/kg, respectively. Table 2 presents the comparison with other authors.

In nature, the radionuclides in the ^{238}U and ^{232}Th series are approximately in a state of secular equilibrium, in which the activities of all radionuclides within a chain are nearly equal. Consequently, the total dose produced by the ^{238}U chain is acquired by the dose summation of decay products. However, an exception is observed in ^{232}Th decay chain. The decay probability of ^{208}Tl in this chain is 0.36 s^{-1}. Thus, to calculate the total dose in this chain, ^{208}Tl dose should be multiplied by 0.36 and then added with the results of other isotopes. Finally, considering the activity concentrations of the ^{238}U, ^{232}Th and the ^{40}K in different provinces of Iran, the effective dose rate in units of nSv per hour has been calculated by the following formula:

The effective dose rate (nSv h^{-1}) = concentration of nuclide (Bq kg^{-1}) × effective dose conversion factor (nSv h^{-1} per Bq kg^{-1}) (2)

In the UNSCEAR 1993 Report, the Committee used 0.8 for the indoor occupancy factor, i.e. the fraction of time spent indoors and outdoors is 0.8 and

Table 1 Soil composition.

Element	Mass fraction	
	Silty soil	This work
H	0.021	0.0375
C	0.016	0.059
O	0.577	0.428
Si	0.271	0.346
Al	0.050	0.009
Fe	0.011	0.024
Ca	0.041	0.045
K	0.013	0.008
B	----	0.0075
Mg	----	0.036

Table 2 Effective dose conversion factors reported in several studies.

Effective dose conversion factors (nSv/h per Bq/kg)			Reference
^{238}U	^{232}Th	^{40}K	
0.301	0.466	0.0295	Beck et al. [8]
0.350	0.51	0.033	Eckerman & Ryman [9]
0.324	0.423	0.0292	Saito and Jacob
0.329	0.4	0.0295	Markkanen [11]
0.280	0.381	0.0279	Clouvas et al. [12]
0.318	0.408	0.030	Quindos et al. [13]
0.461	0.337	0.0209	D. Krstic [14]
0.383	0.314	0.019	This Work

0.2, respectively [7].

The outdoor and indoor AED (mSv) from the radioactivity content of the soil can be calculated using the following formula:

AED (mSv) = the effective dose rate (nSv h^{-1}) × (365 × 24h) × the outdoor or indoor occupancy factors (0.2 and 0.8, respectively) × indoor shielding factor (0.1) (3)

Due to these of concrete building material in Iranian houses, the indoor shielding factor can be considered 0.1.

3. Results

3.1 Determination of Optimum Radius and Depth

The optimum radius and depth are evident for the ^{40}K, ^{232}Th and the ^{238}U sources in Figs. 1 and 2, respectively. As expected in the environmental exposure, there would be an increase in the amount of effective dose with radius (depth) of source. But, from the specified radius (depth), according to the mean free path of emitted photons, the effective doses do not change significantly. Thus, regarding determining the minimum radius (depth) in the saturation region, an accurate estimation of the effective dose coefficients can be obtained.

The soil composition used in Krstic's paper [14] (as SiO_2) and the FGR12 (Federal Guidance Report No. 12) research (Table 1), was employed in the MCNP code and the same dimensions with this work were obtained as cylindrical sources dimensions.

Fig. 3 also presents a comparison between the absorbed dose results of the considered isotopes in

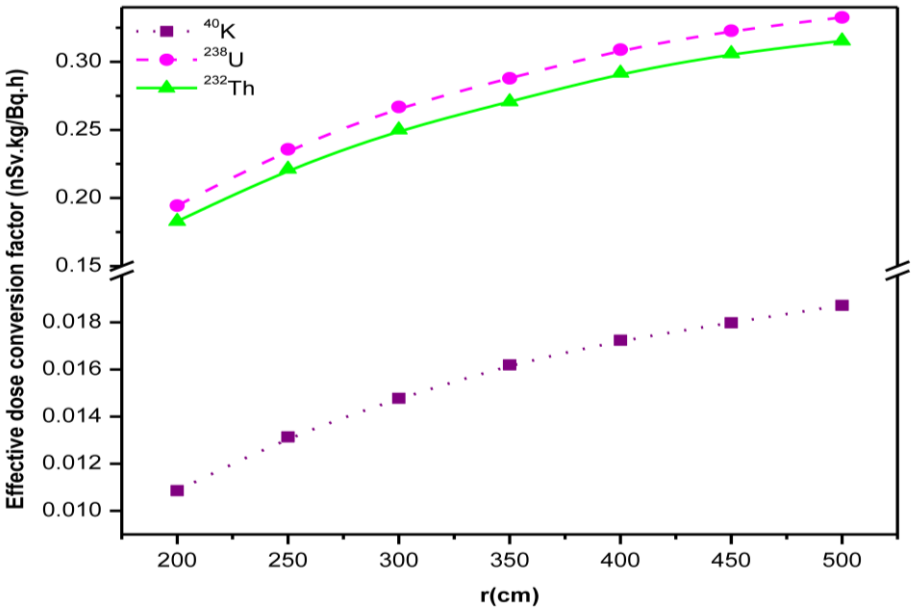

Fig. 1 Determination of optimum radius for ^{238}U, ^{232}Th and ^{40}K Sources, considering the soil composition of this work.

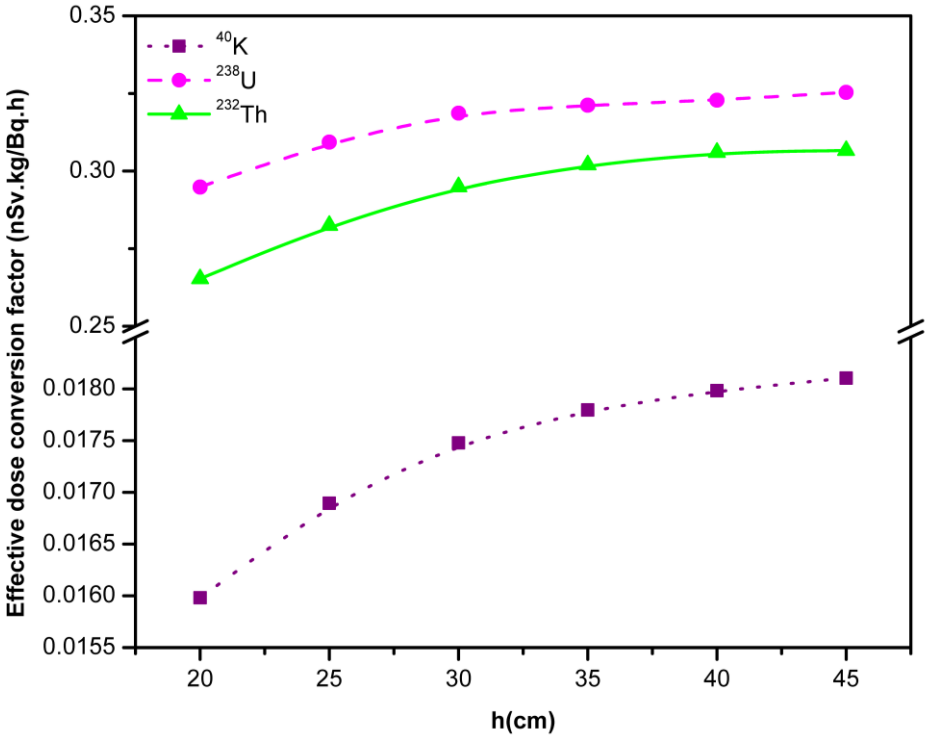

Fig. 2 Determination of optimum depth for ^{238}U, ^{232}Th and ^{40}K Sources, considering the soil composition of this work.

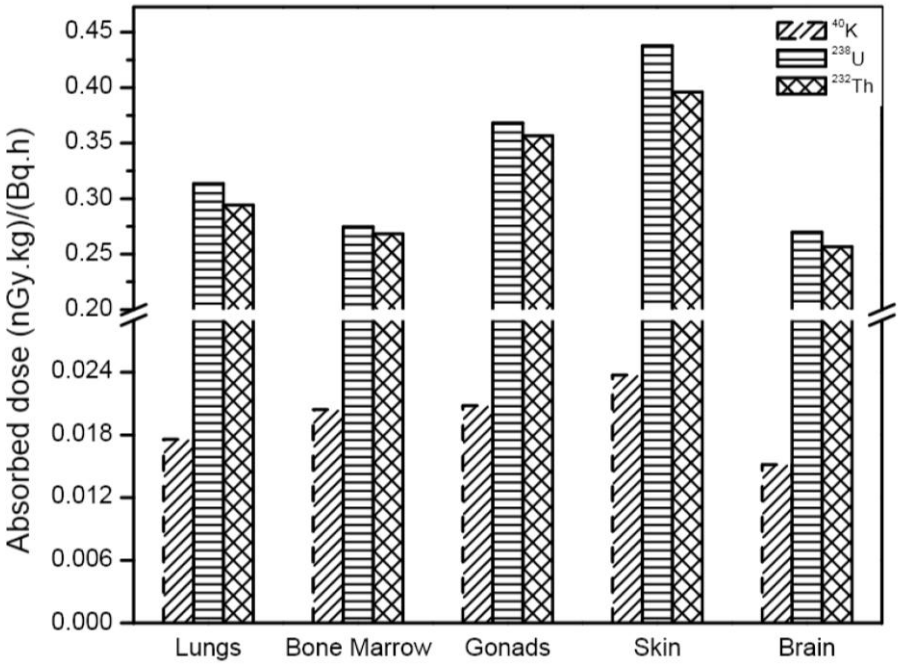

Fig. 3 Determination of absorbed dose in some issues from ^{238}U, ^{232}Th and ^{40}K sources.

several tissue samples. The absorbed dose is dependent upon the distance from the sources position to the tissues. Therefore, it is expected to that the amount of stored dose in the thyroid is less than the amount in the lower body areas that are closer to the source position. On the other hand, radiation exposure on the body surface is more than the internal organs. Hence, the dose received by the

body surface such as the skin, breasts, and gonads will be more larger than the does received by other internal organs such as the hearts. The conversion factors from activity to the effective dose of the ^{238}U series, the ^{232}Th series and the ^{40}K in soil, as calculated in this work are 0.383, 0.314 and 0.019 nSv/h per Bq/kg, respectively.

3.2 Effect of Soil Composition

The effective dose conversion factors of the ^{238}U, ^{232}Th series and the ^{40}K in different soils considered by FGR12, D. Krstic [14]and this work are compared in Table 3. A number of researchers have determined the radioactivity content of soils in some high background regions of Iran. These regions are listed in Fig. 4.

The range and mean activity concentrations of ^{232}Th, the ^{226}Ra, the ^{238}U and the ^{40}K in these provinces measured by other investigators are presented in Table 4. In Table 5, the obtained results of the effective dose rate for the ^{232}Th and the ^{238}U series, and the ^{40}K in different parts of Iran have been displayed and compared to the dose achieved for Iran by UNSCEAR 2000. Table 6 shows the annual effective doses from terrestrial radiation sources in world and different parts of Iran.

4. Discussion

In Fig. 3, the difference in the absorbed dose values of different tissues is due to the type of gamma interaction of the isotopes in these tissues. The skin receives the highest dose compared to the other body organs, because it is more susceptible to radiation. In addition, because of the position of the source and the phantom, high doses are stored in the gonads.

Table 3 Comparison of effective dose conversion factors in different soils considered by Eckerman, D.Krstic and this work.

Effective dose conversion factors (nSv/h per Bq/kg)			Reference
^{238}U	^{232}Th	^{40}K	
0.390	0.319	0.0191	Eckerman & Ryman (1993) [9]
0.398	0.325	0.0194	D. Krstic (2010) [14]
0.383	0.314	0.0190	This work

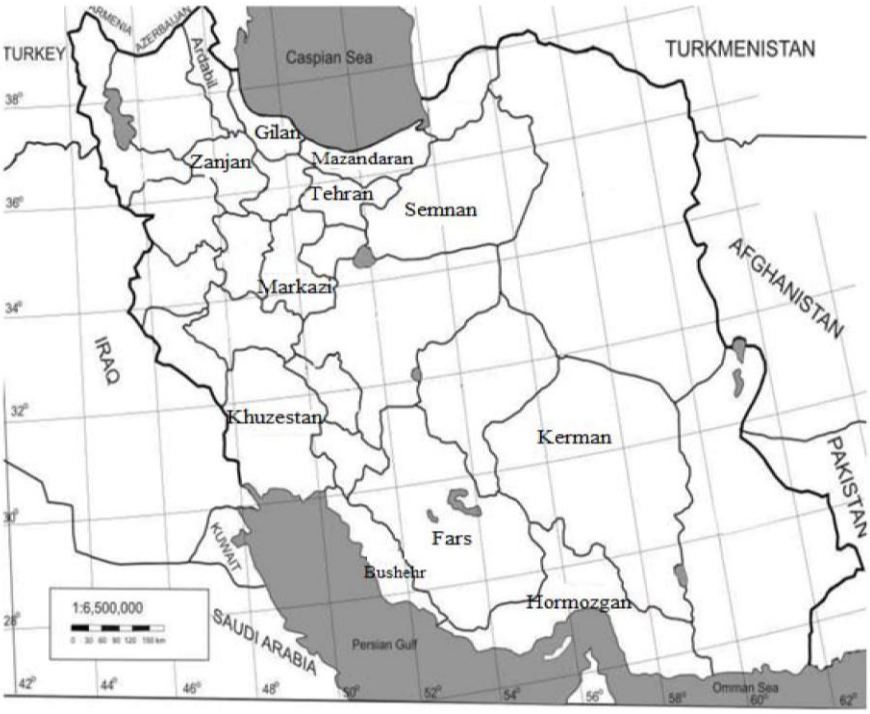

Fig. 4 A map of Iran, showing the nuclear sites of Iran.

Table 4 Activity concentration of concerned radionuclide measured in different parts of Iran.

Province		Activity concentration (Bq/kg)				Reference
		^{238}U	^{226}Ra	^{232}Th	^{40}K	
Ardabil	Range	–	–	7-38	709-940	Sohrabi [15]
Bushehr	Range	12-75	–	8-33	108-520	M.R.Abdi [16]
Gilan	Mean	–	24 ±6	26 ±11	548 ±138	A.Sadermomtaz [17]
Hormozgan	Range	29-385	–	9-156	140-1172	M.R.Abdi
Kerman	Mean	23.8 ±3.6	–	28.8 ±4.3	489.6 ±48.9	S.Hafezi [18]
Khozestan	Range	–	–	6-17	250-773	Sohrabi
Markazi	Range	–	–	9-30	528-840	Sohrabi
Mazandaran	Mean	–	1188.5 ±7838.4	64.92 ±162.26	545.1 ±139.4	M.Abbaspour [19]
Semnan	Range	–	–	7-25	634-897	Sohrabi
Tehran	Mean	24	–	28	635	S.Hafezi
Fars	Range	–	–	12.7-25	224-447	S.Hafezi
Zanjan	Mean	–	88.5 ±22.9	–	497.4 ±162.6	F.Saghatchi [20]

Table 5 A comparison between effective dose rates assessment for the ^{232}Th and ^{238}U series and ^{40}K, in the soil of different parts of Iran in this work and UNSCEAR 2000.

Province		Effective dose rate (nSv h^{-1})				Total effective dose rate (nSv h^{-1})
		^{238}U	^{226}Ra	^{232}Th	^{40}K	
Ardabil	Range	–	–	2.2-11.93	13.3-17.64	15.5-29.57
Bushehr	Range	4.6-28.7	–	2.5-10.36	2.03-9.76	9.13-48.84
Gilan	Mean	–	9.19±2.3	8.16 ±3.45	10.28 ±2.59	27.64 ±8.3
Hormozgan	Range	11.1-147.45	–	2.82-48.97	2.63-22	16.56-218.42
Kerman	Mean	9.11 ±1.38	–	9.04 ±1.35	9.19 ±0.92	27.34 ±3.65
Khozestan	Range	–	–	1.88-5.34	4.69-14.5	6.57-19.85
Markazi	Range	–	–	2.82-9.42	9.91-15.77	12.73-25.18
Mazandaran	Mean	–	455.18 ±3002.03	20.38 ±50.93	10.23 ±2.62	485.79 ±3055.58
Semnan	Range	–	–	2.2-7.84	11.9-16.84	14.1-24.68
Tehran	Mean	9.192	–	8.789	11.92	29.9
Fars	Range	–	–	3.99-7.85	4.2-8.4	8.2-16.24
Zanjan	Mean	–	33.89 ±8.5	–	9.34 ±3.05	43.23 ±11.59
Iran(UNSCEAR 2000)	Mean		–	–	–	71

Table 6 A comparison between AED (annual effective doses) from terrestrial radiation sources in different parts of Iran.

Province		Total annual effective dose (mSv)	AED (outdoors)	AED (indoors)
Ardabil	Range	0.04-0.07	0.027-0.052	0.011-0.021
Bushehr	Range	0.022-0.12	0.016-0.085	0.006-0.034
Gilan	Mean	0.068 ±0.02	0.048 ±0.015	0.019 ±0.006
Hormozgan	Range	0.041-0.53	0.029-0.383	0.012-0.15
Kerman	Mean	0.067 ±0.009	0.048 ±0.006	0.019 ±0.002
Khozestan	Range	0.016-0.049	0.012-0.035	0.005-0.014
Markazi	Range	0.031-0.062	0.022-0.044	0.009-0.018
Mazandaran	Mean	1.19 ±7.49	0.85 ±5.35	0.34 ±2.14
Semnan	Range	0.034-0.06	0.025-0.04	0.01-0.017
Tehran	Mean	0.07	0.052	0.021
Fars	Range	0.02-0.04	0.014-0.03	0.0057-0.011
Zanjan	Mean	0.11 ±0.03	0.076 ±0.02	0.03 ±0.008
UNSCEAR 2008 (World)	Mean	0.03-1	0.07	0.41

Table 1 presents the comparison with other authors [8, 10-14]. All of these authors, with the exception of D. Krstic [14], calculated the absorbed dose in the air (the specific absorbed dose rate in the air outdoors) in units (nGy/h per Bq/kg) due to the radioactivity in soil. The discrepancy between the literature and our results is evident in Table 1, and may be explained by differences in methodology and the gamma spectrum used in calculation. The authors, except D. Krstic, calculated the dose in appoint in air and converted it to the effective dose by multiplying with a factor of 0.7. The second reason is that the literature values were

obtained for the most intensive lines in the spectrum, while many more gamma lines were used in this work (209 lines for the ^{238}U and 105 for ^{232}Th).

The differences between obtained data from D. Krstic and this work caused by several factors, including differences in soil composition considered, gamma lines used (649 lines for the ^{238}U and 318 for ^{232}Th in D. Krstic paper and 209 lines for the ^{238}U and 105 for ^{232}Th in this work), sources dimensions and tissue weighting coefficients used (calculations in D. Krstic paper were done according to ICRP 74 recommendations, while we have used ICRP 103).

According to Table 3, the effect of soil composition can be investigated. It seemed that nuclear data used, are the main reason for the differences of the effective dose conversion factors.

5. Conclusion

In this present paper, the absorbed doses in organs of human body per one photon due to naturally occurring radionuclide in the soil have been calculated. By using of MCNP-4C code, the absorbed doses were calculated for all "main organs" and organs of "remainder". The effective dose conversion factors obtained here are 0.383, 0.314 and 0.019 in nSv/h per Bq/kg for the ^{238}U series, ^{232}Th series and the ^{40}K, respectively. Discrepancy from other authors can be explained with somewhat different methodology and used the gamma spectrum. From the measured activity content of the soil, the annual effective gamma dose rates and the AED were calculated. The activity concentration table of the radionuclides shows that the Mazandaran province has more radioactivity content so that the inhabitants of the Mazandaran can receive a more dose than the people living in the other regions.

References

[1] N. Akhtar, M. Tufail, M. Ashraf, M. MohsinIqbal, Measurement of environmental radioactivity for estimation of radiation exposure from saline soil of Lahor, Pakistan. Radit. Measur. 39 (1) (2005) 11-14.

[2] M.H. Mamaney, E.M. Khater, Environmental characterization and radio-ecological impacts of nonnuclear industries on the Red Sea coast, J. Environ. Radioactivity 73 (2004) 151-168.

[3] G. Perez, V.P. Perelyguin, E. Herrera, L. Desdin, A. Hernandez, D. Gonzalez, et al., Determination of naturally radioactive elements in construction materials by means of gamma spectroscopy, track registration techniques and neutron activation analysis, J. Radioanal. Nucl. Chem. 176 (1993) 315–323.

[4] G. Faghihian, D. Rahi, M. Mostajaboddavati, Study of natural radionuclides in Karun river region, J. Radioanal. Nucl. Chem. 292 (2) (2012) 711-717.

[5] K.F. Eckerman, M. Cristy, J.C. Ryman, The ORNL mathematical phantom series Retrieved from http://ordose.ornl.gov/resources/Mird.pdfS, 1996.

[6] D. Barisic, Dose rate conversion factors, soil thickness and their Influence on natural background dose rate in air above carbonate terrains, J. Environ. Radioactivity 31 (1) (1996) 51-70.

[7] United Nations. Sources and Effects of Ionizing Radiation, United Nations Scientific Committee on the Effects of Atomic Radiation, 1993 report to the general assembly, with scientific annexes. United Nations sales publication E.94.IX.2. United Nations, New York, 1993.

[8] H.L. Beck, J. DeCampo, G. Gogolak, In Situ Ge (Li) and Na (Tl) Gamma-Ray Spectrometry, Technical report, Jan. 1972.

[9] K.F. Eckerman, J.C. Ryman, External Exposure to Radionuclides in Air, Water, and Soil, Federal Guidance Report, 1993.

[10] K. Saito, P. Jacob, Gamma ray fields in the air due to sources in the ground, Radiat. Prot. Dosim. 58 (1) (1995) 29-45.

[11] M. Markkanen, Radiation Dose assessments for Materials with Elevated Natural Radioactivity, STUK-B-STO 32, Helsinki, 1995.

[12] A. Clouvas, S. Xanthos, M. Antonopoulos-Domis, J. Silva, Monte Carlo calculation of dose rate conversion factors for external exposure to photon emitters in soil, Health Phys. 78 (3) (2000) 295-302.

[13] L.S. Quindos, P.L. Fernandez, C. Rodenas, J. Gomez-Arozamena, J. Arteche, Conversion factors for external gamma dose derived from natural radio- nuclides in soils, J. Environ. Radioact. 71 (2004) 139-145.

[14] D. Krstic, D. Nikezic, Calculation of the effective dose from natural radioactivity in soil using MCNP code, Applied Radiation and Isotopes 68 (2010) 946-947.

[15] M. Sohrabi, Natural Radioactivity of Soil Samples in some High Level Natural Areas of Iran, National Radiation Protection Department, Atomic Energy Organization of Iran, 1997.

[16] M.R. Abdi, H. Faghihian, M. Mostajaboddavati, A. Hasanzadeh, M. Kamali, Distribution of natural radionuclides and hot points in coasts of Hormozgan, J. Radioanal. Nucl. Chem. 270 (2) (2006) 319-324.

[17] A. Sadremomtaz, M. VahabiMoghaddam, S. Khoshbinfar, A. Moghaddasi, A comparative study of field Gamma-ray spectrometry by NaI (Tl) and HPGe detectors in the South Caspian region, Caspian J. Env. Sci. 8 (2) (2010) 203-210.

[18] S. Hafezi, A. Shokraei, H. Sajadi, A. Najafi, The effective dose to the public of Kerman province from gamma emitter terrestrial radionuclides, International Journal of Low Radiation 6 (1) (2009) 1-7.

[19] M. Abbaspour, F. Moattar, A. Okhovatian, M. Kharrat Sadeghi, Relationship of soil terrestrial radionuclide concentrations and the excess of lifetime cancer risk in western Mazandaran province, Iran, Radiat. Prot. Dosimetry 142 (2-4) (2010) 265-272.

[20] F. Saghatchi, M. Salouti, A. Eslamiand, A. Sharafi. Natural radioactivity levels of ^{226}Ra and ^{40}K in soil of Zanjan province, Iran, Radiat. Prot. Dosimetry. 141 (1) (2010) 86-89.

Journal of Pharmacy and Pharmacology
Volume 2, Number 1, January 2014
David Publishing Company
240 Nagle Avenue #15C, New York, NY 10034, USA
Tel: 1-323-984-7526, 323-410-1082; Fax: 1-323-984-7374, 323-908-0457
http://www.davidpublishing.com
pharmacy@davidpublishing.com, pharmacy@davidpublishing.org

ISSN 2328-2150
01